Creating, Validating, and Using Synthetic Power Flow Cases:

A Statistical Approach to Power System Analysis

by

Eran Schweitzer

A Dissertation Presented in Partial Fulfillment
of the Requirement for the Degree
Doctor of Philosophy

Approved November 2018 by the
Graduate Supervisory Committee:

Anna Scaglione, Chair
Kory W. Hedman
Thomas J. Overbye
Antonello Monti
Lalitha Sankar

ARIZONA STATE UNIVERSITY

May 2019

ABSTRACT

Synthetic power system test cases offer a wealth of new data for research and development purposes, as well as an avenue through which new kinds of analyses and questions can be examined. This work provides both a methodology for creating and validating synthetic test cases, as well as a few use-cases for how access to synthetic data enables otherwise impossible analysis.

First, the question of how synthetic cases may be generated in an automatic manner, and how synthetic samples should be validated to assess whether they are sufficiently "real" is considered. Transmission and distribution levels are treated separately, due to the different nature of the two systems. Distribution systems are constructed by sampling distributions observed in a dataset from the Netherlands. For transmission systems, only first-order statistics, such as generator limits or line ratings are sampled statistically. The task of constructing an optimal power flow case from the sample sets is left to an optimization problem built on top of the optimal power flow formulation.

Secondly, attention is turned to some examples where synthetic models are used to inform analysis and modeling tasks. Co-simulation of transmission and multiple distribution systems is considered, where distribution feeders are allowed to couple transmission substations. Next, a distribution power flow method is parametrized to better account for losses. Numerical values for the parametrization can be statistically supported thanks to the ability to generate thousands of feeders on command.

DEDICATION

Für Melanie

ACKNOWLEDGEMENTS

I am deeply grateful to my advisor, Prof. Anna Scaglione, for her insight, direction, and advice regarding the PhD and otherwise. Though painful at times, I am a convert to the opinion that problems should be formulated cleanly, and reformulated, until insight can be grasped. This work has greatly benefited from her scrutiny and insight.

I had the privilege of continuing a collaboration with Prof. Antonello Monti past my Masters into the PhD. The two summers I spent back at the Institute for the Automation of Complex Power Systems, were both highly productive and enjoyable, as well as a refreshing escape from Tempe summers. I would also like to thank the rest of my committee—Prof. Kory Hedman, Prof. Lalitha Sankar, and Prof. Thomas Overbye—for their input and feedback, both specific and general, to the work presented here. I am grateful to Jason Fuller and Jacob Hansen, as well as the rest of the Electricity Infrastructure group at the Pacific Northwest National Laboratory for hosting me for a summer. Thank you to Dr. Giuliano Andrea Pagani for his assistance with the Netherlands data. I would also like to thank Ray Zimmerman for his patient guidance in developing for MATPOWER and beyond.

Thank you to all the SINE Lab members. I never met a student that didn't complain about PhD life, but I always tried to include a note of gratitude in my complaints that at least I have such great colleagues, who are both friendly and knowledgeable in so many different areas.

Thank you to my parents, Yael and Ronen, and siblings, Leeor and Na'ama, as well as friends in Portland, Aachen and elsewhere who probably got more than they bargained for on occasion, when asking how I was doing. Finally, I would not have made it to the finish line if my wife, Melanie, had not been so supportive, and visited regularly. Thank you for getting to know Arizona better than me and showing me around.

TABLE OF CONTENTS

CHAPTER Page

CHAPTER Page

CHAPTER Page

CHAPTER Page

APPENDIX Page

LIST OF TABLES

LIST OF FIGURES

Figure Page

Figure Page

LIST OF ALGORITHMS

LIST OF ACRONYMS

Acronym	Meaning
ADMM	Alternating Direction Method of Multipliers.
BFS	Breadth First Search.
cdf	Cumulative Distribution Function.
DistFlow	Baran and Wu Distribution Power Flow [Baran and Wu(1989)].
DSO	Distribution System Operator.
EA	Evolutionary Algorithm.
EI	Eastern Interconnect.
ER	Erdős Rényi.
ERCOT	Electric Reliability Council of Texas.
FERC	The Federal Energy Regulatory Commission.
HV	High Voltage.
KCL	Kirchhoff's Current Law.
KDE	Kernel Density Estimate.
KL	Kullback Leibler.
KS	Kolmogorov-Smirnov.
LMP	Locational Marginal Price.
LPF	Linear Power Flow.
MILP	Mixed Integer Linear Program.
MIP	Mixed Integer Programming.
MV	Medium Voltage.
NOB	Normally Open Branches.
OPF	Optimal Power Flow.
pdf	Probability Density Function.
PNNL	The Pacific Northwest National Laboratory.
PTDF	Power Transfer Distribution Factor.

Acronym	Meaning
RT	RTnested-SmallWorld.
SIL	Surge Impedance Loading.
TnD	Transmission and Distribution.
UC	Unit Commitment.
WECC	Western Electricity Coordinating Council.

LIST OF SYMBOLS

Symbol	Description
$\mathscr{N}$	Set of nodes/buses.
$\mathscr{L}$	Set of lines/branches.
$\{i, j\}$	An undirected branch between nodes i and j.
$\ell \Leftrightarrow \{i, j\}$	A one-to-one *and* onto mapping between edge index ℓ and unordered pair $\{i, j\}$.
(i, j)	A directed branch *from* node i *to* node j.
$f(\ell), t(\ell)$	For an edge (i, j) with index ℓ, $(f(\ell), t(\ell)) = (i, j)$.
$f^{-1}(i), t^{-1}(j)$	Inverses of $f(\cdot)$ and $t(\cdot)$ returning the set of branches $\{\ell : f(\ell) = i\}$, $\{\ell : t(\ell) = j\}$, respectively.
Φ_j	Set of phases at node j. As superscript, projects onto set, by removing extra phases and replacing missing ones with 0.
V_j	$\lvert\Phi_j\rvert \times 1$ complex voltage vector at node i.
v_j	$\lvert\Phi_j\rvert \times 1$ vector with the magnitudes of V_j.
θ_j	$\lvert\Phi_j\rvert \times 1$ vector with the angles of V_j.
I_ℓ	$\lvert\Phi_{t(\ell)}\rvert \times 1$ complex current vector on branch ℓ.
z_ℓ	$\lvert\Phi_{t(\ell)}\rvert \times \lvert\Phi_{t(\ell)}\rvert$ complex impedance matrix for branch ℓ.
s_j^Y	$\lvert\Phi_j\rvert \times 1$ wye-connected constant power load at node j.
s_j^Δ	3×1 delta-connected constant power load at node j.
$\mathbb{I}$	Identity matrix. Subscripts used to state size explicitly.
$\lvert x\rvert$	Magnitude or cardinality of x.
x^T	Transpose of x.
x^*	The complex conjugate of x.
x^H	Conjugate transpose of x.
$\mathrm{D}(x)$	Returns a square matrix with vector x on the diagonal.

Symbol	Description
d(X)	Returns the diagonal of square matrix X as a vector.
vec(X)	Stacks the columns of X into a vector.
$A\otimes$B	Kronecker product of matrix A with matrix B
$\delta(\cdot)$	The Kronecker delta function.
$u(\cdot)$	The Heaviside step function.

CHAPTER 1

INTRODUCTION

The electric grid is the largest machine created by humans, and it is critical for the functioning of developed economies. Research and development work concerning the power grid rely heavily on computational models, allowing studies to be conducted without disturbing the critical day-to-day operation of the system. This work considers where these models come from, how they are created, and why automating their creation opens doors to new insights and types of studies. Conceptually, this is done in two main parts. Part one, Chapters 2 and 3, considers the automatic creation and assessment of power system models, while the second part, Chapters 4 and 5, utilizes the models to both explore and improve power flow calculations. In that respect part two answers both why part one matters and how it might be used.

1.1 Power System Test Cases

Power system test cases are the foundation on which most studies in the field are conducted, and the starting point for many research, development, or educational lines of inquiry. However, due to national security and utility proprietary issues, real test case data is often hard to get, and when obtained, comes with non-disclosure agreements. As a result, reproducibility of published results is often complicated, and algorithms or demonstrations are frequently only tested or conducted on a relatively small set of cases. Some of the work presented here is part of a larger effort to expand the library of power system test cases available to the community at large [ARPA-E Grid Data(2017)].

The most common transmission test cases available in literature either come from [Power Systems Test Case Archive(2018)], where they are either reduced por-

tions of real systems and/or the product of a working group like the Reliability Test System [Grigg *et al.*(1999)]. On the distribution side, many of the available cases can be found in [IEEE PES Distribution Test Feeders(2018)], where some like [Kersting(2001), Arritt and Dugan(2010)] were published in IEEE transactions, as well as a few others like [Schneider *et al.*(2008)]. This work strives for a fundamentally different approach, where cases are created completely automatically, thus increasing the number of available samples to be arbitrarily large. Doing so relies on analyzing statistics of real systems and then developing methods to exploit these statistics in synthesis algorithms.

Insisting on automatic generation comes with certain benefits, as well as costs. The power grid is a highly engineered system, which means that it exhibits some highly idiosyncratic behaviors. It is extremely difficult to capture very rare corner cases in a statistical approach, and as such, very rich detail is difficult to obtain. At the same time, the statistical approach relies at its core on an *ensemble* of results. Following basic Monte Carlo reasoning, the idea is that a sufficiently large number of cases will capture the distribution of situations encountered in the real world systems (at the chosen level of abstraction). Seen in this light, the presented approach to synthetic test case generation, is an initial tool for a different way of conducting power system studies. Instead of presenting results on a particular (or a handful) of cases, while varying certain parameters of interest, with automatically generated synthetic test cases, studies are run on large ensembles of cases and make evaluations based on the distributions of result statistics.

The objectives of Chapters 2 and 3 can be summarized as:

> Creating steady-state power flow models, at both the distribution and transmission levels, that are automatically generated, such that in principle, a large number of models can enable Monte Carlo like statistical

testing.

Power systems are traditionally split into two classes: transmission (high voltage) and distribution (medium and low voltage). Accordingly, the algorithms presented tackle the two systems separately. Chapter 2 deals with distribution system feeders, while Chapter 3 addresses the bulk transmission system.

1.1.1 Related Work

Beginning in the late 1990s and into the 2000s there several works characterized the power system as a complex network, focusing mainly on the topology of transmission grids. In [Watts and Strogatz(1998)] the grid is compared to small-world graphs, and in the subsequent year [Barabási and Albert(1999)] compared it to preferential attachment models which form scale free networks, where the node degree distribution exhibits a power-law behavior. Following the 2003 Northeast blackout in the U.S. [US-Canada Power System Outage Task Force *et al.*(2004)], many papers were written analyzing the grid's vulnerability through the lens of the topological analysis that had already begun. Work on cascading failure, such as [Albert *et al.*(2004), Rosato *et al.*(2007), Rosas-Casals *et al.*(2007)], effectively consider emergent behaviors relating to connectivity on a graph under removal of edges or nodes. Much of the literature in this vein is summarized in [Pagani and Aiello(2013)].

Beginning with [Wang *et al.*(2010a)] these topology models began to be exploited, in order to synthesize realistic grid topologies. Where [Wang *et al.*(2010a)] focused on the small-world tendencies of power systems, [Deka *et al.*(2016)] and [Cloteaux(2013)] employ a more preferential attachment model approach, and [Hu *et al.*(2015)] exploits clustering related observations. Soltan and Zussman present a geographically embedded topology model in [Soltan and Zussman(2016)] and [Soltan and Zussman(2015)], where Gaussian Mixture Models of population are used to sample node locations,

that are then connected by a tunable weight spanning tree procedure. As the complex network community increased its interaction with the power system community, some warnings began to appear about the efficacy of the complex network approach. [Hines *et al.*(2010)] suggests that a strictly topological view is insufficient to assess the vulnerability of the power grid, [Cotilla-Sanchez *et al.*(2012), Cotilla-Sanchez *et al.*(2013),Hines *et al.*(2016)] use the so-called "electric distance" described in [Klein and Randić(1993)] to capture an alternative graph representation of the system. Both [Brummitt *et al.*(2013)] and [Rosas-Casals *et al.*(2015)] summarize some of the challenges of combining the generalities of the complex network approach, with the idiosyncrasies of the power system.

As a partial response, current work began to pay more attention to the intricacies of the power system. Still from a strictly topological perspective, [Aksoy *et al.*(2017)] considers the relationship between voltage levels connected by transformers, by combining Chung-Lu random graphs representing the voltage levels, with star graphs representing transformers. Most similar to the work presented in Chapter 3 are [Elyas and Wang(2016a), Elyas and Wang(2016b)], which identify different bus types in a topology based on defined entropy measures. Notably, [Birchfield *et al.*(2016), Birchfield *et al.*(2017b)] created as part of the ARPA-E Grid Data project [ARPA-E Grid Data(2017)], present a much more engineering decision focused, almost greenfield planning, style approach, which draws on many publicly available data. For instance, topologically, the grid is assembled by selecting edges from the Delaunay triangulation of geographically placed loads and generators. Loads are sited at post-office zip-codes and sized based population data, while real geographical coordinates of generating units from the Energy Information Administration are used. It should be noted that these are no longer fully automated cases. The possibility to create large ensembles of such cases is therefore somewhat limited, however, they offer a level of detail far

greater than any of the other models discussed.

At the distribution level, there has been much less system level analysis in terms of complex networks. One notable exception is [Pagani and Aiello(2011)], which presents a first analysis of the data that is used extensively in Chapter 2. While creating their prototypical feeders, [Schneider *et al.*(2008)] also performs some similar analysis on feeders from various U.S. regions. This analysis contributes to the feature vector, used to clustering real feeders and produce the final set of 24.

Recently, [Kadavil *et al.*(2016)] described a method for generating stochastic feeder data in The Pacific Northwest National Laboratory (PNNL)'s GridLAB-D [GridLAB-D(2018)] environment. However, this approach is mainly designed to enhance the load model as seen from the transmission system, and does not, therefore, go into much detail on how the distribution system is constructed.

Several works from the planning field are also quite related to the synthetic generation area. All [Rotering *et al.*(2011), Carrano *et al.*(2006), Mateo *et al.*(2011)] perform an optimization to create some sort of optimal distribution system. These algorithms bare some similarity to [Birchfield *et al.*(2017b)], in that they take as a starting point fixed load (and generation) points embedded in space. As such, they solve the problem of how to best serve this load given various geographic and other constraints, and are treated as either greenfield or brownfield planning problems. A few representative Europeans systems are created using the Reference Network Model from [Mateo *et al.*(2011)] and are presented in [Mateo *et al.*(2018)]. The same model is also adapted for the single and double phase laterals found in the U.S and used to create a few systems in the SMART-DS project from the National Renewable Energy Laboratory [SMART-DS(2018)]. While these models offer a great deal of detail, the planning approach taken makes it relatively costly to produce new models and therefore, large numbers of samples are difficult to achieve. Finally, a completely different

approach is taken by the OpenGridMap project [Rivera *et al.*(2016)], which attempts to crowdsource data collection to create models of the real grid.

1.2 Co-Simulating Transmission and Distribution

Chapter 4 considers co-simulation regimes for coupled Transmission and Distribution (TnD) systems. As distribution systems become more active, meaning that power is both withdrawn and injected, there is growing need to regularly simulate their behavior. Increased interaction between transmission and distribution also reduces the efficacy of typical assumptions, where either side treats the other as a fixed known: constant power loads for transmission and constant voltage source for distribution. A growing area of research into co-simulating TnD is developing to serve this need.

Imbalance in distribution systems stems from several factors including load imbalances, lack of transposition, and the prevalence of single and double-phase laterals in the U.S. [Kersting(2012)]. Therefore, in the U.S., modeling in three phase detail has become the norm. At the transmission level, balanced assumptions are more valid and positive sequence modeling is prevalent. Distribution system models tend to view transmission nodes as perfect voltage sources, while transmission generally views distribution as a load, modeled as a current sink (voltage dependent or not). While methods for solving large electrical circuits in pieces have been around for decades [Kron(1963)], the different modeling regimes and assumptions make the direct application of techniques such as Diakoptics problematic. One can chose to create fictitious voltage or current sources in Diakoptics [Brameller *et al.*(1969)], however, this particular application would require both.

Where real systems are concerned, all relevant models should already exists, however, to conduct more exploratory studies about the influence of TnD on each another,

or simply assess the performance of co-simulation routines, test cases are needed. These require one transmission and many distribution models. Chapter 4 uses the PNNL taxonomy feeders [Schneider *et al.*(2008)] since three-phase models are needed, however, similar constructions using generated synthetic feeders would also be of great interest.

1.2.1 Related Work

A three-phase/three-sequence co-simulation approach is proposed in [Huang and Vittal(2016)] for power flow and dynamic studies. All distribution segments are assumed to connect to transmission at one and only one node, simplifying the translation of the distribution system to a load. A Master-Slave-Splitting powerflow approach for integrated TnD is proposed in [Sun *et al.*(2015)]. Current loops via the distribution system are allowed, and handled by adding equivalent branches to the master (transmission system) problem. However, [Sun *et al.*(2015)] neither derives the equivalent branch model, nor provides any validation against a combined TnD model.

In [Huang *et al.*(2017)], the FNCS co-simulation platform developed at PNNL is introduced in its use for dynamic TnD simulations. Unlike other works in the area, the co-simulation is decoupled, meaning that there is no iteration between federates within a single time-step. Similar to most literature, it only considers a single point of coupling per feeder. The impact of tighter coupling vis-à-vis the need for iteration is the motivation for the work in Chapter 4, and Section 4.2.3 addresses it specifically. Finally, a method for converting transmission system sequence model to three-phase detail is developed in [Jain *et al.*(2016)]. As pointed out in [Huang and Vittal(2016)] and [Huang *et al.*(2017)], this approach excludes established algorithms and applications developed for transmission systems in the sequence domain.

1.3 Distribution Power Flow

Similar to the interest in co-simulation, increased activity at the distribution system level due to integration of distributed generation, has led to renewed research interest in power flow and Optimal Power Flow (OPF) solutions at the distribution level. Distribution feeders generally employ a radial topology that can be exploited by power flow algorithms [Kersting(2012), Baran and Wu(1989)]. At the same time, multiphase modeling is often necessary as opposed to the single phase, positive sequence modeling in transmission analyses, which requiring some algorithmic modifications [Garcia *et al.*(2000)].

Chapter 5, explores one distribution specific power flow method, the Baran and Wu Distribution Power Flow [Baran and Wu(1989)] (DistFlow) formulation, and expands it to better account for line losses using a parameter. Single and multiphase formulations are developed as matrix-vector equations with similarities noted between the two derivations. In fact, combining the equations into matrix-vector forms helps illuminate the relationship between DistFlow and several linearized power flow methods for meshed networks.

The parametrization to approximate line losses and reduce error is performed numerically utilizing synthetic feeders from Chapter 2. This chapter thus provides the most concrete validation and justification for the automatic synthesis of test cases. Obtaining the necessarily number of cases (multiple thousands) for the numerical studies performed would have otherwise been immensely difficult if not impossible.

1.3.1 Related Work

Kersting's forward-backward sweep has long been used for distribution power flow [Kersting(2012)]. The DistFlow model and its simplified linearized solution are first

proposed in [Baran and Wu(1989)]. The non-linear DistFlow considers power flows instead of currents, but is otherwise very similar to Kersting's method. The formulation is expanded to three-phase circuits in [Gan and Low(2014)] utilizing a Semidefinite Relaxation to solve an OPF. In a balanced radial system, [Low(2014a)] and [Low(2014b)] establishes the convex relaxation OPF solution is exact, which makes the approach particularly interesting. A similar observation is made in [Jabr(2006)], where conic-programing is used to solve the power flow in a radial system. As in the DistFlow formulation, v^2 is used as an independent variable instead of v.

Three-phase modeling is expanded to include delta loads in [Zhao *et al.*(2017)], as well as [Bernstein *et al.*(2018)], although the latter does not utilize the same set of DistFlow equations but rather a Y_{bus} formulation. Furthermore, the linear formulations in [Bernstein *et al.*(2018)] require either a linearization about an operating point or a single fixed-point iteration.

The use of v^2 as an independent variable in the DistFlow formulation draws parallel to its use in recent transmission system power flow and OPF studies. In [Yang *et al.*(2018b)], a linearized power flow method using v^2 is developed with results in [Yang *et al.*(2018a)] showing that linearization errors are reduced. Fatemi *et al.* also develop a linearized power flow in v^2 that includes an additional factor of 0.95 to improve the linearization error [Fatemi *et al.*(2015)]. The parameter α introduced in this study is similar to the factor in [Fatemi *et al.*(2015)] with additional justification embedded in the physics-based analyses used to quantify and tune α for a particular distribution network. Chapter 5.1.3 shows how formulations using v^2 as an independent variable naturally arise by generalizing the radial DistFlow equations to meshed networks.

— PART I —

Generating Synthetic Power System Models

CHAPTER 2

RADIAL DISTRIBUTION FEEDERS

2.1 Overview of Methodology

The dataset used to inform the distribution system algorithm described in this chapter comprises the Medium Voltage (MV) system from one of the Distribution System Operators in the Netherlands, covering an area around 8200 square kilometers. Summary statistics are provided in Table 2.1. Data was provided in several `.vnf` files, the proprietary format of the Vision software from Phase2Phase[1]. From there, the data was exported to Excel and imported to a PostgreSQL[2] database for easier manipulation.

[1] `http://www.phasetophase.nl/en_products/vision_network_analysis.html`

[2] https://www.postgresql.org/

Table 2.1: Data component overview

(a) Buses: 21,118

Voltage Level	#
220 kV	6
110 kV	53
20 kV	708
10 kV	18,357
3 kV	1979
400 V	15

(b) Branches: 23,041

Type	#
Underground Cables	21,274
Transformers	711
Link	996
Overhead Lines	7
Reactance Coils	53

(c) Node Objects

Type	#
HV Grid Connection	64
Transformer Loads	17,548
Loads	1494
Generators	461

2.1.1 Feeder Identification

For the purposes of analysis, a feeder is defined as a section of the distribution system fed by a *single* primary substation MV bus, plus the High Voltage (HV) source bus on the other side of the distribution transformer. To identify the feeders, the complete system data is gathered into a large graph, $G(\mathscr{N}, \mathscr{L})$, with buses as the vertices, $\mathscr{N}$, and all the branch elements as the edges, $\mathscr{L}$. Importantly, only branches that are connected at both ends are used. There are 20,903 of these branches as opposed to the full count shown in Table 2.1.

Beginning at each HV source, b, all its neighbors in G are collected in set, η. Two nodes, i and j are neighbors, if there exists an edge $\ell \Leftrightarrow \{i, j\}$, with $\ell \in \mathscr{L}$. Each $r \in \eta$ is used as the starting point of a Breadth First Search (BFS) [Kepner and Gilbert(2011)] that excludes HV source s and its other neighbors, $\eta \setminus \{r\}$. All of the nodes found in the BFS constitute the feeder. The HV node, b is referred to as the *source*, and r as the *root* of the feeder. Around 100 such feeders are identified in the data.

An additional set of feeders is generated by grouping nodes that are separated by very small impedances[3]. These "reduced" feeders are used for much of the analysis since the difference between a large busbar or two smaller busbars connected by negligible impedance is, for this analysis, immaterial.

2.1.2 Feeder Analysis

The nodes and edges of each feeder are analyzed for various properties. These include topological properties such as node degree, and hop distance from the source, h, where hop distance is the number of edges along a path between two nodes. Note

[3]These are primarily the "Link" branch type that has $R = X = 1\,\mu\Omega$.

that, in contrast to meshed transmission networks, e.g. [Wang *et al.*(2010a)], distribution circuits are limited to trees, which are representative of feeders. Therefore, since at this stage open connections are ignored, there is no ambiguity about the class of graph under consideration.

For tree graphs representing distribution feeders, h can be thought of as similar in spirit to the betweenness centrality [Brandes(2001)], while the distribution of h gives a sense for the average path length (both common metrics in literature). In fact, in the context of a radial feeder, the one path of interest for each node is the one between it and the substation. Other common topological features such as clustering coefficients do not make sense for this analysis, since clustering on a tree is, by definition, zero.

Additionally, electrical properties like load at nodes, as well as actual and nominal branch currents are collected. From the graph perspective, these are different weights or attributes. Analysis of specific properties is conducted over all the nodes or edges in all the feeders, granting access to a larger sample pool and therefore, more reliable statistics.

The main objective of the analysis is to identify clear distributions in the data that can be exploited in a synthesis process. Distributions that are a good fit to the cumulative data are compared to each individual feeder to determine the range of deviation at the feeder level from the cumulative trend. Note that although the dataset comprises one distribution system, it comprises about a hundred independent feeders, which are the meaningful sample cases under analysis.

2.1.3 Verification Methodology

Evaluation of how well the synthetic feeders match real data is performed using the Kullback Leibler (KL)-Divergence [Kullback and Leibler(1951)],

$$D_{KL}(p\|q) = \int_{-\infty}^{\infty} p(x) \log\left(\frac{p(x)}{q(x)}\right) \, \mathrm{d}x, \tag{2.1.1}$$

which is often used to characterize the distance between two distributions[4]. In all tests, $q(x)$ is an analytical functional law, while $p(x)$ will be the empirically observed distribution/histogram of the data. Meaningful ranges for the KL-Divergence are determined in the following way:

1. The functional law is determined by considering aggregate data from *all* the feeders, for higher statistical relevance. Out of several possible distribution functions, the one that exhibits minimal D_{KL} with respect to the data is selected.

2. KL-Divergences between *each* individual feeder and the selected functional law are considered. These provide a weighted range for D_{KL}, given the selected function.

In Chapter 3.1, when transmission systems are considered, an additional distance measure is introduced.

[4]The operational meaning of KL distance is as follows: an observer trying to determine if data come from the distribution $p(x)$ rather than $q(x)$ will be wrong with a probability that decays exponentially in the number of independent observations, with a rate that is the KL distance. Therefore, a small KL distance means that a significant number of samples can be generated form distribution $p(x)$, that look indistinguishable from data generated from the statistic $q(x)$ [Dembo and Zeitouni(2009)].

2.2 Data Analysis

Analysis presented in this chapter is used to inform the synthesis algorithm in Section 2.3. In each section, trends in the form of distributions are identified, which are later exploited for synthesis. Intuition is provided as to why a particular distribution is a reasonable modeling choice for the data. This intuition is important for potential expansion and manipulation of the algorithm. By adjusting the parameters of the various distributions, the generation logic is preserved while more extreme or conservative results are achieved, which may be of interest.

2.2.1 Node Generation

The radial assumption is fundamental to the synthesis algorithm because it allows each node to be characterized in terms of distance in *hops* away from the HV source, which is by design the first node in the feeder. For example, root node, r, as described in Section 2.1.1 is by definition one hop away from the source, denoted as $h_r = 1$. Figure 2.2.1 shows the distribution of hop distances in the dataset as well as a fit line following the Negative Binomial distribution,

$$f(x; n, p) = \frac{\Gamma(n + x)}{x!\Gamma(n)} p^r (1 - p)^x, \tag{2.2.1}$$

where $n > 0$, $0 \leq p \leq 1$, $x = 0, 1, \ldots, \infty$, and $\Gamma(\cdot)$ is the Gamma function. The KL-Divergence for this fit, as well as the other distributions in this section and the next, is given in Appendix A.1 Table A.1, and the values for the parameters in (2.2.1) are reported in Table A.2.

The intuition behind the Negative Binomial is its interpretation as an over-dispersed Poisson distribution. In other words, in the random process of deciding how far a node is from its source, the variance does not equal the mean, however, a mean and a variance are sufficient to describe the process.

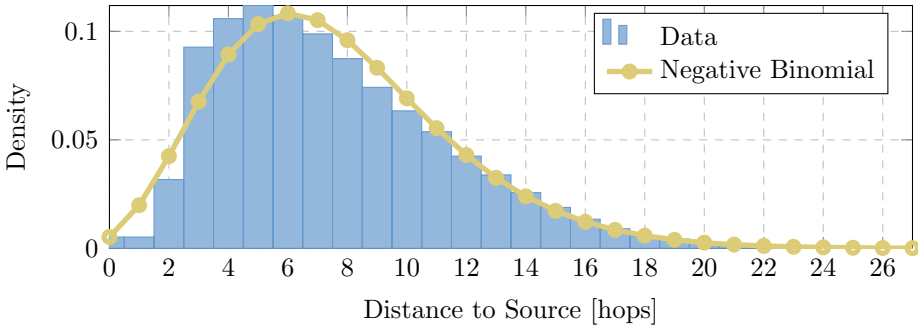

Figure 2.2.1: Distribution of hop distances, h, and the Negative Binomial fit.

2.2.2 Feeder Connection

By restricting the topology, the degree distribution actually reveals a fair amount about the feeder. The degree distribution, $f(k)$, describes the frequency of each degree, k, in the graph, and is widely used in Complex Network Analysis [Lewis(2009)],

$$f(k) = \frac{1}{|\mathcal{N}|} \sum_{n \in \mathcal{N}} \delta(d_n - k), \tag{2.2.2}$$

where d_n is the degree of node n—the number branches incident on node n.

The empirical degree distribution for all feeders is fit by a mixture of Gamma distribution,

$$f(x; p, a_1, b_1, a_2, b_2) = p \cdot g(x; a_1, b_1) + (1 - p) \cdot g(x; a_2, b_2) \tag{2.2.3}$$

with,

$$g(x; a, b) = \frac{1}{b^a \Gamma(a)} x^{a-1} e^{-x/b}, \tag{2.2.4}$$

where $a_{1,2}, b_{1,2} > 0$, $x > 0$, and $g(x; a, b)$ is the Gamma distribution Probability Density Function (pdf). The exponential degree distribution of transmission grids has been widely discussed in literature [Wang *et al.*(2010b), Cotilla-Sanchez *et al.*(2012), Watts and Strogatz(1998), Albert *et al.*(2004)], while in [Pagani and Aiello(2011)] a

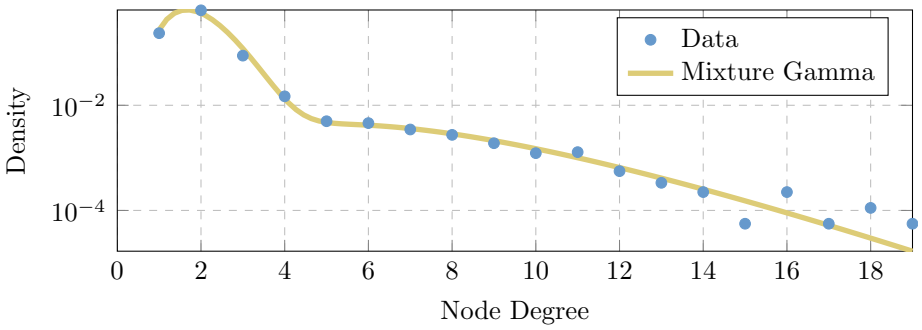

Figure 2.2.2: Degree distribution with a mixture of Gamma distributions fit line.

more split view is given on the appropriateness of an exponential decay versus a power law for distribution systems.

The data displays a clear bimodal behavior as seen in Figure 2.2.2, with two very evident rates of decay. As the conjugate prior of the Exponential distribution, a mixture of Gamma distributions is a natural choice for modeling the two rates. This also fits with the findings in [Deka and Vishwanath(2013)] that a sum of Exponential distributions provided a good fit to the degree distribution.

2.2.3 Node Properties

At present, the node properties considered are the powers associated with each node. Only the real power is considered, with the understanding that the reactive power is handled by a power factor distributed according to the Cumulative Distribution Function (cdf) in Table 2.2 . Three types of nodes are identified: intermediate (no load), generation (negative load), consumption (positive load). Since the number of intermediate nodes and generation nodes is quite small, single feeder statistics are omitted in Table A.1.

Table 2.2: Power Factor CDF

Power Factor	cdf(Power Factor)
0.85	0.1649
0.90	0.2700
0.95	1

2.2.3.1 Intermediate Nodes

Some nodes in the data have neither positive nor negative load, $p_n = 0$. Such intermediate nodes are normally either junctions from which several sub-feeders spring, or nodes associated with normally open connections. The fraction of intermediate nodes per feeder is fit with a Beta distribution, shown in Figure 2.2.3a. The Beta distribution,

$$f(x;,\alpha,\beta) = \frac{1}{\mathrm{B}(\alpha,\beta)} x^{\alpha-1}(1-x)^{\beta-1}, \tag{2.2.5}$$

with $0 < x < 1$, and $\mathrm{B}(\cdot)$ the Beta function, is a common choice when modeling fractional quantities.

Next, the distance of intermediate nodes from the HV source in terms of hops is considered. Figure 2.2.3b shows the histogram as well as a mixture Poisson distribution fit to the data. The mixture poisson is defined as,

$$f(x;p,\mu_1,\mu_2) = p\frac{\mu_1^x}{x!}e^{-\mu_1} + (1-p)\frac{\mu_2^x}{x!}e^{-\mu_2}, \tag{2.2.6}$$

where $x = 0, 1, \ldots, \infty$, $p \in [0, 1]$, and $\mu_{1,2} > 0$. Nodes serving as feeder junctions occur predominantly close to the primary substation, where the main sub-feeders separate from each other. Less frequently, junction points occur one third to halfway down the feeder, which may reflect further geographical splitting, or even a transition to another voltage level[5]. This physical interpretation helps justify the mixture model,

[5]Secondary voltage levels are currently not implemented in the subsequent analysis and algorithm.

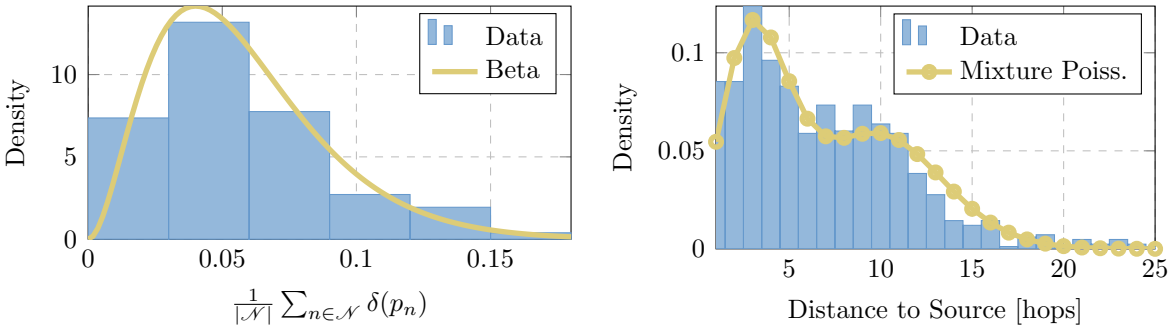

(a) Fraction of intermediate (zero load) nodes

(b) Hop distance of intermediate nodes

Figure 2.2.3: Distributions for intermediate node assignment.

and the Poisson distribution is a natural choice for a random process on the integers.

2.2.3.2 Negative Load Nodes

Negative load, or power injections, represent the "active" part of the feeder. In principle, the load at a given node is a combination of the power injected and consumed at that node. Presently, the sum total is considered and as such, nodes that have a net negative load, $p_n < 0$, are of interest.

Again, the fraction of injection nodes is analyzed and fit with a Beta distribution (cf. Figure 2.2.4a). Also similar to the intermediate nodes, the hop distance for each injection node is considered. Here however, h_n is normalized by the maximum hop distance on the feeder. Figure 2.2.4b shows the histogram along with a mixture Normal distribution described as,

$$f(x; p, \mu_1, \sigma_1, \mu_2, \sigma_2) = p \cdot g(x; \mu_1, \sigma_1) + (1 - p) \cdot g(x; \mu_2, \sigma_2), \tag{2.2.7}$$

where $0 \leq p \leq 1$, and $g(x; \mu, \sigma)$ is the normal distribution pdf with mean μ and standard deviation σ. The normalization is found to help rectify discrepancies between longer and shorter feeders. As might be expected, the main mode is close to the primary substation, where small generators, larger photovoltaic installations, or

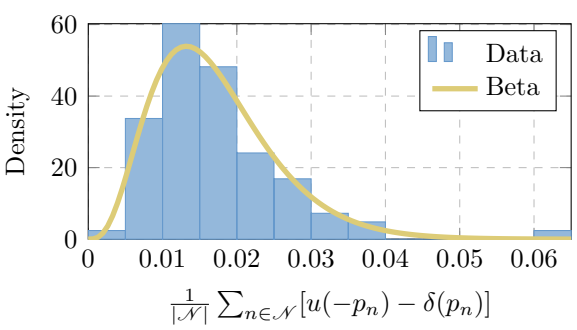

(a) Fraction of injection nodes

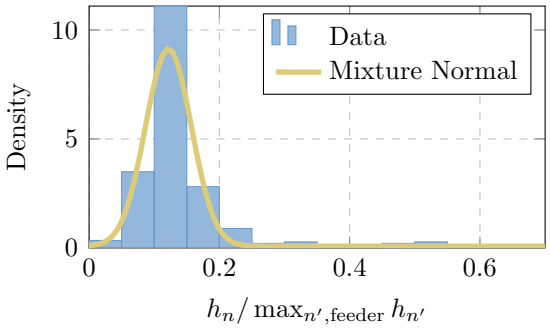

(b) Normalized hop distance of injection nodes

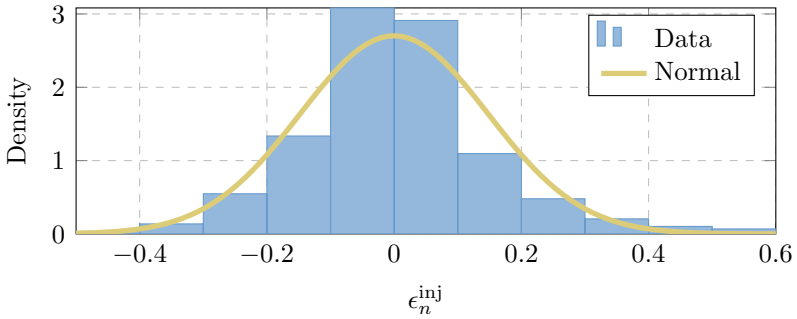

(c) Deviation in (2.2.8) of power injection from uniform distribution

Figure 2.2.4: Distributions for power injection assignment.

even single wind turbines are likely to connect. The slight bump further down the feeder is most likely caused by lower voltage feeders that are feeding back power due to the current loading scenario. While fairly rare, this does happen and is expected to become more frequent as penetration of distributed generation increases.

Finally, Figure 2.2.4c shows the distribution of deviation between each power injection—normalized so that all injections on a single feeder sum to one—and the uniform distribution $1/N_{\text{inj}}$. where N_{inj} is the number of injection nodes. The "error",

$$\epsilon_n^{\text{inj}} = \frac{|p_n| \cdot u(-p_n)}{\sum_{n'\in\mathcal{N}} |p_{n'}| \cdot u(-p_{n'})} - \frac{1}{N_{\text{inj}}} \tag{2.2.8}$$

is found to be normally distributed. This seems reasonable, suggesting power injection magnitudes on a given feeder are similar to one another.

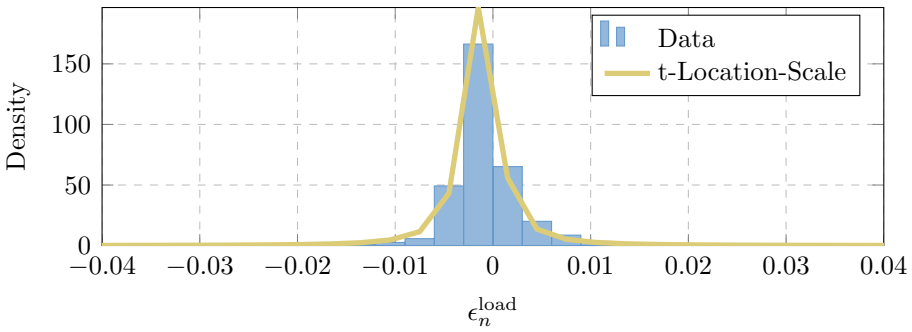

Figure 2.2.5: Histogram of the deviation in (2.2.9) of the load from the uniform distribution.

2.2.3.3 Positive Load Nodes

Distribution feeder design principles are such that the utility attempts to distribute the load evenly across a feeder [Kersting(2012)]. Therefore, the error, ϵ_n^{load}, between the actual power consumed and the uniform distribution is an interesting quantity to consider,

$$\epsilon_n^{\text{load}} = \frac{p_n \cdot u(p_n)}{\sum_{n' \in \mathcal{N}} p_{n'} \cdot u(p_{n'})} - \frac{1}{|\mathcal{N}|}, \tag{2.2.9}$$

where each load has been normalized so that all loads on a single feeder sum to one.

Figure 2.2.5 shows the histogram generated by (2.2.9), which is indeed tightly centered around zero. The t-Location-Scale distribution,

$$f(x;\mu,\sigma,\nu) = \frac{\Gamma\left(\frac{\nu+1}{2}\right)}{\sigma\sqrt{\nu\pi}\cdot\Gamma\left(\frac{\nu}{2}\right)}\left[1+\frac{1}{\nu}\left(\frac{x-\mu}{\sigma}\right)^2\right]^{-\frac{\nu+1}{2}}, \tag{2.2.10}$$

where $\sigma, \nu > 0$, is used to fit the data, reflecting the fact that the load is symmetrically distributed around the Uniform distribution, but with heavy tails. In fact, as can be seen from the parameters in Table A.2, the distribution is close to being Cauchy, which is the case when $\nu = 1$.

2.2.4 Cable Type

Node j is *downstream* of node i, denoted $i \to j$, if the path from the source to j passes through i. Similarly, node i is said to be *upstream* of node j. Define β_i as the

set of all nodes downstream of i, including i:

$$\beta_i = \{j : i \to j\} \cup \{i\}. \tag{2.2.11}$$

The downstream apparent power at node i is defined as,

$$s_i^{\mathrm{dn}} = \sum_{j \in \beta_i} s_j. \tag{2.2.12}$$

Neglecting losses, the power flowing in each branch of the feeder can be estimated by simply summing all downstream powers. If $\ell \Leftrightarrow \{i, j\}$ and $j \in \beta_i$ then $S_\ell^{\mathrm{dn}} = s_j^{\mathrm{dn}}$.

Assuming nominal voltage, the current magnitude on branch ℓ can be estimated as:

$$|I_\ell^{\mathrm{est}}| = \frac{|S_\ell^{\mathrm{dn}}|}{\sqrt{3}|V_\ell^{\mathrm{nom}}|}. \tag{2.2.13}$$

For notational simplicity the magnitude signs are neglected in the following. The Exponential distribution,

$$f(x; \mu) = \frac{1}{\mu} e^{-x/\mu}, \tag{2.2.14}$$

with $\mu > 0$, and $x \geq 0$, describes the ratio between estimated current and nominal cable current, $I_\ell^{\mathrm{est}}/I_\ell^{\mathrm{nom}}$, as shown in Figure 2.2.6. Since some of the feeders analyzed are not 100% radial, the calculation of S_ℓ^{dn} is slightly erroneous, leading to minor errors in I_ℓ^{est}. The discrepancy is quite small, given its low frequency, and it is observed that there is no significant difference between using I_{est} as given in (2.2.13) or the currents calculated from the power flow in the Vision program. Since the power flow requires conductor parameters, which have not yet been assigned, using I_ℓ^{est} offers a significant advantage.

This last point deserves reiteration. The most powerful result of the radial assumption is that the power flow can be fairly accurately estimated *without* knowing line parameters. If the radial assumption is lifted, this is no longer valid. Since distribution systems are operated radially, there is still a deal of utility even in radial models. In

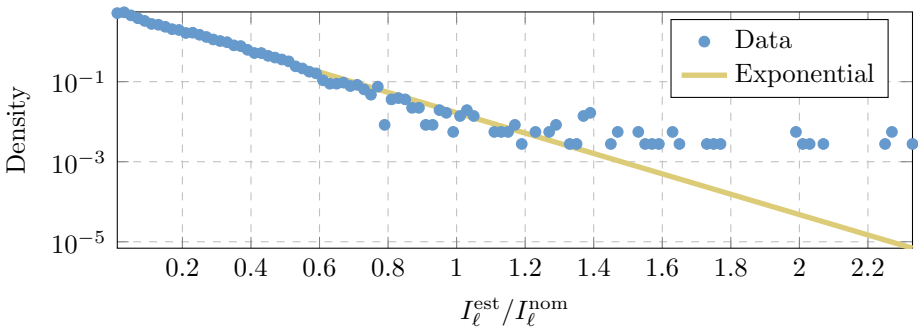

Figure 2.2.6: Exponential fit to the ratio of estimated current, I_{est}, and nominal cable current, I_{nom}.

fact, most of the publicly available test systems, such as the IEEE8500 bus feeder [Arritt and Dugan(2010)] or all the feeders available from PNNL's project [Schneider *et al.*(2008)], are radial. Nonetheless, reconfiguration options should be available, and there are non-radial distribution systems as well. The former is addressed in Chapter 2.5.

2.2.5 Conductor Length

While investigating the distribution of cable lengths, a clear exponential decay in the magnitude of the empirical characteristic function—the Fourier transform of the histogram—was observed, which can be seen in Figure 2.2.7b. Considering common characteristic functions, only the Cauchy distribution with characteristic function,

$$\phi_x(t; x_0, \gamma) = e^{jx_0 t - \gamma|t|}, \tag{2.2.15}$$

exhibits such a decay in magnitude. A modified Cauchy distribution is therefore fit to the data,

$$f(x; x_0, \gamma) = \left[\arctan\left(\frac{x_0}{\gamma}\right) + \frac{\pi}{2}\right]^{-1} \left[\frac{\gamma}{(x - x_0)^2 + \gamma^2}\right] \tag{2.2.16}$$

where $x_0 \in \mathbb{R}, \gamma > 0$, and the modification cuts the support of the distribution from $x \in \mathbb{R}$ to $x > 0$. Figure 2.2.7a shows that the fit matches the data well.

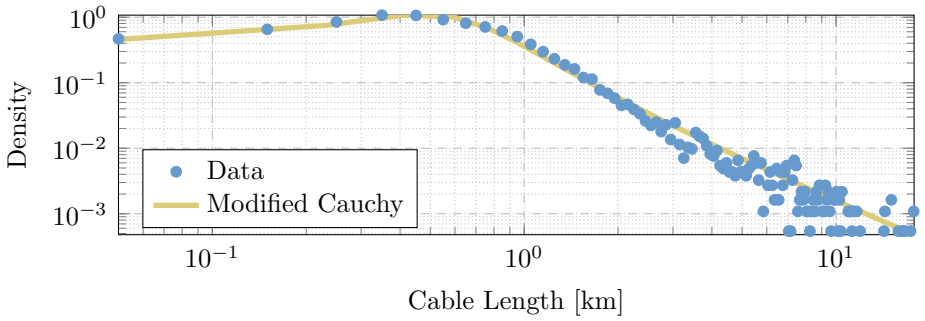

(a) Histogram

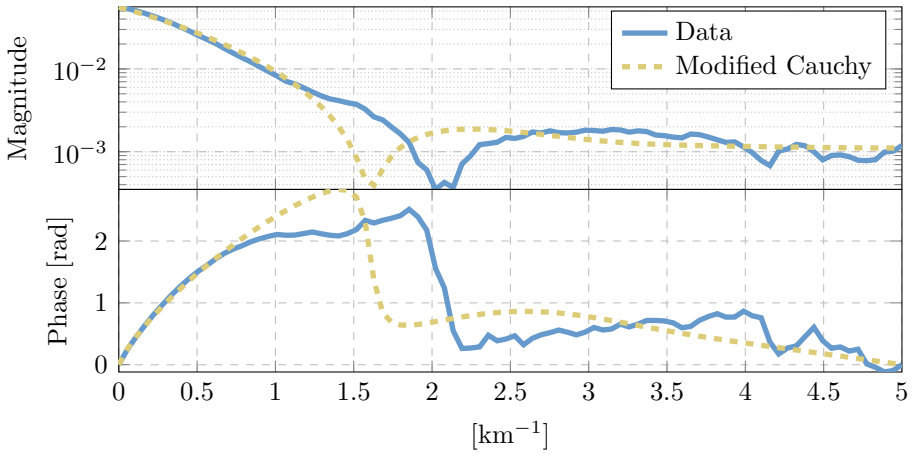

(b) FFT of histogram representing the characteristic function

Figure 2.2.7: Distribution of cable lengths and modified Cauchy fit.

2.2.6 Clipping Distributions

Most of the distributions introduced thus far have either the whole real line or the positive real line as support. Since several of them are heavy tailed distributions, extreme values occur at non-negligible frequencies. However, from fundamental engineering principles, certain situations do not make physical sense. For example, constraints on acceptable voltage drop limit the length of a distribution conductor given the nominal voltage. Therefore, for several of the distributions, bounds are needed to restrict the range returned when sampling. All of these bounds are expressed in terms of the node's hop distance, h_n, from the source. In this way the

graph description of the feeder is again leveraged to identify trends in physical node and edge properties.

2.2.6.1 Maximum Degree

From the basic design principles of a distribution feeder, branching occurrences are expected to diminish as the distance from the primary substation increases [Dickert *et al.*(2013)]. The maximum degree for each hop level in the dataset, shown in Figure 2.2.8, exhibits this trend, which is fit by a power law function,

$$g_{d_{\max}}(h_n) = a \cdot h_n^b, \tag{2.2.17}$$

where h_n is the hop distance, and a and b are fit to minimize squared error. The specific fit parameters can be found in Table A.2. This function will be used in constraining the degree assigned to nodes.

2.2.6.2 Maximum Nominal Current

Since the Exponential distribution for $I_\ell^{\text{est}}/I_\ell^{\text{nom}}$ places a significant weight on very low ratios, it is possible that sampling would result in very large I_ℓ^{nom}. However, as Figure 2.2.9 shows, the largest cables are not used beyond several hops away from the source. This is, if nothing else, an economics issue, since larger capacity cables

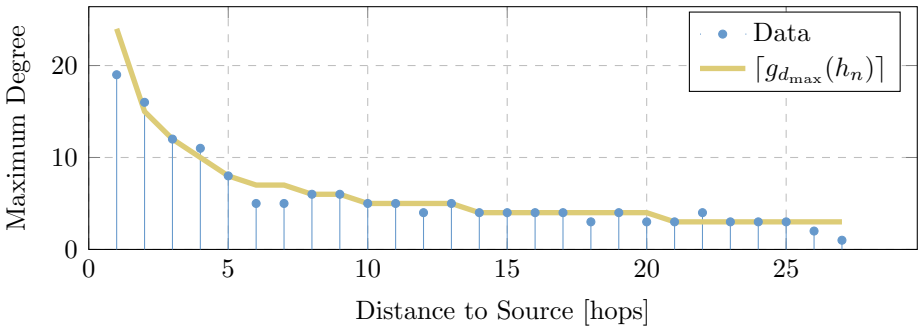

Figure 2.2.8: Maximum degree at each hop distance along with a power law fit.

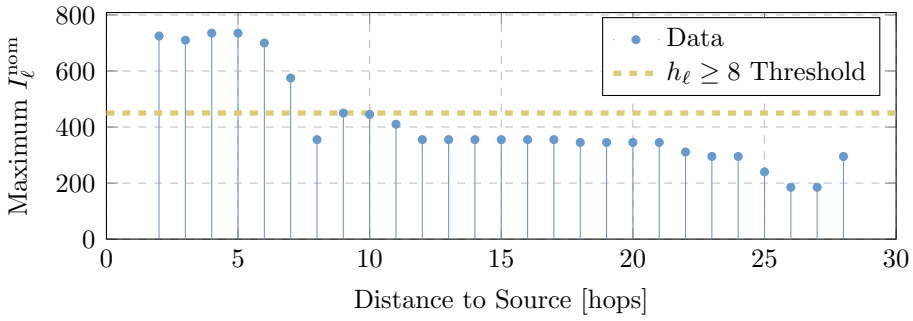

Figure 2.2.9: Maximum I_ℓ^{nom} for cables at each hop distance from the source. The dotted line is the threshold chosen for nodes at $h \geq 8$.

are much more expensive. Therefore, a threshold is selected that for hop distances, $h_\ell \geq 8$, the nominal current is $I_\ell^{\text{nom}} \leq 450\,\text{A}$. The hop distance for branch ℓ relates to its end nodes similarly to the downstream power in Section 2.2.4. That is, if $\ell \Leftrightarrow \{i, j\}$ with $j \in \beta_i$ then $h_\ell = h_j$.

2.2.6.3 Maximum Length

Given the heavy tails of the modified Cauchy distribution, physically unrealizable lengths could be drawn. Figure 2.2.10a shows the maximum length at each hop distance, h_ℓ, as well as an exponential fit,

$$g_{l_{\max}}(h_\ell) = a \cdot e^{b \cdot h_\ell}. \tag{2.2.18}$$

Since the data falls on both sides of $g_{l_{\max}}(h_\ell)$, the errors made by using the function instead of the empirical data are considered. The objective is to not overly constrain the algorithm, that is, force a cable to be much shorter than it could be. Figure 2.2.10b plots two different error functions. The first shows the fraction of cables that are longer than the value returned by (2.2.18) at each hop distance,

$$g_1(\tilde{h}) = \frac{\sum\limits_{\ell \in \mathscr{L}} \left[u(l_\ell - g_{l_{\max}}(h_\ell)) - \delta(l_\ell - g_{l_{\max}}(h_\ell))\right] \delta(h_\ell - \tilde{h})}{\sum\limits_{\ell \in \mathscr{L}} \delta(h_\ell - \tilde{h})} \tag{2.2.19}$$

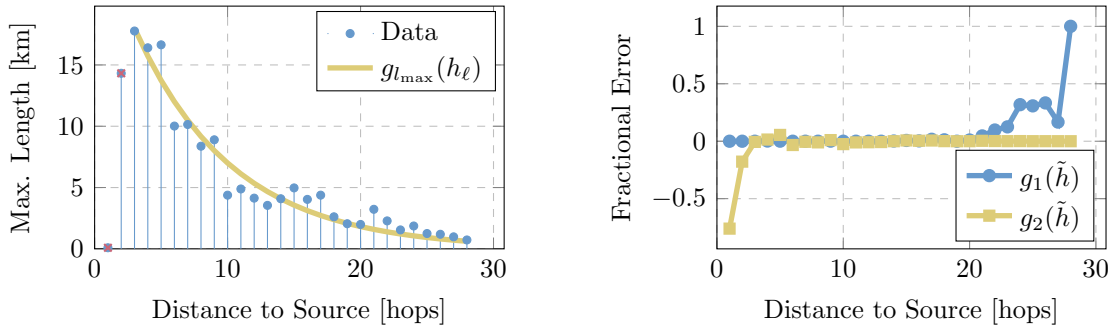

(a) Maximum cable length at each hop distance and Exponential fit to the data.

(b) Analysis of error from using $g_{l_{\max}}$ to bound maximum branch lengths.

Figure 2.2.10: Clipping Function for Length Assignment.

where l_ℓ is the length of branch ℓ. The second function shows the maximum fractional error in length with respect to (2.2.18),

$$g_2(\tilde{h}) = \frac{\max_{\ell \in \mathscr{L}} \delta(h_\ell - \tilde{h}) \cdot l_\ell - g_{l_{\max}}(\tilde{h})}{g_{l_{\max}}(\tilde{h})}. \tag{2.2.20}$$

These two tests reveal that when $g_2(\tilde{h})$ (fractional error) is large, the fraction of cables that are *longer* than $g_{l_{\max}}(h_\ell)$, is negligible, i.e., $g_1(\tilde{h}) \approx 0$. Alternatively, as $g_1(\tilde{h})$ increases, meaning there are more cables longer than $g_{l_{\max}}(h_\ell)$, the fractional error in length is negligible, i.e., $g_2(\tilde{h}) \approx 0$. Therefore, it is reasonable to conclude that (2.2.18) is a good bounding function for the length sampling.

2.2.6.4 Effect of Clipping

From the modeling perspective, applying the bounds is akin to applying a condition to the distributions, from $f(x)$ to $f(x|x < x_{max}(h))$. The effect of such conditioning is to redistribute the weight from outside the constrained domain, to the domain, depending on parameter h. Put another way, there is a relationship between the support of the distribution and h. In the case of the degree distribution, the influence

is fairly minimal, since so much is already dictated by the radial assumption. For example, the average degree is fixed to $2 - 2/N$.

Consider the weighted adjacency matrix A, where the nodes have been sorted based on h_n. The effect of clipping the degree based on h_n is to shift more of the non-zero entries of A to the upper rows. For edge properties, such as length, the clipping function is somewhat like a diagonal matrix with decreasing values that multiplies A. Note, however, that clipping effects were trends observed in the real data.

2.2.7 Analysis Used for Validation

In addition to the previously introduced distributions, which, as will be shown in the next section, are used to synthesize feeders, two additional distributions are considered. The natural emergence of the same trends observed in the data further validate the algorithm's ability to synthesize realistic distribution system feeders. The emergence of statistical behavior for edge and node properties is the main validation of the work.

The first additional trend is the downstream power distribution (cf. Figure 2.2.11a). Downstream power for node i, p_i^{dn}, is defined just like (2.2.12) except that s is substituted with p, i.e., real instead of apparent power. For example, the HV source has downstream power equal to the sum of all loads minus generation in the feeder. The histogram is plotted in Figure 2.2.11a, is a normalization of downstream power by the total load in the feeder, $\sum_{n\in\mathscr{N}} p_n \cdot u(p_n)$. Each node in this distribution is highly dependent on the others, which is the main reason why this distribution does not easily lend itself to be used in the synthesis algorithm.

The second emergent distribution considered is the estimated voltage drop magnitude over a cable, expressed as a fraction of the nominal voltage. This can be

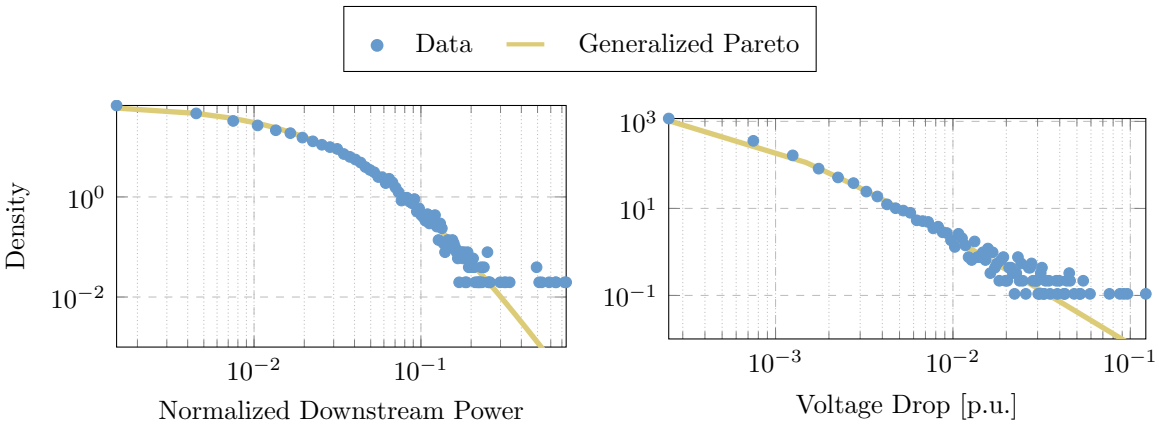

(a) Downstream power distribution with Generalized Pareto fit line.

(b) Per unit voltage drop distribution with Generalized Pareto fit line.

Figure 2.2.11: Two additional distributions, not explicitly used in synthesis, that are used to validate the effectiveness of the generation algorithm.

calculated using the estimated current, I_ℓ^{est}, and impedance, z_ℓ, of branch ℓ:

$$\Delta V_\ell = \frac{|I_\ell^{\text{est}}| \cdot |z_\ell|}{V_\ell^{\text{nom}}}, \tag{2.2.21}$$

where I_ℓ^{est} is as in (2.2.13), and z_ℓ is calculated using per distance cable data and length, l_ℓ.

Both the downstream power, Figure 2.2.11a, and the voltage drop, Figure 2.2.11b, distributions are fit by a Generalized Pareto distribution:

$$f(x; k, \sigma, \theta) = \frac{1}{\sigma}\left(1 + k \cdot \frac{x - \theta}{\sigma}\right)^{-1-\frac{1}{k}}, \tag{2.2.22}$$

where, $x > \theta$, and $k > 0$. The KL-Divergence for both reported in Table A.1.

2.3 Radial Feeder Synthesis Algorithm

The statistical laws and limiting distributions from the previous section are put together to create the synthesis algorithm. Figure 2.3.1 provides an overview of the algorithm. The parts that follow mirror those in Section 2.2 and describe how the analysis is exploited in synthesis.

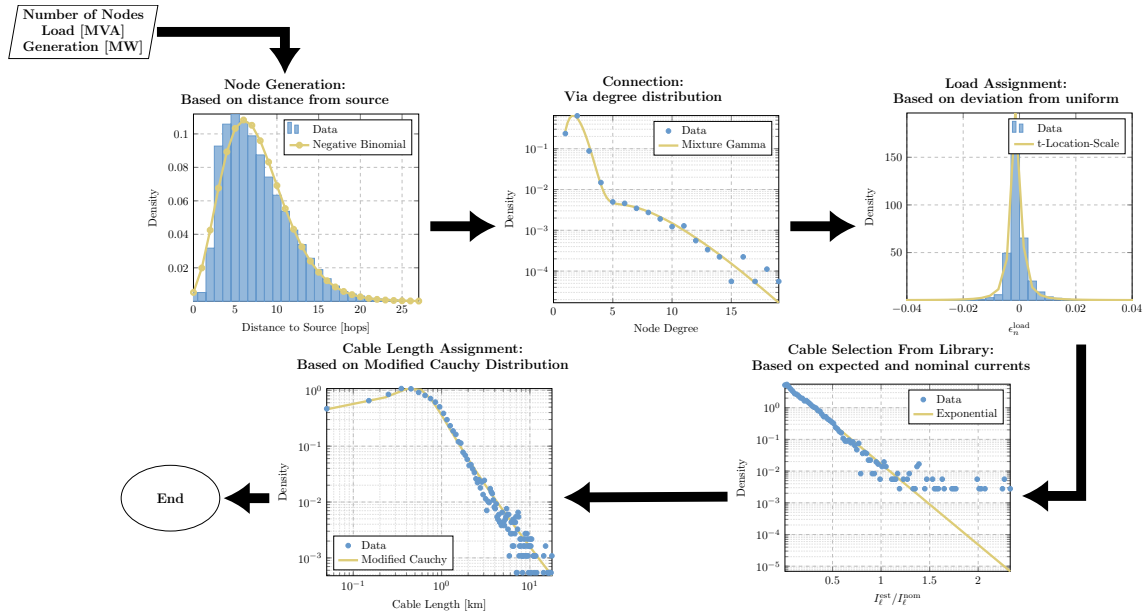

Figure 2.3.1: Radial Feeder Synthesis Algorithm Flowchart.

2.3.1 Node Generation

Algorithm 1 uses samples from (2.2.1) to assign a hop distance property to each node. In addition to the hop distance, a power factor is assigned to each node, from an empirical cdf given in Table 2.2, which greatly simplifies further manipulations, allowing to focus on real power.

The final step adjusting hop distances simply avoids gaps. It would be impossible, for example, to have a node, j with $h_j = 20$, without any node, i, with $h_i = 19$. The nodes are therefore shifted in until the hop distances are consecutive. An alternative approach could be to add extra nodes to fill the holes.

2.3.2 Connection via Degree Distribution

Once the nodes have been created, Algorithm 2 is used to connect them into a tree rooted at the root (MV bus) and by extension the source (HV bus). Due to the radial structure, nodes with maximum distance from the source must be leaves and therefore

Algorithm 1 Node Generation

procedure GENERATE NODES(Power Factor cdf, Negative Binomial distribution)
    The first node is by design the source at $h_1 = 0$
    The second node is by design the only node at $h_2 = 1$
    for $i = 3, 4, \ldots, |\mathscr{N}|$ **do**
        power factor$_i$ $\leftarrow$ power factor from input cdf
        $h_i \leftarrow$ sample from the Negative Binomial distribution
    end for
    Adjust hop distances so there are no gaps
end procedure

have degree one. Additionally, by design only the root, r, has $h_r = 1$, the degree of the source, b, with $h_b = 0$ must also be one. Finally, all nodes $\{i : h_i = 2\}$ and the source must connect to the root, so its degree is also deterministically known following the hop distance assignment. For the remaining nodes, a degree is assigned based on the bimodal Gamma. The distribution is clipped based on the hop distance of each node using function $g_{d_{\max}}(h_n)$, described in Section 2.2.6.1. In this way, excessive degrees further down the feeder are avoided.

Once each node has an assigned degree, $d_n^\star$, Algorithm 2 starts at the leaf nodes and works its way up towards the root. Each step adds an edge ℓ between nodes i and j such that $(f(\ell), t(\ell)) = (i, j)$, where node i is called the predecessor of node j. For each node j, predecessor i is picked from the viable set $\mathscr{P}_j = \{i : h_i = h_j - 1\}$, i.e. nodes one hop closer to the source. Predecessor, i, is chosen as the one with *actual* degree[6], d_i, furthest below its assigned degree $d_i^\star$:

$$f(\ell) \leftarrow \arg\min_{i \in \mathscr{P}} d_i - d_i^\star, \tag{2.3.1}$$

where $t(\ell) = j$.

[6]The number of edges already incident on node i.

Algorithm 2 Node Connection

procedure CONNECT NODES(Mixture Gamma, $g_{d_{\max}}(\cdot)$)
  for all $n \in \{n : (h_n = \max_{n \in \mathscr{N}} h_n) \cup (h_n = 0)\}$ **do** ▷ leaf nodes
    $d_n \leftarrow 1$
  end for
  $d_2 \leftarrow 1 + \sum_{n \in \mathscr{N}} \delta(h_n - 2)$ ▷ Degree of root node
  for all $n \in \mathscr{N}$ **do**
    if No degree assigned **then**
      repeat
        $d_{\text{tmp}} \leftarrow$ sample from the mixture Gamma distribution
      until $d_{\text{tmp}} \leq \lceil g_{d_{\max}}(h_n) \rceil$
      $d_n^\star \leftarrow d_{\text{tmp}}$ ▷ Assigned degree
    end if
  end for
  Sort nodes into ascending order in h, i.e., $h_i \leq h_j$ if $i < j$.
  for $j = |\mathscr{N}|, |\mathscr{N}| - 1, \ldots, 2$ **do** ▷ Moving from leaves towards source
    Connect node j to a viable predecessor, $i \in \mathscr{P}_j$ via (2.3.1)
  end for
end procedure

2.3.3 Node Properties

Intermediate and injection nodes are somewhat special due to their small number. For this reason they are handled first, after which, all the a remaining nodes are assigned positive load.

2.3.3.1 Intermediate Nodes

Intermediate nodes are marked first, so that load will not be assigned to them by the subsequent procedures. Algorithm 3 sets the number of zero load nodes, $N_{\text{intermediate}}$, by sampling a Beta distribution for the fraction of intermediate nodes.

Next, the HV source is designated as having zero load. For each of the remaining intermediate nodes, a sample is chosen from a mixture Poisson distribution, to determine at what hop distance the node should be.

Algorithm 3 Intermediate Node Assignment

procedure INTERMEDIATE(Intermediate Beta Distribution, Mixture Poisson Distribution)
    $N_{\text{intermediate}} \leftarrow \lfloor |\mathcal{N}| \cdot \epsilon \rfloor$, where $\epsilon \sim$ Beta distribution
    Mark source node as intermediate.
    for $i = 1, 2, \ldots, N_{\text{intermediate}} - 1$ **do**
        $\epsilon \leftarrow$ sample from mixture Poisson distribution
        Mark a node n with $h_n = \epsilon$ as intermediate.
    end for
end procedure

2.3.3.2 Power Injections

Since the algorithm only produces the sum total of load and generation at a node, several nodes are picked in Algorithm 4, based on observations from the data, to have a net negative load. The number of injection nodes, N_{inj}, is determined using a ratio sampled from a Beta distribution and the hop distance for each injection node is then selected by sampling a mixture Normal distribution. Finally, real power injection is assigned by solving (2.2.8) for $|p_n|$. Note that $p_{\text{inj,total}}$ is one of the algorithm inputs.

The Algorithm 4 module is an instance where the statistical distributions could potentially be modified to achieve progressively more "active" feeders. One simple way would be to vary the parameters of the Beta distribution, thus increasing the fraction of injection nodes.

Algorithm 4 Power Injection Node Assignment

procedure POWER INJECTION(Injection Beta Distribution, Mixture Normal Distribution, Normal Distribution)
  $N_{\text{inj}} \leftarrow \text{round}(|\mathscr{N}| \cdot \epsilon)$, where $\epsilon \sim$ Beta distribution
  for $i = 1, 2, \ldots, N_{\text{inj}}$ **do**
    $\epsilon \leftarrow$ sample from mixture Normal distribution
    Select one node, n, with $h_n = \lceil \epsilon \cdot \max_{n' \in \mathscr{N}} h_{n'} \rceil$
    repeat
      $\epsilon \leftarrow X \sim$ Normal
    until $1/N_{\text{inj}} + \epsilon > 0$
    $p_n \leftarrow -P_{\text{inj,total}} \left(1/N_{\text{inj}} + \epsilon\right)$
    $q_n \leftarrow p_n \cdot \tan\left[\cos^{-1}(\text{power factor}_n)\right]$
  end for
end procedure

2.3.3.3 Load

After both intermediate and injections have been selected, the remaining nodes are assigned load in Algorithm 5. All the procedure does is solve (2.2.9) for p_n, generating ϵ by sampling the t-Location-Scale distribution. Once again, note that P_{total} is derived from the total MVA algorithm input. Following all assignments, a normalization step scales powers to match the inputs.

Algorithm 5 Load Node Assignment

procedure POSITIVE LOAD(t-Location-Scale Distribution)
  for $n = 2, 3, \ldots, |\mathscr{N}|$ **do**
    if n is not an intermediate or an injection node **then**
      repeat
        $\epsilon \leftarrow X \sim$ t-Location-Scale
      until $1/|\mathscr{N}| + \epsilon > 0$
      $p_n \leftarrow P_{\text{total}} \left(1/|\mathscr{N}| + \epsilon\right)$
      $q_n \leftarrow p_n \cdot \tan\left[\cos^{-1}(\text{power factor}_n)\right]$
    end if
  end for
end procedure

2.3.4 Cable Selection

In a separate analysis, all nominal currents I_ℓ^{nom}, incident on a given node are considered. In roughly two-thirds of the cases, all are found to be the same. A library of conductors is supplied, selected from the data via a k-means clustering algorithm based on nominal current and r/x ratio. The library contains all the cable data, as well as the frequency of occurrence for each cable type and can be seen in Appendix A.2.

The key idea in Algorithm 6, is that I_ℓ^{nom} serves as an identifier of the cable. Once a desired I_ℓ^{nom} is calculated, the cable which most closely matches it out of the library is chosen.

The procedure performs three main functions. In two-thirds of the cases, a cable is assigned by picking the largest cable connected to the downstream node[7], in line with the finding that roughly two-thirds of nodes have only one type of cable incident upon them. In the rest of the cases, the Exponential distribution is used to sample a ratio, $I_\ell^{\text{est}}/I_\ell^{\text{nom}}$, and then solve for I_ℓ^{nom}. There are some implementation details regarding how parallel conductors are handled and how the cable type frequencies are used to weight the cable selection, but these are left out of the present discussion. Finally, branches with no current are given an I_ℓ^{nom} taken as the average over the incident branches on the upstream node, since the procedure using the ratio, $I_\ell^{\text{est}}/I_\ell^{\text{nom}}$, does not work in this case.

Note that Algorithm 6 does not explicitly show the threshold from Section 2.2.6.2 for clarity considerations. In implementation, however, if the threshold is exceeded, a new sample is drawn from the Exponential distribution. While the threshold is currently a scalar, it could be expanded to a step function if finer control is desired.

[7]Assuming there *is* a downstream node, i.e., for non-leaf nodes.

Algorithm 6 Cable Assignment

procedure CABLE TYPE(Cable Library, Exponential Distribution)
  Sort branches by h_ℓ, i.e. $h_\ell \leq h_{\ell'}$ if $\ell < \ell'$.
  for $\ell = |\mathscr{L}|, |\mathscr{L}| - 1, \ldots, 1$ **do** ▷ moves from the furthest branches towards source.
    if $I_\ell^{\text{est}} \neq 0$ **then**
      $r \leftarrow \mathcal{U}(0,1)$ ▷ Sample uniform distribution $\mathcal{U}(0,1)$
      if $r < 2/3$ and $I_{\ell'}^{\text{nom}}$ assigned to branches $\ell' \in f^{-1}(t(\ell))$ **then**
        $I_\ell^{\text{nom}} \leftarrow \max_{\ell' \in f^{-1}(t(\ell))} I_{\ell'}^{\text{nom}}$
      else
        $\hat{I}_{\text{nom}} \leftarrow I_\ell^{\text{est}}/\epsilon$, where $\epsilon \sim$ Exponential.
        $I_\ell^{\text{nom}} \leftarrow$ cable from library with closest I_{nom} to $\hat{I}_{\text{nom}}$, considering parallel cable options and expected frequencies of cable types in the feeder.
      end if
    end if
  end for
  for $\ell = 1, 2, \ldots, |\mathscr{L}|$ **do**
    if $I_\ell^{\text{est}} = 0$ **then**
      $\hat{I}_{\text{nom}} \leftarrow$ average of maximum and minimum $I_{\ell'}^{\text{nom}}$ attached to node $i = f(\ell)$.
      $I_\ell^{\text{nom}} \leftarrow$ cable from library with closest I_{nom} to $\hat{I}_{\text{nom}}$
    end if
  end for
end procedure

2.3.5 Conductor Length

Since cable types are assigned, and the cable library contains all the per distance parameters, all that remains is to assign length to each branch so that a total impedance could be calculated. Algorithm 7, thus simply assigns length by sampling from (2.2.16). Since this is a heavy tailed distribution, extreme values will inevitably occur. However, there is a physical limit to how long a particular branch can be, which is addressed by function (2.2.18). The modified Cauchy distribution is sampled for each cable ℓ, until the result falls below $g_{l_{\max}}(h_\ell)$.

Algorithm 7 Length Assignment

procedure CABLE LENGTH(Modified Cauchy Distribution, $g_{l_{\max}}(\cdot)$)
  for $\ell \in \mathscr{L}$ **do**
    repeat
      $\hat{l} \leftarrow$ Sample from Modified Cauchy Distribution.
    until $\hat{l} \leq g_{l_{\max}}(h_\ell)$
    $l_\ell \leftarrow \hat{l}$
  end for
end procedure

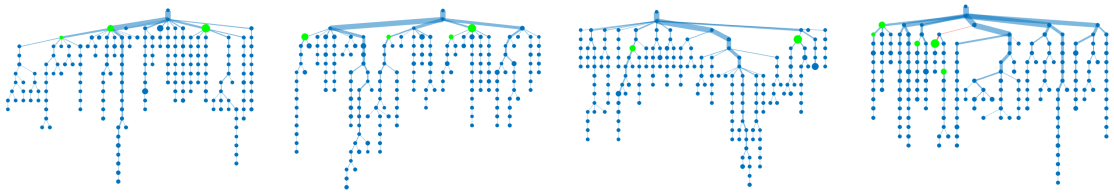

(a) (b) (c) (d)

Figure 2.4.1: Three samples generated with the following inputs: $|\mathscr{N}|$: 195, Load: 23 MVA, and Generation: 3 MVA. The width of each line represents the relative real power flow magnitude. Edges with reverse flow are marked in red. The size of each node represents the relative magnitude of real load/injection. Injection nodes are identified with green. The fourth feeder is a real feeder from the data set with the same $|\mathscr{N}|$, Load, and Generation. The real feeder is identified in Appendix A.3.

2.4 Feeder Generation Results

2.4.1 Individual Inspection

A visual test of the algorithm is done by using data from one of the real feeders to generate some samples. Figure 2.4.1 shows three generated samples as well as the real feeder from the dataset. As a fun exercise, the reader is encouraged to try and pick out the real feeder before inspecting the solution provided in Appendix A.3.

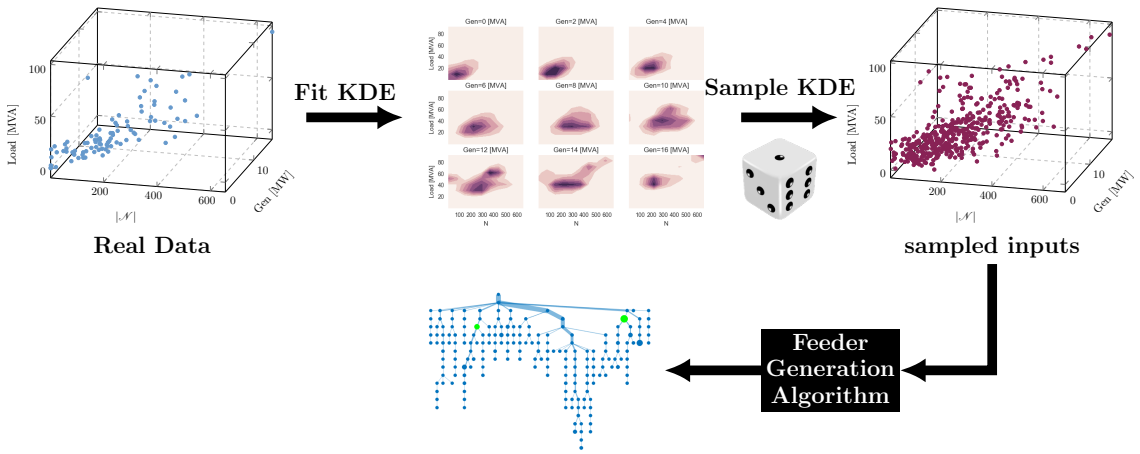

Figure 2.4.2: Procedure used to generate ensemble of synthetic samples.

2.4.2 Ensemble Testing

In addition to visual comparison of individual samples, 427 synthetic samples are generated to observe the cumulative statistics. Input parameters to the algorithm are drawn from a three dimensional Kernel Density Estimate (KDE) for the data vector ($|\mathscr{N}|$, Load, Generation). The input variables should therefore, be similar to the dataset. Figure 2.4.2 shows a flow chart for the process used to create the ensemble of synthetic feeders. The scatter plots and KDE slices shown in the figure are from the real data, and reveal that in fact the inputs are similarly distributed.

Using the cumulative dataset, the distributions identified in Section 2.2 can be evaluated. The distributions introduced in Section 2.2.7, which are not considered in the synthesis process, are also assessed to further evaluate the realism of the synthetic feeders' behavior. These are found to naturally emerge with the same trends observed in the data, further validating the algorithm's ability to synthesize realistic distribution system feeders. The emergence of statistical behavior for edge and node properties is, in fact, the main validation of the work.

Figure 2.4.3 shows the various distributions from the synthetic data along with

Table 2.3: KL-Divergences Results Comparison

Property	Distribution	Real Cumulative D_{KL}	Synthetic Samples
Hop Distance	Negative Binomial	0.0173	0.0101
No-Load			
Fraction	Beta	0.0014	0.0242
Hop Distance	Bimodal Poisson	0.0755	0.0233
Power Injection			
Fraction	Beta	0.0620	0.2968
Hop Distance	Bimodal Normal	0.1706	0.4240
Deviation From Uniform	Normal	0.0459	0.2031
Load Deviation From Uniform	tLocationScale	0.0008	0.1329
Degree Distribution	Bimodal Gamma	0.0211	0.0147
$I_\ell^{\text{est}}/I_\ell^{\text{nom}}$	Exponential	0.0098	0.0102
Cable Length	Modified Cauchy	0.0247	0.0108
Downstream Power	Generalized Pareto	0.0111	0.0243
Voltage Drop	Generalize Pareto	0.0917	0.0216

the original functions fit to the *real data*. Visual inspection suggests fairly good matches, including for the emergent downstream power, Figure 2.4.3f, and the voltage drop, Figure 2.4.3g, distributions. The KL-Divergence for each sample is reported in Table 2.3, where relatively low values further support a good match.

2.4.3 Overload Testing

Next, the effect of inputs on output statistics is considered. A second set of feeders is created from the same input data, except that the load is doubled. Two illuminating results are shown in Figure 2.4.4. Because the input vectors are further separated from

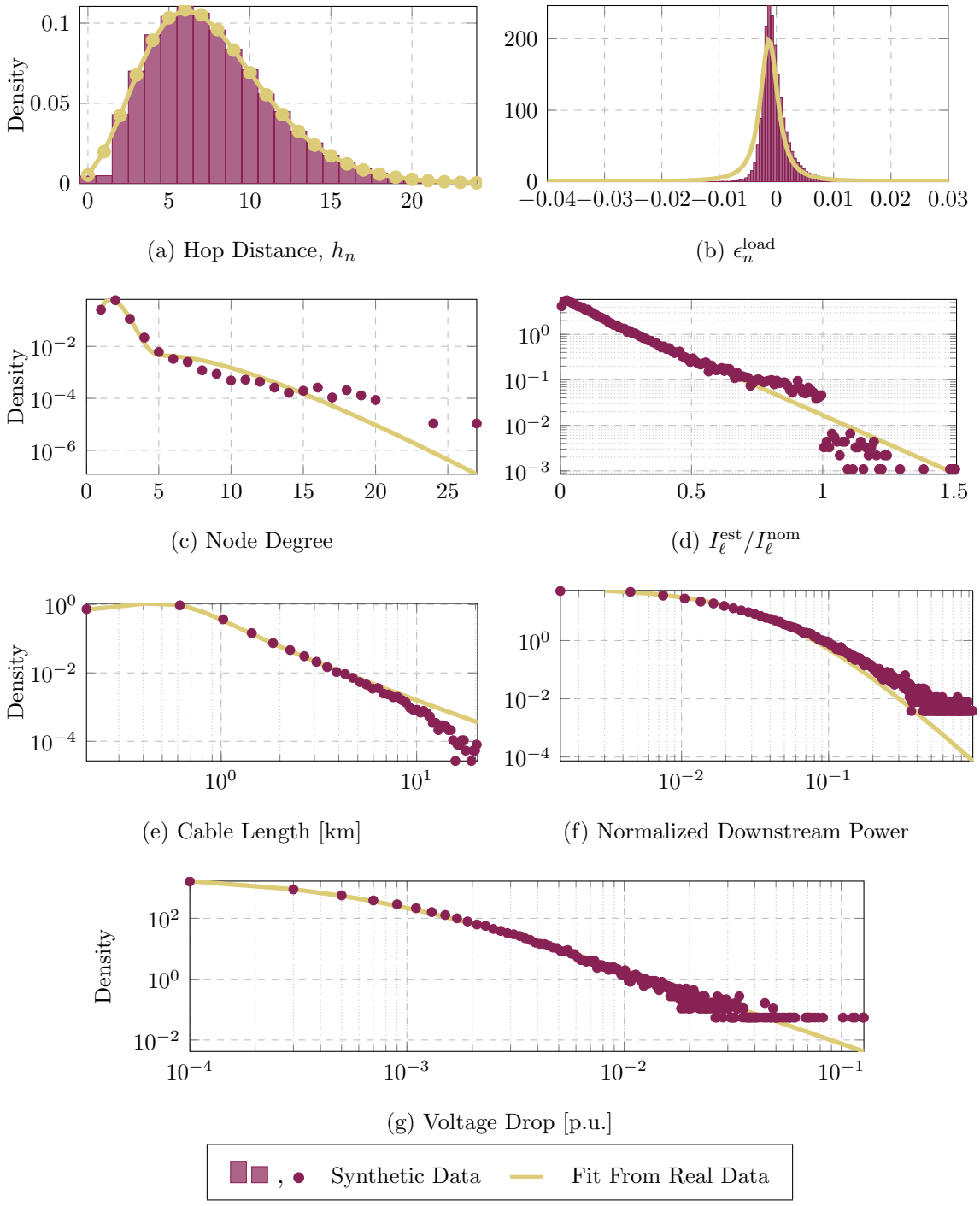

(a) Hop Distance, h_n

(b) ϵ_n^{load}

(c) Node Degree

(d) $I_\ell^{\text{est}}/I_\ell^{\text{nom}}$

(e) Cable Length [km]

(f) Normalized Downstream Power

(g) Voltage Drop [p.u.]

Figure 2.4.3: Results from the generated synthetic samples using procedure in Figure 2.4.2.

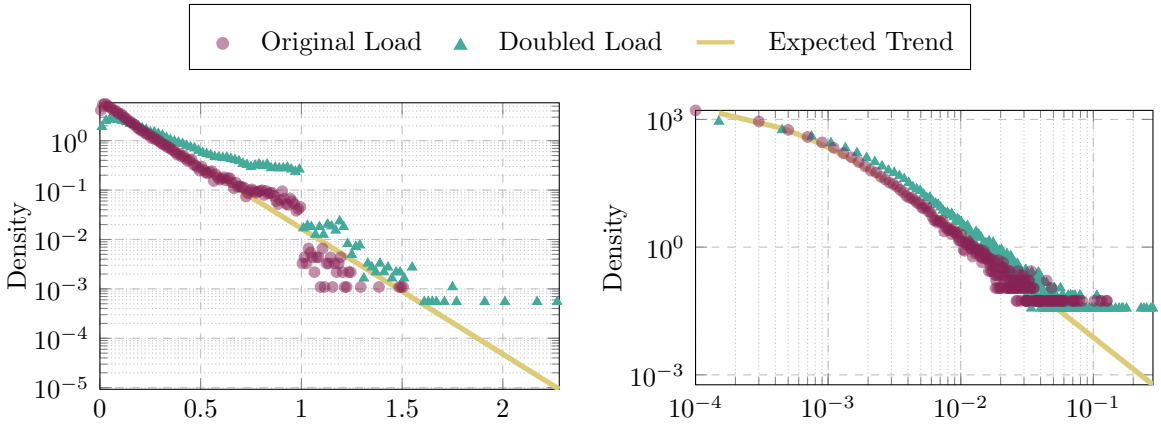

(a) $I_\ell^{\text{est}}/I_\ell^{\text{nom}}$ (b) Voltage Drop [p.u.]

Figure 2.4.4: As the input vectors to the algorithm are more distant from those seen in the dataset, certain properties begin to diverge from the expected trend. Numerically D_{KL} increases: 0.21 for $I_\ell^{\text{est}}/I_\ell^{\text{nom}}$ instead of 0.01 with the original inputs, and 0.13 instead of 0.02 for voltage drop.

the actual data, the ensemble contains a larger concentration of extreme cases. As a result, some emergent distributions diverge more strongly from their expected trend. If the load on a given feeder were to double, more heavily loaded conductors and larger voltage drops would be expected, exactly as seen in Figure 2.4.4, where the data lies further above the expected trend line than in Figure 2.4.3. Correspondingly, the KL-divergence between the empirical distribution and expected trends has increased by roughly an order of magnitude.

2.5 Combining Feeders

This section addresses the question of how the radial feeders created up to this point can be joined to form full distribution systems.

2.5.1 Feeder Allocation

Feeder allocation refers to assigning feeder groups to an HV source bus. Figure 2.5.1c shows that there are either 1, 2, or 3 feeders connected to a given source. This is consistent with [Short(2014), Table 1.2] that lists 2 as a common value of transformers per substation. Figure 2.5.1 also shows that the Rayleigh distribution is a reasonable fit at both the 1 and 2 feeder levels, to the total power delivered by the HV bus. The Rayleigh distributions is,

$$f(x;\mu,\sigma) = \frac{x-\mu}{\sigma^2} e^{-(x-\mu)^2/(2\sigma^2)} \tag{2.5.1}$$

where $\mu \in \mathbb{R}$ and $\sigma > 0$. Note that normally μ is not a parameter of the distribution and it is taken as 0.

Algorithm 8 describes how feeder allocation is done on a set of feeders $\mathcal{P}$. The size of the group, M, is drawn from the empirical distribution in Figure 2.5.1c. Then the desired power, C, is sampled from the corresponding Rayleigh distribution, where the parameters for $M = 1, 2$ are known (cf. Figure 2.5.1), and those for $M = 3$ are linearly extrapolated. The set of remaining feeders and inputs C, M are passed to the optimization problem in (2.5.2), which selects the optimal feeder group. The process is repeated until there are no feeders left unallocated. The optimization performed in Algorithm 8 simply tries to pick the combination of M feeders, with total load P_i, whose power consumption most closely matches C:

$$\underset{t,u}{\textbf{Minimize}} \quad t \tag{2.5.2a}$$

$$\textbf{Subject to} \quad \sum_i u_i = M \tag{2.5.2b}$$

$$t + \sum_i P_i u_i \geq C, \quad t - \sum_i P_i u_i \geq -C \tag{2.5.2c}$$

$$t \geq 0, \quad u_i \in \{0,1\}\ \forall i \in \mathcal{P} \tag{2.5.2d}$$

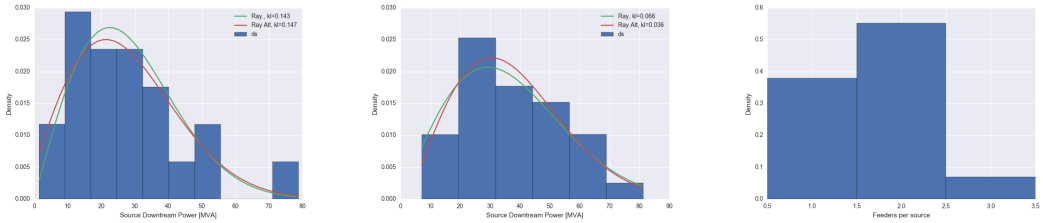

(a) Sources with 1 feeder (b) Sources with 2 feeder (c) Feeders Per Source

Figure 2.5.1: Grouping Statistics for Feeders.

Algorithm 8 Feeder Allocation

procedure FEEDER ALLOCATION($\mathcal{P}$)
  repeat
    $M \leftarrow \{1, 2, 3\}$ Sampled from empirical distribution
    $C \leftarrow \text{Rayleigh}(\mu_M, \sigma_M)$
    $g \leftarrow$ Group of M feeders from $\mathcal{P}$ as returned by optimization in (2.5.2)
    $\mathcal{P} \leftarrow \mathcal{P} \setminus g$
  until $\mathcal{P} = \emptyset$
end procedure

2.5.2 Adding Normally Open Branches

The task remaining for completing the system topology is to add Normally Open Branches (NOB). In doing so, the following quantities are considered:

1. H^{hop} hop distance assortativity: the two dimensional distribution of the hop distance for end nodes of NOBs. For example, there would be a +1 added to $H^{\text{hop}}_{5,5}$ for every NOB where both end nodes have a distance of 5 hops to the source node.

2. H^{deg} degree assortativity: the two dimensional distribution of the node degree for end nodes of NOBs. For example, there would be a +1 added to $H^{\text{deg}}_{1,1}$ for every NOB where both end nodes have node degree 1 *in their feeder*. It is important to note that the degree is now treated as a *fixed* number, i.e.,

attaching an NOB to a branch does not increase its degree.

3. H_f fraction of NOBs that are intra-feeder, i.e., both end nodes belong to the same feeder. That is $H_f = N_{\text{NOB intra-feeder}}/N_{\text{total NOB}}$.

4. H_s fraction of NOBs that share the same source. These can be nodes on the same feeder *or* nodes on feeders grouped by Algorithm 8.

5. H_{frac} average ratio of normally open to normally closed branches per feeder.

This problem greatly suffers from dimensionality, since it contains roughly $|\mathscr{N}|^2/2$ binary variables, where $|\mathscr{N}|$ is the total number of nodes in the system[8]. Considering the Netherlands dataset with $|\mathscr{N}| \approx 20 \times 10^3$, that is around 200 million binary variables. To combat the dimensionality, the problem is split into parts. First intra-feeder NOBs are added and then inter-feeder ones, where in the inter-feeder step only a small subset of "neighbor" feeders is considered.

2.5.2.1 Intra Feeder Normally Open Branches

For each feeder, the set of possible NOBs is constricted to connecting nodes that are not at hop 0 or 1, and whose upstream branch has the same nominal current. The nominal current requirement comes from observations in the data, as well as some basic engineering judgment. Open branches are there to allow for reconfiguration, therefore, they are likely to handle load similar to the edges they are incident upon.

The optimal selection from set u of all possible NOBs, is made based on optimization problem (2.5.4). If entry $u_{i,j} = 1$ then an NOB exists between nodes i and j. Note that u is symmetric, and therefore only the upper triangular part is considered.

[8]The exact number is $|\mathscr{N}|\,(|\mathscr{N}|-1)/2 - (|\mathscr{N}|-1)$, for the total number of edges in a complete graph minus the closed branches in the tree.

The fraction of desired intra-feeder edges to closed branches is $H_{\text{frac}} \times H_f$. Therefore, the number of NOBs to add, N_f, for a given feeder with $|\mathscr{L}|$ closed edges is,

$$N_f = |\mathscr{L}| \times H_{\text{frac}} \times H_f. \tag{2.5.3}$$

The optimization in (2.5.4) attempts to match the hop and degree distributions on an entry by entry basis through constraints (2.5.5c) and (2.5.4d), while getting as close to the desired number of NOBs through constraint (2.5.4e). Constraint (2.5.4b) only allows one NOB edge to be incident on any given node. Finally, weights are available in vector w to allow more or less influence to the different requirements. The complete formulation is:

$$\underset{t,u}{\textbf{Minimize}} \quad w^T t \tag{2.5.4a}$$

$$\textbf{Subect to} \quad \sum_j u_{i,j} \leq 1 \qquad \forall i \tag{2.5.4b}$$

$$t_{\text{hop}} + \frac{1}{N_f} \sum_{\substack{h_{i'}=i \\ h_{j'}=j}} u_{i',j'} \geq H^{\text{hop}}_{i,j},\ t_{\text{hop}} - \frac{1}{N_f} \sum_{\substack{h_{i'}=i \\ h_{j'}=j}} u_{i',j'} \geq -H^{\text{hop}}_{i,j} \quad \forall i,j \tag{2.5.4c}$$

$$t_{\text{deg}} + \frac{1}{N_f} \sum_{\substack{d_{i'}=i \\ d_{j'}=j}} u_{i',j'} \geq H^{\text{deg}}_{i,j},\ t_{\text{deg}} - \frac{1}{N_f} \sum_{\substack{d_{i'}=i \\ d_{j'}=j}} u_{i',j'} \geq -H^{\text{deg}}_{i,j} \quad \forall i,j \tag{2.5.4d}$$

$$t_N + \sum u \geq N_f,\ t_N - \sum u \geq -N_f \tag{2.5.4e}$$

$$t_{\text{hop}}, t_{\text{deg}}, t_N \geq 0, \quad u_{i,j} \in \{0,1\}\ \forall i,j \tag{2.5.4f}$$

where $t = [t_{\text{hop}}\ t_{\text{deg}}\ t_N]^T$.

2.5.2.2 Inter Feeder Normally Open Branches

To complete the NOB assignment, branches are added between feeders. For a given feeder with $|\mathscr{L}|$ closed branches and the previously defined quantities, the following values can be calculated:

$N_{\text{tot}} = \lvert\mathscr{L}\rvert \times H_{\text{frac}}$	Total number of desired NOBs
$N_s = H_s \times N_{\text{tot}}$	Number of NOBs with the same source
$N_f = H_f \times N_{\text{tot}}$	Number of NOBs on the same feeder
$N_{\text{same}} = N_s - N_f$	Number of NOBs with same source but different feeder
$N_{\text{diff}} = N_{\text{tot}} - N_s$	Number of NOBs with different sources
$N_+ = N_{\text{same}} + N_{\text{diff}}$	Number of new NOBs to add

For the inter-feeder problem the potential edges that qualify need to have *exactly one* node in the feeder under consideration, the hop distance must be greater than one, and the upstream nominal current must be the same for both end nodes, much like in the intra-feeder problem. Additionally, only feeders that are $\pm D_{\max}$ are considered, which refers to the difference between id numbers assigned to the feeders. The value $D_{\max} = 4$ is chosen, which means that if feeder 10 is considered, the only nodes in the feasible set are on feeders 6 through 14. Feeder distance is calculated with a modulus so that the highest numbered feeder is considered one away from feeder 0. The sets of edges connecting a given feeder to feeders that are distance n away is denoted with η_n . For example, the NOB connecting node i on feeder 4 and node j on feeder 6 is in set η_2: $(i, j) \in \eta_2$, indicating that it connects two feeders a distance of 2 apart.

Optimization problem (2.5.5) selects the NOBs out of set u to connect feeders to one another. Constraints (2.5.5c), (2.5.5d), and (2.5.5b) work exactly the same way in this optimization problem as in the inter-feeder one. Constraints (2.5.5e) and (2.5.5f) do the same thing as (2.5.4e) except that the summation is partitioned in two. Function $b(n)$ returns the source node for node n. Finally, the sum of added NOBs to feeders at different distances is added to objective along with weights c, allowing some control on how these connections are handled. The complete formulation is,

$$\underset{t,u}{\textbf{Minimize}} \quad w^T t + \sum_{n=1}^{D_{\max}} \left(c_n \sum_{(i,j)\in\eta_n} u_{i,j} \right) \tag{2.5.5a}$$

$$\textbf{Subect to} \quad \sum_j u_{i,j} \leq 1 \qquad \forall i \tag{2.5.5b}$$

$$t_{\text{hop}} + \frac{1}{N_+} \sum_{\substack{h_{i'}=i \\ h_{j'}=j}} u_{i',j'} \geq H^{\text{hop}}_{i,j},\ t_{\text{hop}} - \frac{1}{N_+} \sum_{\substack{h_{i'}=i \\ h_{j'}=j}} u_{i',j'} \geq -H^{\text{hop}}_{i,j} \qquad \forall i,j \tag{2.5.5c}$$

$$t_{\text{deg}} + \frac{1}{N_+} \sum_{\substack{d_{i'}=i \\ d_{j'}=j}} u_{i',j'} \geq H^{\text{deg}}_{i,j},\ t_{\text{deg}} - \frac{1}{N_+} \sum_{\substack{d_{i'}=i \\ d_{j'}=j}} u_{i',j'} \geq -H^{\text{deg}}_{i,j} \qquad \forall i,j \tag{2.5.5d}$$

$$t_{\text{same}} + \sum_{b(i)=b(j)} u_{i,j} \geq N_{\text{same}},\ t_{\text{same}} - \sum_{b(i)=b(j)} u_{i,j} \geq -N_{\text{same}} \tag{2.5.5e}$$

$$t_{\text{diff}} + \sum_{b(i)\neq b(j)} u_{i,j} \geq N_{\text{diff}},\ t_{\text{diff}} - \sum_{b(i)\neq b(j)} u_{i,j} \geq -N_{\text{diff}} \tag{2.5.5f}$$

$$t_{\text{hop}}, t_{\text{deg}}, t_{\text{same}}, t_{\text{diff}} \geq 0, \quad u_{i,j} \in \{0,1\}\ \forall i,j \tag{2.5.5g}$$

where $t = [t_{\text{hop}}\ t_{\text{deg}}\ t_{\text{same}}\ t_{\text{diff}}]^T$.

2.5.3 Results

The above procedures were applied to the feeders generated in Section 2.4. Table 2.4 shows a comparison of the input data described in Section 2.5.2 for the real data and the resulting synthetic system. The results demonstrate that from the perspective of these metrics a valid, large scale, distribution system is created.

2.6 Related Publications

The radial feeder algorithm was published in [Schweitzer *et al.*(2017a)]. An implementation, called `synfeeder`, is freely accessible on GitHub at: `https://github.com/eranschweitzer/synfeeder`, where a conversion function to the MATPOWER format is also available. An earlier incarnation focusing on topology was published

in [Schweitzer *et al.*(2015)], but is mainly related in that statistics from the Netherlands system were used, as the actual algorithm differs greatly. The work on combining feeders was published in an internal technical report for the Flexible Elektrische Netze Consortium [Schweitzer and Monti(2017)].

Table 2.4: Real vs. Synthetic Statistics for Connecting Feeders

Feature	**Real**	**Synthetic**
H_f	77%	77%
H_s	84%	83%
Average H_{frac}	10%	15%
NOB node degree assortativity	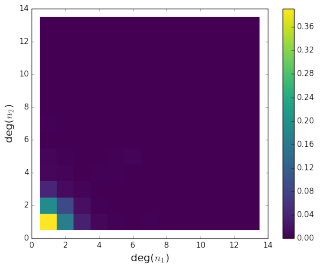	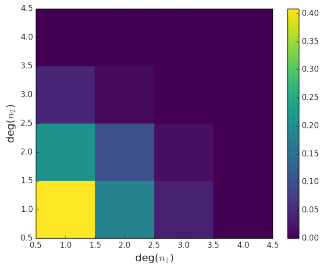
NOB hop assortativity	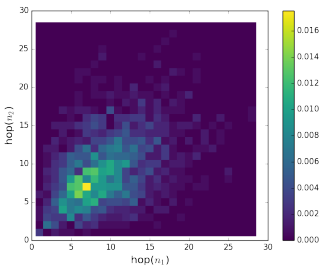	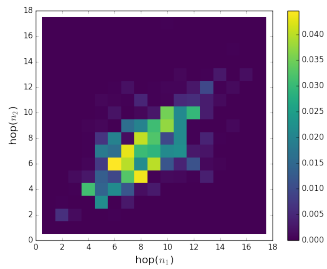

CHAPTER 3

TRANSMISSION CASES

Where the previous chapter considered radial distribution systems, attention is turned in this chapter to meshed transmission systems. Analysis is first presented in Section 3.1, that demonstrates the origin of a few properties, used to assess realism. The difference between operational and topological tests is stressed. Section 3.2 shows an example of how topological features can influence operational ones, and thus helps justify the selection of validation tests from Section 3.1.

The focus of the remaining sections is the automated generation of transmission cases by placing load, generation, and conductor properties on a topology. Sections 3.3 and 3.4 describe the basic problem formulation as a Mixed Integer Linear Program (MILP) and some tools used decompose the problem and make it more solvable. Section 3.5 provides results, which also highlight further modeling challenges. These are tackled in Section 3.6, which is a completely non-MILP solution to the original problem posed in Section 3.3.

3.1 Analysis

An important element of creating synthetic cases, is determining ways in which to validate them. As a first step, real data must be analyzed to extract various rules and relationships that can then be tested for in the synthetic data. The data analyzed in this section and the next comes mainly from The Federal Energy Regulatory Commission (FERC) through a freedom of information request, and comprises the three U.S. interconnects: the Eastern Interconnect (EI), the Western Electricity Coordinating Council (WECC), and the Electric Reliability Council of Texas (ERCOT). Additional data, used mainly in sections 3.3 and beyond comes from publicly available cases in

the MATPOWER software [Zimmerman *et al.*(2011)].

There is an endless number of possible metrics to consider in the analysis of power system cases. Many of the metrics developed for the ARPA-E Grid Data project [ARPA-E Grid Data(2017)], of which this work is a part, are published in [Birchfield *et al.*(2017a)]. Two new features, not often considered, are discussed in the following. Additionally, a new divergence measure, the Hellinger distance [Hellinger(1909)],

$$D_H(p||q) = \sqrt{1 - \int_{-\infty}^{\infty} \sqrt{p(x)q(x)}\, \mathrm{d}x}, \tag{3.1.1}$$

is used to assess similarity between distributions, along with the KL-distance introduced in Section 2.1.3. The Helligner distance is shown in [Comaniciu *et al.*(2003)] to obey the triangle inequality, which is an attractive property. Another benefit of using the Hellinger distance, is that it relates to the total variation distance, $\delta(p, q)$ as:

$$D_H^2(p, q) \leq \delta(p, q) \leq \sqrt{2} D_H(p, q). \tag{3.1.2}$$

Therefore, the Hellinger distance provides a bound on how far the two distributions could differ from each other at any given point. For all $D_H(p, q) < 1/\sqrt{2}$ this gives a non-trivial upper bound on the most extreme error between an estimate q and the empirical distribution p.

3.1.1 Traditional Topological Studies

There have been many studies into the topology of the electric grid. These tend to focus on three topological metrics: the node degree distribution, average path length, and the clustering coefficient. The degree distribution is generally distinguished by its tail. Small-world models as in [Watts and Strogatz(1998)], exhibit exponential tails, while the preferential attachment model in [Barabási and Albert(1999)] has power-law tails.

Exponential tail are also found in Erdős Rényi (ER) random graphs [Erdős and Rényi(1959)], with average path length similar to power systems. However, the clustering coefficient[1] is greater in power systems compared to ER graphs [Wang *et al.*(2010a)]. The relationship between the clustering coefficient and triangles, which are the smallest possible cycle, is the motivation behind the following study of the cycle distribution.

3.1.2 Cycle Distribution

Cycles offer a way to describe the meshed structure of the system. They also relate directly to classic circuit mesh analysis. In fact, Kirchhoff's work [Kirchhoff(1847)] used fundamental cycle bases for the application of his famous voltage law. Cycle bases are however, non-unique, so to obtain a better level of consistency, minimum cycle bases are used in the following analysis, which are calculated using the algorithm in [Berger *et al.*(2004)].

A minimum cycle basis is one where the sum of the weights of all cycles is minimum. When unit weight is assigned to each edge, this translates to meaning that it is the collection of the smallest cycles that form a basis for the graph. While this collection is also non-unique, its distribution is. A cycle distribution is a count of how many cycles of each size form the basis of the graph. For the distribution to change, the count between different cycle sizes must change, which means that some cycle is broken into smaller constituent parts. This, however, contradicts the definition of a minimum cycle distribution, and explains why the distribution is unique even if the

[1]The clustering coefficient has two different but very similar definitions. In one form [Newman(2003), pp. 183–184] it gives the probability that a path of length 2 will form a triangle. In the other, popularized by [Watts and Strogatz(1998)] a local ratio of neighbors who are themselves connected is calculated, and then averaged over the whole network.

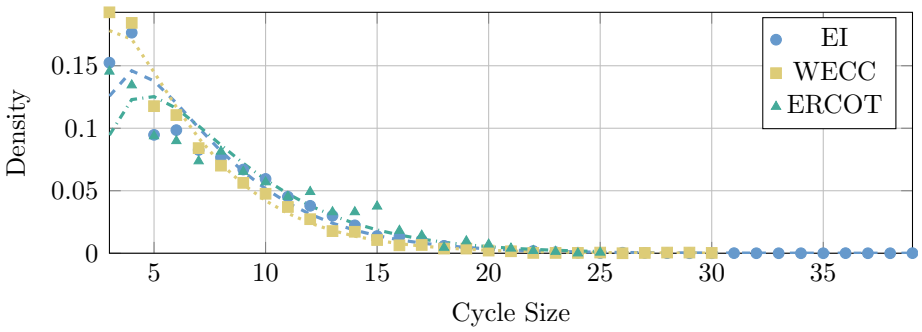

Figure 3.1.1: Minimum cycle distributions for topology graphs. The corresponding Negative Binomial fit is shown in a line with matching color.

Table 3.1: Negative Binomial Fit Parameters and Divergence Measures to Cycle Distribution

	p	n	D_{KL}	D_H
EI	0.27	1.60	0.02	0.08
WECC	0.27	1.32	0.01	0.05
ERCOT	0.26	1.76	0.04	0.11

cycles making it up can be selected in different ways.

The distribution of minimum cycles is found to fit the Negative Binomial distribution (2.2.1) nicely, as seen in Figure 3.1.1. Note that letting $\tilde{x}$ denote cycle size, (2.2.1) is evaluated at $x = \tilde{x} - 3$, i.e, cycles with three edges map to the integer zero, since no cycles are smaller than 3, yet the Negative Binomial distribution domain starts at zero. Table 3.1 shows that the Negative Binomial parameters are tightly clustered for the three interconnect cases.

3.1.3 Surge Impedance Loading

While topological tests can indicate potential structural issues with synthetic samples, operational criteria are of most interest for researchers who will be using synthetic cases. In an attempt to link system structure to its operation in terms of power

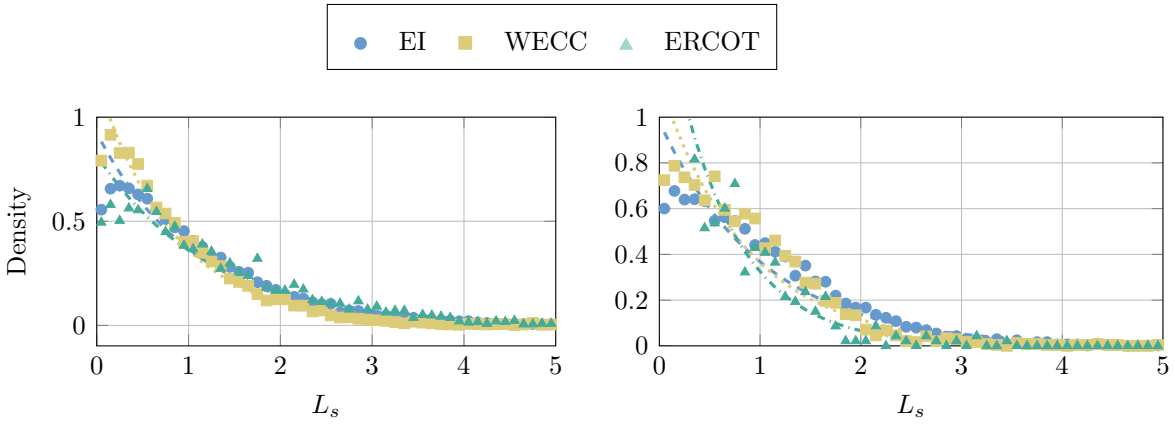

(a) $80 < v_{\text{nom}} < 200\text{kV}$ (b) $200 < v_{\text{nom}} < 400\text{kV}$

Figure 3.1.2: Fraction of SIL loading, L_s, distributions for two voltage ranges. Exponential fit lines are plotted with corresponding colors.

flow, line loading is considered as a fraction of its Surge Impedance Loading (SIL). SIL represents an impedance matched termination for a lossless line, in the sense that there is no voltage drop when the line delivers its SIL [Glover *et al.*(2012)]. Defining the ratio between actual loading and SIL as,

$$L_s = \frac{\text{Actual MVA flow}}{\text{SIL MVA rating}}, \tag{3.1.3}$$

L_s is used to evaluate system loading. Figure 3.1.2 shows, for two different voltage ranges, that L_s roughly follows an exponential distribution (2.2.14). Values for parameter μ and divergences are given in Table 3.2.

It is worth noting that $\mu \approx 1$ has some physical intuition, suggesting that lines are *on average* loaded at their SIL rating. Since at SIL, the voltage profile is flat and power systems operation attempt to maintain voltages close to 1 p.u., an average SIL around one is quite logical.

Table 3.2: Exponential Fit to L_s

	$80 < v_{nom} < 200$kV			$200 < v_{nom} < 400$kV		
Case	μ	D_{KL}	D_H	μ	D_{KL}	D_H
EI	1.08	0.02	0.08	1.04	0.04	0.11
WECC	0.85	0.02	0.07	0.88	0.06	0.13
ERCOT	1.23	0.04	0.11	0.63	0.05	0.13

3.2 Modifying cases

A natural question when dealing with validation is: what impact does property x have? In other words, to justify why a particular property is used for validation, it is helpful to at least provide some intuition as to its effect. To that end, the relationship between the cycle and L_s distributions is investigated in this section. The ACTIVSg2000 case [Birchfield *et al.*(2017b)] is used, since in its original form it showed both a different cycle distribution, as well as a somewhat different L_s. A comparison is made to the EROCT interconnect since the two cases roughly cover the same geographic footprint.

3.2.1 Modifying Cycles

Considering that cycles imply parallel paths, an intuitive reasoning based on Kirchhoff's Current Law (KCL) suggests a relationship between the cycle basis of the power system graph and the resulting loading distribution. To test this hypothesis, the ACTIVSg2000 case is rewired to target a cycle distribution more similar to the ERCOT system. A simple greedy approach to achieve this is outlined in Figure 3.2.1.

Using the fit parameters in Table 3.1, Equation (2.2.1), and the total number of

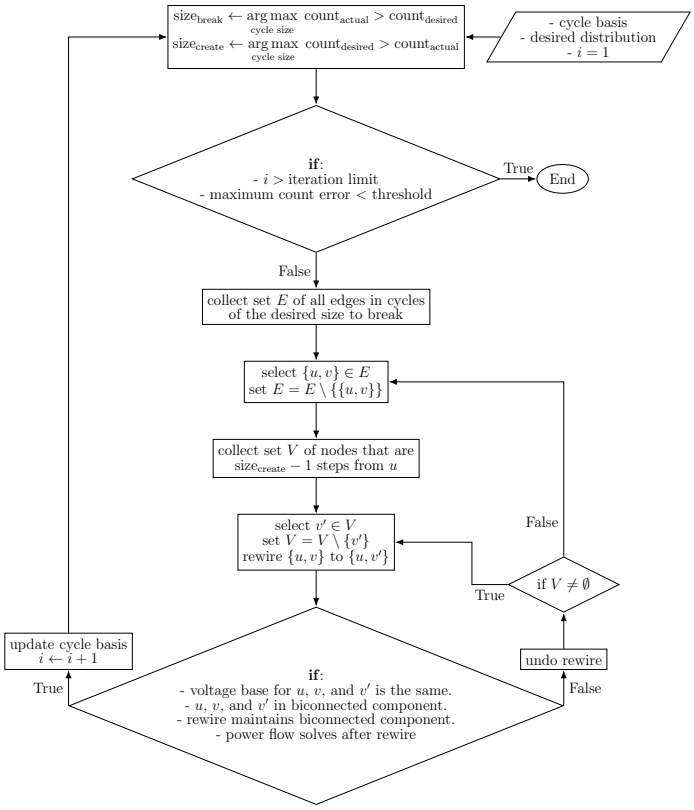

Figure 3.2.1: Flowchart describing how cases are rewired to target a specific cycle distribution

cycles[2], the desired number of cycles at any size can be calculated. The procedure in Figure 3.2.1 selects the cycle size that is most *over represented* in the current cycle basis as the type of cycle to break ($\text{size}_{\text{break}}$), while the most *under represented* cycle is the one to target ($\text{size}_{\text{create}}$). Edges participating in cycles of the appropriate size to break are collected in a set E, and one by one, new neighbors are sought, until one is found which fulfills the following requirements:

- The voltage basis of the new neighbors is the same (as it does not make sense to rewire transformers).
- System biconnectivity is unaltered.

[2]The total number of cycles does not change since by Euler's equation it is $|\mathscr{L}| - |\mathscr{N}| + 1$ where $|\mathscr{L}|$ is the number of edges, $|\mathscr{N}|$ the number of nodes, and 1 is the number of connected components.

- A power flow solution exists.

Since the calculation of a minimum cycle basis is rather expensive, an update algorithm is used, which is a modification of [Horton(1987)], in the main loop of Figure 3.2.1. At the end of the procedure the full cycle distribution is calculated again to catch any possible errors caused during successive updates[3].

Figure 3.2.2 shows the minimum cycle distribution of the original and modified ACTIVSg2000 cases, as well as the original ERCOT case for reference. It is visually clear, that the desired change is achieved. Numerically, the change is evaluated by considering the KL-divergence between the empirical distribution and the desired Negative Binomial distribution parametrized by the ERCOT values in Table 3.1. The empirical distribution simply refers to the histogram of the data, which could have bins with no associated weight. This differs from the chosen Negative Binomial *model*, which will map any value in its domain to an associated weight, irrespective of the underlying data used to initially fit the model. For example, there might not be cycles of size 52 in the dataset, but (2.2.1) can certainly be evaluated at $x = 52 - 3$. The following notation is used:

- p_i refers to the *empirical* cycle distribution for case i. Whether the original or modified case is intended is indicated either with a superscript or elsewhere.
- q_i refers to the Negative Binomial distribution with parameters for case i. For ERCOT the parameters are given in Tabe 3.1. For ACTIVSg2000 they are $p = 0.73$ and $n = 12.66$.

Using this convention, the change in KL-divergence values is tabulated in Table 3.3. The numbers strongly support the visual from Figure 3.2.2 that the cycle distribution

[3]It is experimentally found that the update does not perform perfectly. However, the error, on the order of 0.1%, is minimal.

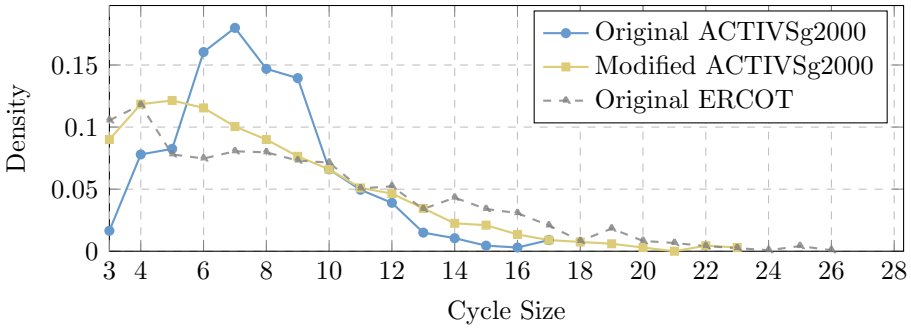

Figure 3.2.2: Cycle distribution for the ACTIVSg2000 case before and after modification. The targeted ERCOT case is also shown for reference.

Table 3.3: KL-Divergence of ACTIVSg2000 Cycle Distribution

	original case	modified case
$D_{KL}(p_{\text{ACTIVSg2000}} \mid q_{\text{ERCOT}})$	0.2050	0.0157
$D_{KL}(p_{\text{ACTIVSg2000}} \mid q_{\text{ACTIVSg2000}})$	0.0240	0.2316

for the modified ACTIVSg2000 case closely matches that of the original ERCOT case, and furthermore, no longer matches the original ACTIVSg2000 case.

3.2.2 Effects On Operations

Having established the desired structural change, attention is turned to how system loading is (or is not) impacted. A simple Unit Commitment (UC) determines an economically optimal dispatch for both the original and modified cases, followed by an AC OPF solved using MATPOWER [Zimmerman *et al.*(2011)], which also accounts for losses, voltage deviations, etc., that are not captured by the DC model used for UC. Line limits are neglected in the OPF since they are not considered during topology manipulation, and could therefore introduce infeasibility that is merely an artifact of the modification algorithm. As all cases are handled in the same manner, the comparison is still fair and considers two identical cases but for a topological

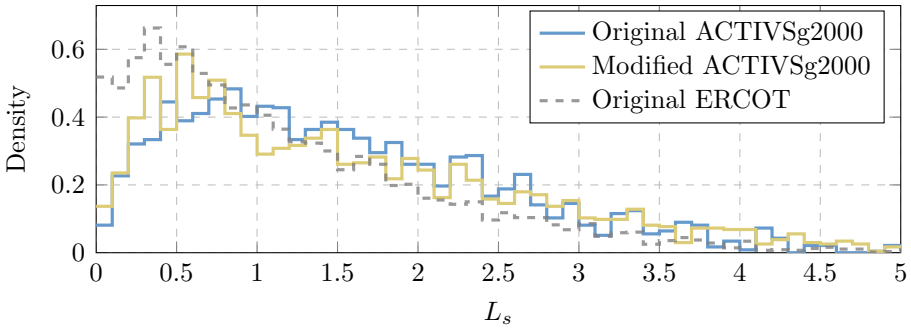

Figure 3.2.3: Distribution of L_s for ACTIVSg2000 case before and after modification. The ERCOT case is also shown for reference.

manipulation. Once the operating point for both cases is established, statistics can be compared.

Figure 3.2.3 shows the distribution of L_s for the original and modified ACTIVSg2000 cases. One can see that the peak of the distribution shifts in a desirable direction, where desirable means more similar to the ERCOT case, although the change is admittedly not very significant. Table 3.4, however, provide further evidence to the changes. First, losses increase following the modification, which agrees with the simultaneously observed increase in average L_s. That loading in the system increase is further supported by a slight increase in the average $\Delta\theta$ between adjacent buses, suggesting higher real power flows. Furthermore, it is noteworthy that L_s behaves more like an Exponential distribution, which is seen by the decrease in the KL-divergence between L_s and the Exponential distribution parametrized by the Maximum Likelihood Estimator, which in the case of Exponential is simply the mean value, μ_{L_s}.

The change also manifests itself in the cost to operate the system, which increases slightly. In this particular case, further insight is possible since generator commitment happens to be unaffected by the modification. Letting $\bar{p}$ be the average of all the Locational Marginal Prices (LMPs), C and l total cost and losses respectively, and

Table 3.4: ACTIVSg2000 Operational Values

Quantity	Original	Modified Case
Cost [$]	1,220,002.12	1,222,871.83
Average LMP [$/MW]	19.62	19.70
Losses [MW]	1389.19	1539.84
Average L_s	1.5498	1.6050
Average $\Delta\theta$ [degree]	1.50	1.63
$D_{KL}(L_s \vert \text{Exp}(\mu_{L_s}))$	0.1625	0.0979

using subscripts 0 and m for original and modified cases,

$$(C_m - C_0) - \bar{p}(l_m - l_0) = -\$97.46. \tag{3.2.1}$$

In words: the cost difference between the two scenarios is largely attributed to losses.

3.2.3 Interpretation

Each of the changes demonstrated is on its own rather small. However, the accumulation of all of these effects strongly suggest that altering the cycle distribution did in fact change the operational behavior of the power system. Furthermore, this change largely agrees with the initial hypothesis. The basic intuition that cycles imply parallel current paths, suggests that a higher density of larger cycles means more parallel paths, and therefore, reduces loading on any individual branch. Decreases in losses, L_s, $\Delta\theta$, and cost, all support this hypothesis. Finally, as the cycle distribution changed, the loading distribution, measured by L_s, also shifted. The results presented are one rewiring example. Out of 25 additional runs, only two show a different behavior in terms of cost, one in terms of losses (coinciding with one of the two cost cases), and none showed a different trend in terms of average L_s.

While the direction of change is clear, its magnitude is fairly small. This test shows

Table 3.5: KL-Divergence of ERCOT Cycle Distribution

	original case	modified case
$D_{KL}(p_{\text{ERCOT}}\|q_{\text{ACTIVSg2000}})$	0.5243	0.4224
$D_{KL}(p_{\text{ERCOT}}\|q_{\text{ERCOT}})$	0.0584	0.0891

that the cycle distribution impacts the loading distribution, however, it is clearly one of many marginal effects. In other words, it affects but does not *determine*. The implication is that a correct cycle distribution is not *sufficient* for correct operation statistics. Since only a marginal effect is considered, rather than the full joint distribution of all variables, a definitive claim of necessity is problematic to make. The impact, however, is clear and therefore, if this feature is not matched others may have to be adversely manipulated to achieve desirable operational behaviors.

3.2.4 A Reverse Experiment

In an effort to further strengthen the argument, another test is performed where the ERCOT case is modified targeting the original ACTIVSg2000 case's cycle distribution. The results of the cycle modification are shown in Figure 3.2.4. While the mode appears to visually move in the "right" direction, closer numerical evaluation show this is far less successful a modification than Sections 3.2.1 and 3.2.2. Table 3.5 shows the KL-divergence for the original and modified cases similar to Table 3.3. While the modified ERCOT case is *more* similar to the original ACTIVSg2000 case it is still quite different. At the same time, the modified case remains closer, at least in the KL-divergence sense, to the original ERCOT case than to the original ACTIVSg2000 case.

With the caveat that the structural change is less successful, a similar and opposite trend is still seen in the operational statistics. Table 3.6 shows that as the cycle

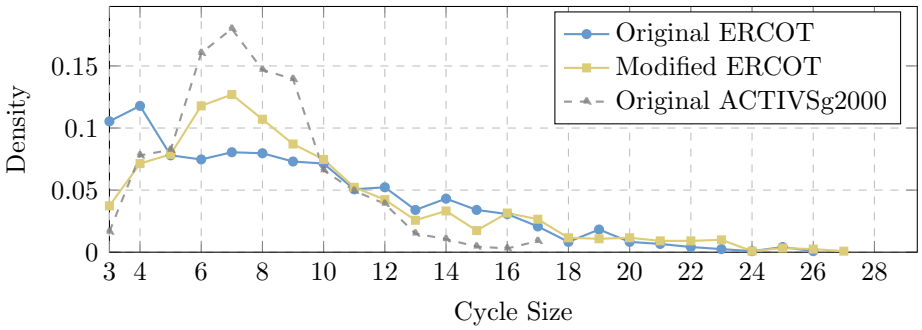

Figure 3.2.4: Cycle distribution for the ERCOT case before and after modification. The targeted original ACTIVSg2000 case is also shown for reference.

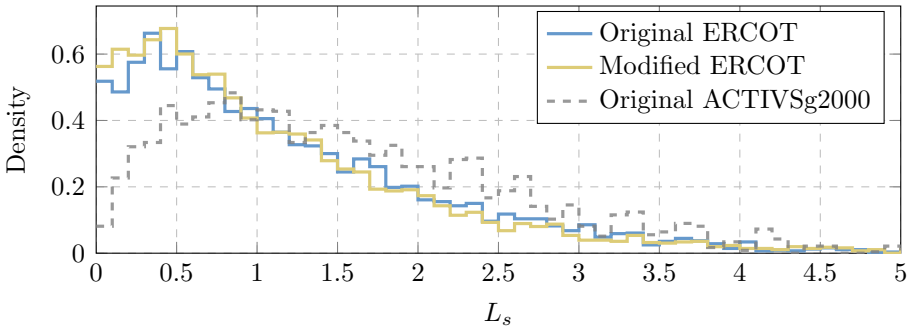

Figure 3.2.5: Distribution of L_s for the ERCOT case before and after modification. The original ACTIVSg2000 case is also shown for reference.

Table 3.6: ERCOT Operational Values

Quantity	Original	Modified Case
Cost [$]	1,740,845.88	1,739,953.28
Average LMP [$/MW]	20.15	20.12
Losses [MW]	1570.72	1412.80
Average L_s	1.2065	1.1422
Average $\Delta\theta$ [degree]	2.42	2.41
$D_{KL}(L_s \vert \text{Exp}(\mu_{L_s}))$	0.0358	0.0278

distribution is pushed towards something more like the original ACTIVSg2000 case losses *decrease*, as does average L_s, and $\Delta\theta$. These changes similarly translate to a *decrease* in the total cost, however, in this case the UC is altered and therefore, it is no longer possible to attribute the change in cost directly to the losses. Since the structural change is much smaller as previously discussed, the observed changes are also smaller compared to those in Section 3.2.2. Still, the fact that the changes are consistent with those in Section 3.2.2 further supports the hypothesis that structural cycles impact the loading distribution in the system.

3.2.5 Results from Modified Algorithm

Following the observations discussed above, a tweak was made to the ACTIVS algorithm [Birchfield *et al.*(2017b)] to address the cycles issue. A second 2000 bus case on the ERCOT footprint was created, referred to here as `ACTIVSg2000 v2`. Figure 3.2.6a shows that the algorithm tweak in fact alters the cycle distribution to be more similar to that observed in the ERCOT case. The fit parameters to the Negative Binomial distribution are, $p = 0.31$, and $n = 1.53$, which are significantly closer to the ERCOT values in Table 3.1.

Since there are many other elements involved in the generation of cases, conclusions from a direct comparison are limited. For example, the original version has around 10% more load, which obviously impacts the loading distribution. In fact the average L_s in the new case is 0.9, significantly lower than either value in Table 3.4. Nonetheless, figure 3.2.6b shows the L_s distribution has also changed and in a manner similar to Figure 3.2.3, i.e., the peak shifting somewhat to the left. While the change cannot be strictly attributed to the change in cycle distribution, the agreement with the previous findings serve as further support for the hypothesis.

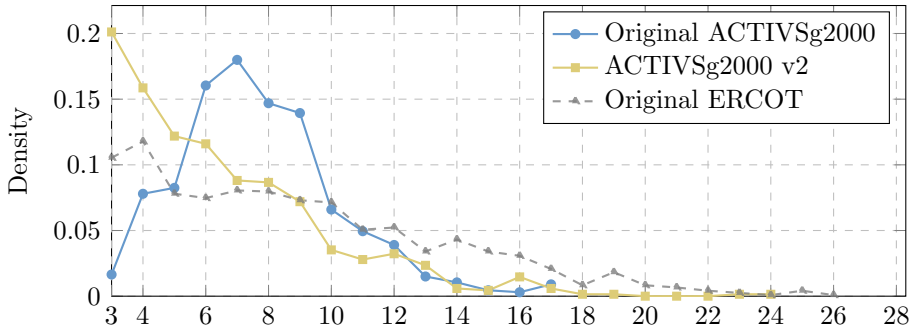

(a) Cycle Size

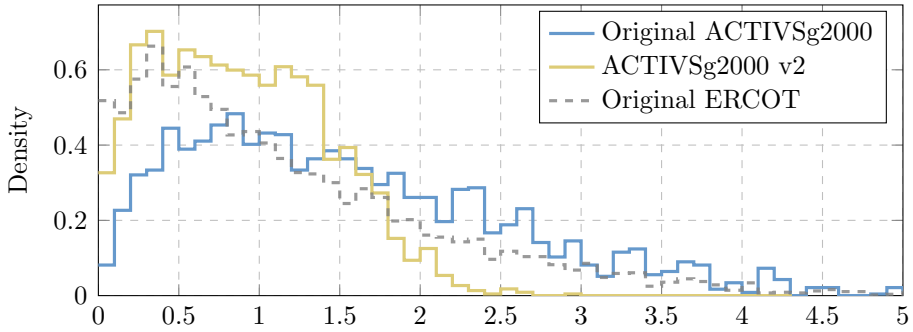

(b) L_s

Figure 3.2.6: Cycle and L_s distributions following a tweak to the ACTIVS algorithm to address the cycle distribution.

3.3 Creating Synthetic Transmission Cases

Building on the observations for how topology impacts power flow results, a solution is sought for forming power system cases from constituents parts to obtain realistic operational behavior. The synthesis philosophy in this section is a bit different from Chapter 2. Whereas for distribution the topology itself is synthesized based on observed statistics, in the following, it is assumed that the topological work has already been done in one way or another. Expressed in this manner, the problem can be viewed as permuting input data onto a topology lattice, and is therefore often called a *placement problem* in the following. This section presents a MILP solution to the placement problem.

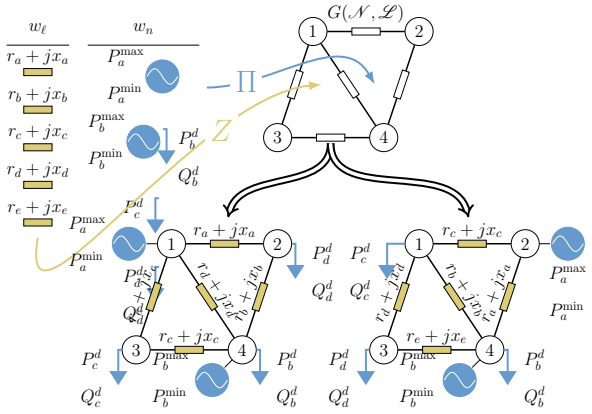

Figure 3.3.1: Conceptual illustration of the placement problem. A map is sought from sets w_ℓ and w_n, via matrices Z and Π respectively, onto topology $G(\mathscr{N},\mathscr{L})$.

3.3.1 Preliminaries

The topology of the power system is described as a graph, $G(\mathscr{N},\mathscr{L})$, where $\mathscr{N}$ and $\mathscr{L}$ are the bus and branch sets, respectively. Figure 3.3.1, illustrates the placement problem: given an $|\mathscr{N}|$ size set w_n of node properties (e.g. load or generation limits) and an $|\mathscr{L}|$ size set, w_ℓ, of branch properties (e.g. line impedance or rating), how should w_n and w_ℓ be permuted when mapped onto $\mathscr{N}$ and $\mathscr{L}$?

No assumptions are placed explicitly on the inputs. Rather, the algorithm does its best to create a well functioning system with those provided. The implicit assumption, therefore, is that the inputs are "reasonable". When the goal is realism, this means that load samples, for example, should have a realistic distribution, or that the topology is realistic. For a "what-if" question, however, samples with more novel distributions could be supplied.

As posed, the tasks of obtaining data samples and creating a full power-flow case are decoupled. The first order statistics encapsulated in w_n, w_ℓ, as well as topological features of G can be relatively easily extracted from already available cases, or other data sources. Higher order statistics, capturing the interactions between these

elements, are far more difficult, since samples are few. For example, there are $|\mathscr{L}|$ admittance samples in a single case. However, that case provides only a single sample of the Y_{bus} matrix, describing how these admittances associate with each other. As formulated the placement problem enables independent data collection, while higher order statistics are addressed via optimization. Furthermore, the literature on random graph generation for grid topologies, such as [Wang *et al.*(2010a)], can be directly used without modification.

In the following, graph G comes either from a reference case or from a topology generation algorithm (see Section 3.5.2). The load data is sampled from a KDE fit to a reference case. Since the generation and branch data exhibit much heavier tails [Schweitzer *et al.*(2018c)], they are sampled directly from a reference case histogram. It should be stressed that samples could be generated in a myriad of ways, whose appropriateness depends on the application at hand.

Even when a single reference case is used, as just described, multiple, distinct synthetic test cases can be created. First of all, the sampling process for w_ℓ and w_n yields different inputs, even if the topology is fixed. Second, given the specified Mixed Integer Programming (MIP) gap[4], it is almost certain that the solution to the problem formulated in Section 3.3.2 is not unique, and therefore, multiple solutions may be found even if the exact same inputs are given. Finally, when the branch permutations are solved for in an Evolutionary Algorithm (EA) approach (introduced in Section 3.4.3) the very structure of the algorithm yields a set of different, distinct, solutions.

[4]The MIP gap measures the difference in objectives between the incumbent and integer-relaxed solutions.

3.3.1.1 Notation

When used as superscripts f and t are used as labels for the *from* and *to* ends of branches, respectively. Otherwise, they are the functions as defined in the List of Symbols. For nodal values such as θ, the difference over a branch ℓ is writen as: $\theta_{ft(\ell)} \triangleq \theta_{f(\ell)} - \theta_{t(\ell)}$. A set of indexes can be used as a subscript to refer to the subset of variables by the same name with indexes in the set.

The $|\mathscr{L}| \times |\mathscr{L}|$ matrix permuting w_ℓ is Z, and the $|\mathscr{N}| \times |\mathscr{N}|$ one permuting w_n is Π. S, P, and Q are used for apparent, real, and reactive power respectively. Superscripts d and g stand for demand and generation, while f and t are used to indicate branch flows. When used as variables, i, v, and $y = g + jb$ indicate currents, voltages, and admittances respectively. The variable u is used for $\ln(v)$ and therefore *does not* represent the step-function as previously.

3.3.1.2 Full Variable Linearized Power Flow

In order to formulate the problem as a MILP, a Linear Power Flow (LPF) formulation that can be embedded in an OPF is required. The chosen LPF is introduced here briefly, noting that a similar approach was recently published in [Li *et al.*(2017)]. Starting from a generic, two port branch model,

$$\begin{pmatrix} I_\ell^f \\ I_\ell^t \end{pmatrix} = \begin{pmatrix} y^{ff} & y^{ft} \\ y^{tf} & y^{tt} \end{pmatrix} \begin{pmatrix} V_{f(\ell)} \\ V_{t(\ell)} \end{pmatrix}, \tag{3.3.1}$$

the complex power at the *from* end of a branch is:

$$\left(S_\ell^f\right)^* = v_f^2 y_\ell^{ff} + V_f^* V_t y^{ft}. \tag{3.3.2}$$

Noting that $|V| = v = e^{\ln(v)}$, and letting $u = \ln(v)$,

$$\left(S_\ell^f\right)^* e^{-u_{f(\ell)}} = y_\ell^{ff} e^{u_{f(\ell)}} + y^{ft} e^{u_{t(\ell)} - j\theta_{ft(\ell)}}. \tag{3.3.3}$$

Expanding the exponentials on the right about zero,

$$\left(S_\ell^f\right)^* e^{-u_{f(\ell)}} \approx y^{ff}(1+u_{f(\ell)}) + y^{ft}(1+u_{t(\ell)})(1-j\theta_{ft(\ell)} - \phi_\ell), \tag{3.3.4}$$

where $\phi_\ell = \theta^2_{ft(\ell)}/2$, the second order term in the expansion of $e^{j\theta_{ft(\ell)}}$. Multiplying through, neglecting further second-order terms, and setting $e^{-u} \approx 1$ on the left:

$$\left(S_\ell^f\right)^* \approx y^{ff}(1+u_{f(\ell)}) + y^{ft}(1-\phi_\ell+u_{t(\ell)}) - jy^{ft}\theta_{ft(\ell)}. \tag{3.3.5}$$

Treatment of S_ℓ^t is identical.

There is a good deal of literature about different linearizations of the OPF, see [Yang *et al.*(2017)] for a comparison of some methods. While the placement problem is embedded inside an OPF formulation, the desired output is not the typical generation dispatch, but the permutation matrices Z and Π. The particular choice of LPF here is due to familiarity with it from working with power flow (not OPF) linearizations, where it showed good behavior, as also reported in [Li *et al.*(2017)]. Whether and how a linearization choice impacts the final placement is an interesting question for future research, but beyond the scope of this work.

3.3.2 Formulation

This section describes how Z and Π are embedded in a linearized OPF to form a MILP for solving the placement problem. Each subsection describes a set of constraints that are gathered together for the final formulation.

3.3.2.1 Nodal balance constraints

Energy balance due to KCL is enforced at each node via,

$$P_n^g - P_n^d - \sum_{\ell \in t^{-1}(n)} P_\ell^t - \sum_{\ell \in f^{-1}(n)} P_\ell^f = 0 \qquad \forall n \in \mathscr{N} \tag{3.3.6a}$$

$$Q_n^g - Q_n^d - \sum_{\ell \in t^{-1}(n)} Q_\ell^t - \sum_{\ell \in f^{-1}(n)} Q_\ell^f = 0 \qquad \forall n \in \mathscr{N}, \tag{3.3.6b}$$

where all Ps and Qs are variables.

3.3.2.2 Linearized Branch Flows

Branch permutation matrix Z is embedded into the LPF formulation (3.3.5), along with line limits r by,

$$-\sum_{\tilde{\ell} \in \mathscr{L}} Z_{\ell,\tilde{\ell}} r_{\tilde{\ell}} \le P_\ell^{f,t}, Q_\ell^{f,t} \le \sum_{\tilde{\ell} \in \mathscr{L}} Z_{\ell,\tilde{\ell}} r_{\tilde{\ell}} \qquad \forall \ell \in \mathscr{L} \tag{3.3.7a}$$

$$\begin{aligned} -(1 - Z_{\ell\tilde{\ell}})\mathcal{M}_{P^f} \le P_\ell^f - g_{\tilde{\ell}}^{ff}(1 + u_{f(\ell)}) - g_{\tilde{\ell}}^{ft}(1 - \phi_\ell + u_{t(\ell)}) \\ -b_{\tilde{\ell}}^{ft}\theta_{ft(\ell)} \le (1 - Z_{\ell\tilde{\ell}})\mathcal{M}_{P^f} \quad \forall \ell, \tilde{\ell} \in \mathscr{L} \end{aligned} \tag{3.3.7b}$$

$$\begin{aligned} -(1 - Z_{\ell\tilde{\ell}})\mathcal{M}_{Q^f} \le Q_\ell^f + b_{\tilde{\ell}}^{ff}(1 + u_{f(\ell)}) + b_{\tilde{\ell}}^{ft}(1 - \phi_\ell + u_{t(\ell)}) \\ -g_{\tilde{\ell}}^{ft}\theta_{ft(\ell)} \le (1 - Z_{\ell\tilde{\ell}})\mathcal{M}_{Q^f} \quad \forall \ell, \tilde{\ell} \in \mathscr{L} \end{aligned} \tag{3.3.7c}$$

$$\begin{aligned} -(1 - Z_{\ell\tilde{\ell}})\mathcal{M}_{P^t} \le P_\ell^t - g_{\tilde{\ell}}^{tt}(1 + u_{t(\ell)}) - g_{\tilde{\ell}}^{tf}(1 - \phi_\ell + u_{f(\ell)}) \\ +b_{\tilde{\ell}}^{tf}\theta_{ft(\ell)} \le (1 - Z_{\ell\tilde{\ell}})\mathcal{M}_{P^t} \quad \forall \ell, \tilde{\ell} \in \mathscr{L} \end{aligned} \tag{3.3.7d}$$

$$\begin{aligned} -(1 - Z_{\ell\tilde{\ell}})\mathcal{M}_{Q^t} \le Q_\ell^t + b_{\tilde{\ell}}^{tt}(1 + u_{t(\ell)}) + b_{\tilde{\ell}}^{tf}(1 - \phi_\ell + u_{f(\ell)}) \\ +g_{\tilde{\ell}}^{tf}\theta_{ft(\ell)} \le (1 - Z_{\ell\tilde{\ell}})\mathcal{M}_{Q^t} \quad \forall \ell, \tilde{\ell} \in \mathscr{L}. \end{aligned} \tag{3.3.7e}$$

In (3.3.7a), Z permutes r to affect the appropriate branch[5]. In (3.3.7b)–(3.3.7e), g and b are the real and imaginary parts of y, and each equality constraint is split into

[5]Since ratings are in $S = \sqrt{P^2 + Q^2}$, which is non linear, another approximation is required. As a conservative measure, the actual rating is scaled by $1/\sqrt{2}$. This way, even if both P and Q flows are at the limit, flow S should not be in violation.

two disjunctive constraints utilizing big multiplier, $\mathcal{M}$[6]. Term $(1 - Z_{\ell\tilde{\ell}})\mathcal{M}$ ensures constraints are only active if $Z_{\ell,\tilde{\ell}} = 1$.

3.3.2.3 Node Permutation

Bus permutation Π is embedded into the OPF formulation via variables P^g, P^d, Q^g, and Q^d, which are assigned or constrained by permuting properties in w_n (indicated with a tilde) by Π:

$$P_n^d = \sum_{\tilde{n}\in\mathcal{N}} \Pi_{n\tilde{n}} \tilde{P}_{\tilde{n}}^d,\ Q_n^d = \sum_{\tilde{n}\in\mathcal{N}} \Pi_{n\tilde{n}} \tilde{Q}_{\tilde{n}}^d \qquad \forall n \in \mathcal{N} \tag{3.3.8a}$$

$$\sum_{\tilde{n}\in\mathcal{N}} \Pi_{n\tilde{n}} \tilde{P}_{\tilde{n}}^{\min} \leq P_n^g \leq \sum_{\tilde{n}\in\mathcal{N}} \Pi_{n\tilde{n}} \tilde{P}_{\tilde{n}}^{\max} \qquad \forall n \in \mathcal{N} \tag{3.3.8b}$$

$$\sum_{\tilde{n}\in\mathcal{N}} \Pi_{n\tilde{n}} \tilde{Q}_{\tilde{n}}^{\min} \leq Q_n^g \leq \sum_{\tilde{n}\in\mathcal{N}} \Pi_{n\tilde{n}} \tilde{Q}_{\tilde{n}}^{\max} \qquad \forall n \in \mathcal{N}. \tag{3.3.8c}$$

Superscripts 'min' and 'max' indicate respective generator limits. For example, if $\Pi_{nk} = 1$, constraint (3.3.8b) forces P_n^g to lie between limits $\tilde{P}_k^{\min}$ and $\tilde{P}_k^{\max}$.

3.3.2.4 Variable Limits

Typical OPF limits are enforced by,

$$-\Delta\theta_{\max} \leq \theta_{ft(\ell)} \leq \Delta\theta_{\max} \qquad \forall \ell \in \mathscr{L} \tag{3.3.9a}$$

$$u_{\min} \leq u_n \leq u_{\max} \qquad \forall n \in \mathcal{N}, \tag{3.3.9b}$$

where $\Delta\theta_{\max}$ is the maximum angle between adjacent buses. Note that voltage limits are mapped to u's logarithmic domain.

[6]For more on how an appropriate size for the various $\mathcal{M}$ can be determined, see Appendix B.1.

3.3.2.5 Binary Permutation Matrices

The definition of Z and Π as permutation matrices is enforced by,

$$\sum_{\tilde{n}\in\mathscr{N}} \Pi_{n\tilde{n}} = 1, \qquad \sum_{\tilde{n}\in\mathscr{N}} \Pi_{\tilde{n}n} = 1 \qquad \forall n \in \mathscr{N} \tag{3.3.10a}$$

$$\sum_{\tilde{\ell}\in\mathscr{L}} Z_{\ell\tilde{\ell}} = 1, \qquad \sum_{\tilde{\ell}\in\mathscr{L}} Z_{\tilde{\ell}\ell} = 1 \qquad \forall \ell \in \mathscr{L} \tag{3.3.10b}$$

$$\Pi_{n\tilde{n}} \in \{0,1\} \quad \forall n, \tilde{n} \in \mathscr{N},\ Z_{\ell\tilde{\ell}} \in \{0,1\} \quad \forall \ell, \tilde{\ell} \in \mathscr{L}. \tag{3.3.10c}$$

Namely, each must be doubly stochastic and binary valued.

3.3.2.6 Minimum losses

For added realism, a minimum loss fraction, $\Omega_{\min}$ is forced on the system,

$$\sum_{n\in\mathscr{N}} P_n^g \geq \sum_{n\in\mathscr{N}} P_n^d \frac{1}{1-\Omega_{\min}}. \tag{3.3.11}$$

For example, [Wong(2011)] gives $\Omega_{\min}$ between 4–8% in California, while [National Grid(2017)] reports losses in England's National Grid to be around 1.5%. Variable ϕ introduced in 3.3.1.2 plays an important role in modeling losses, as an additional real term in (3.3.5). Capturing ϕ's quadratic behavior is addressed next.

3.3.2.7 Polyhedral relaxation

Quadratic behavior in angle difference is modeled via a polyhedral relaxation, much like in [Coffrin and Van Hentenryck(2014)]. This is done by adding $h+1$ constraints, tangential to the quadratic curve, at points spaced d apart over $[-\Delta\theta_{\max}, \Delta\theta_{\max}]$:

$$\phi_\ell \geq -\frac{(-\Delta\theta_{\max} + td)^2}{2} + (-\Delta\theta_{\max} + td)\theta_{ft(\ell)} \quad \forall t \in \{0,1,\ldots,h\}, \forall \ell \in \mathscr{L}. \tag{3.3.12}$$

Figure 3.3.2 illustrates this geometrically for $\Delta\theta_{\max} = 40°$, $h = 4$, and $d = 2\Delta\theta_{\max}/h = 20°$. In the implementation that follows, h is determined by specifying maximum error $\epsilon = \theta_{ft(\ell)}^2/2 - \phi_\ell$, and solving for h: $h = \lceil \Delta\theta_{\max}/\sqrt{\epsilon} \rceil$[7].

[7]See Appendix B.2 for a derivation.

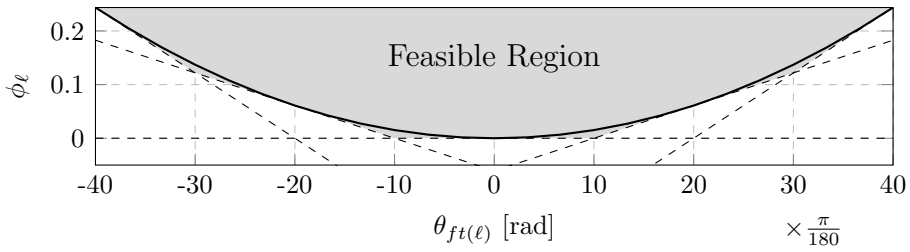

Figure 3.3.2: Polyhedral relaxation of second order term in $\theta_{ft(\ell)}$ expansion.

As noted in [Coffrin and Van Hentenryck(2014)] and [Akinbode and Hedman(2013)], this sort of piecewise linear relaxation can lead to fictitious losses when negative LMPs arise in the system. This problem is commonly circumvented in literature by including binary variables to force selection of the correct linear segment [Akinbode and Hedman(2013), Zhang *et al.*(2013), Fortenbacher and Demiray(2017)]. The present concern, however, is not a perfectly accurate OPF solution, but reasonable permutation matrices Z and Π. The OPF is only a means to reach desirable Z and Π solutions, of which there are many. Therefore, a few fictitious losses are not detrimental to the objective, and accepted as added error in the solution rather than further increase the computational burden with more binaries. Finally, there are other ways of modeling losses, such as "loss factors" [Yang *et al.*(2018b)]. These, however, require generator distribution factors, which would also have to be permuted with matrix Π. This modeling choice is thus not suitable for this particular formulation.

3.3.2.8 Reactive Flow Magnitude

During initial trials, the reactive flows in the generated synthetic cases were unsatisfactorily large. Reactive planning in general, is addressed in a post processing step discussed in Section 3.4.5. However, to encourage the solution to already have smaller magnitude flows variables $q_\ell^f \geq 0$ and $q_\ell^t \geq 0$ are first used to capture the magnitude

of reactive power flow on line ℓ:

$$q_\ell^f + Q_\ell^f \geq 0,\ q_\ell^t + Q_\ell^t \geq 0 \qquad \forall \ell \in \mathscr{L} \tag{3.3.13a}$$

$$q_\ell^f - Q_\ell^f \geq 0,\ q_\ell^t - Q_\ell^t \geq 0 \qquad \forall \ell \in \mathscr{L} \tag{3.3.13b}$$

Adding variables q^f and q^t to the objective function encourages the optimization problem to find a solution with small reactive flow magnitudes. Minimizing reactive flows makes sense from an engineering perspective as well. Reactive power is generally considered a local property and should therefore be provided close to where it is consumed.

3.3.2.9 Problem Statement

Unlike many OPF formulations, the objective function primarily minimizes losses by assuming uniform cost, namely unity, for all generators. This decision and some of its ramifications are further discussed in Section 3.5.3. Variable ϕ must also be minimized to force it to lie on the piecewise linear approximation to the parabola described by (3.3.12). Finally, as mentioned in the previous section, to minimize reactive flow magnitudes, q^f and q^t are also added to the objective. Letting,

$$x = \left\{ Z, \Pi, \theta, u, P^g, Q^g, P^f, Q^f, P^t, Q^t, q^f, q^t, \phi \right\}, \tag{3.3.14}$$

the objective function is,

$$J(x) = \sum_{n \in \mathscr{N}} P_n^g + \sum_{\ell \in \mathscr{L}} \left(\phi_\ell + q_\ell^f + q_\ell^t \right), \tag{3.3.15}$$

and the placement problem is formulated as:

$$\begin{aligned} \underset{x}{\textbf{Minimize}} \quad & J(x) \\ \textbf{Subject to} \quad & \text{constraints (3.3.6) to (3.3.13).} \end{aligned} \tag{3.3.16}$$

Table 3.7: Divergence Between Real and Synthetic 118 Bus Cases

Quantity	D_H
$\theta_{ft(\ell)}$ [°]	0.3106
P_ℓ^f [MW]	0.3963
Q_ℓ^f [MVAr]	0.2517
$\lvert S_\ell^f \rvert$ [MVA]	0.2893

3.3.3 Initial Results

The IEEE 118 bus system, as available in MATPOWER [Zimmerman *et al.*(2011)], is used for a proof-of-concept test. Minimum losses are set to match the case with $\Omega_{\min} = 3\%$. Voltage limits $v_{\min} = 0.9$, and $v_{\max} = 1.05$ are also taken directly from the reference data. Angle limits are chosen to be $\Delta\theta_{\max} = 40°$, and for the polyhedral constraint $\epsilon = 0.001 \Rightarrow h = 23$. Similar to Section 3.1, the Hellinger distance (3.1.1), as well as the empirical quantile function, are used to assess how distributions p and q match each another[8]. Note that these are distributions for a single snapshot, there is no consideration of time-series data.

Figure 3.3.3 shows both pdfs and quantile functions of several properties for the synthetic case, created by solving (3.3.16), and the original 118-bus reference case. Visually, the distributions appear well matched. Table 3.7 reports the corresponding D_H values. Considering the small size of $\mathscr{L}$, the statistics are likely to be noisy, and therefore the values seem satisfactory. Improved values on a larger system in subsequent Section 3.5.1 further support this claim.

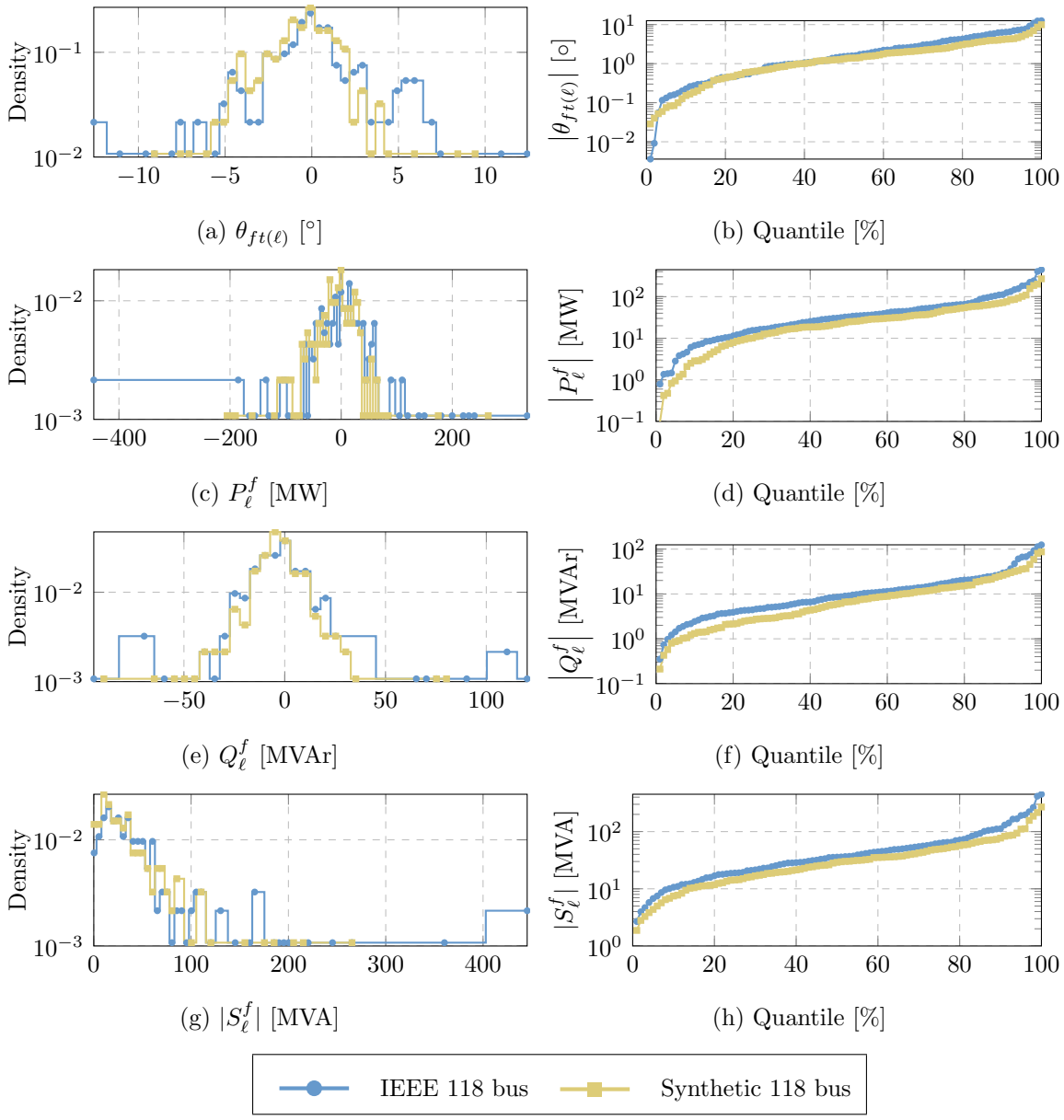

Figure 3.3.3: Comparison of solving (3.3.16) to original IEEE 118-bus case.

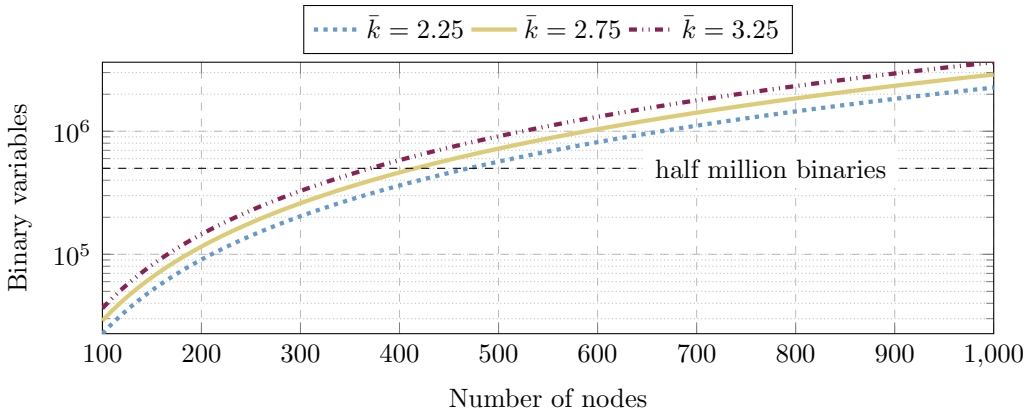

Figure 3.4.1: Relationship between topology and number of binary variables. For typical power systems, the number of binaries cross half a million around $|\mathscr{N}| = 400$.

3.4 Scaling Up

While the 118 bus case provides a proof-of-concept, the real value of automating test case creation will come from making a larger number of large cases available. With increased size, statistics become more meaningful, and testing on an ensemble of cases can offer new insights.

A node's degree describes how many branches are connected to it, and the average nodal degree, $\bar{k}$, is the average of this quantity over all nodes in $\mathscr{N}$. There are $(\bar{k}/2) \times |\mathscr{N}|$ edges in a graph with average nodal degree $\bar{k}$, and $|\mathscr{N}|$ nodes. The total number of binary variables is therefore, $(1+\bar{k}^2/4)\,|\mathscr{N}|^2$. Quadratic growth of binaries causes (3.3.16) to scale quite poorly. Figure 3.4.1 shows how the number of binary variables grows with $\mathscr{N}$ for typical power systems $\bar{k}$. Power system values of $\bar{k}$ range between 2 and 4, meaning that around 400 buses the problem crosses the half million binaries mark. Since MILP problems with millions of binaries are still too difficult to solve, decomposition becomes necessary.

[8] Since both p and q are empirical distributions the Hellinger distance is better defined. D_{KL} is not defined for $q(x) = 0$, where D_H is.

3.4.1 Separation Into Zones

A spectral decomposition using the graph Laplacian Fiedler vector [Fiedler(1975)] is used to partition the system into a set of zones, $\mathscr{H}$, as shown in Algorithm 9. All Algorithm 9 does is split graphs into two parts based on the sign of the Fiedler vector elements, which according to [Mohar(1992)] has been shown to be a good heuristic for partitioning graphs with small interference, i.e., few edges between the two partitions. The problem of partitioning power systems has been studied quite a bit. The Diakoptics technique [Kron(1963),Brameller *et al.*(1969)] is based on partitioning systems. More recently [Cotilla-Sanchez *et al.*(2013)] describes various methodologies for partitioning. These different methods, either require or are at least intended to be used with additional non-topological information about the system. Since electrical properties have yet to be mapped to the graph, a simple spectral decomposition is a reasonable choice for the strictly topological graph, although alternative methods could be investigated in the future.

The set of nodes and branches in zone i are $\mathscr{N}_i$ and $\mathscr{L}_i$, respectively. Additionally, set $\mathscr{E}_i$ contains all edges connecting zone i to its neighbors. Each boundary edge, ℓ, is associated with real flow, β_ℓ, and reactive flow, γ_ℓ. Two copies of each boundary flow variable exist: one for each of the neighboring zones. Superscripts are used to indicate to which zone a variable belongs. For example, β_ℓ^i is in zone i, while γ_ℓ^j belongs to zone j. The following convention is adopted to clearly indicate which copy is intended:

$$\mathscr{E}_{ij} = \begin{cases} \mathscr{E}_i \cap \mathscr{E}_j & i < j \\ \emptyset & \text{otherwise.} \end{cases} \tag{3.4.1}$$

The β variables between zone i and j belonging to zone i are therefore, $\beta^i_{\mathscr{E}_{ij}}$, while the j copies are $\beta^j_{\mathscr{E}_{ij}}$. Figure 3.4.2 illustrates the different uses of notation.

3.4.2 Decomposed Formulation

Boundary variables β and γ require some constraint modifications. First, nodal balance constraints (3.3.6), are adjusted to include boundary flows:

$$P_n^g - P_n^d - \sum_{\ell \in t^{-1}(n)} P_\ell^t - \sum_{\ell \in f^{-1}(n)} P_\ell^f + \sum_{\ell \in t^{-1}(n) \cap \mathscr{E}_i} \beta_\ell^i - \sum_{\ell \in f^{-1}(n) \cap \mathscr{E}_i} \beta_\ell^i = 0 \quad \forall i \in \mathscr{H}, \forall n \in \mathscr{N} \tag{3.4.2a}$$

$$Q_n^g - Q_n^d - \sum_{\ell \in t^{-1}(n)} Q_\ell^t - \sum_{\ell \in f^{-1}(n)} Q_\ell^f + \sum_{\ell \in t^{-1}(n) \cap \mathscr{E}_i} \gamma_\ell^i - \sum_{\ell \in f^{-1}(n) \cap \mathscr{E}_i} \gamma_\ell^i = 0 \quad \forall i \in \mathscr{H}, \forall n \in \mathscr{N}. \tag{3.4.2b}$$

Second, the minimum loss constraint (3.3.11) is modified to consider exported and imported real power:

$$\sum_{n \in \mathscr{N}_i} \left(P_n^g + \sum_{\ell \in t^{-1}(n) \cap \mathscr{E}_i} \beta_\ell^i - \sum_{\ell \in f^{-1}(n) \cap \mathscr{E}_i} \beta_\ell^i \right) \geq \sum_{n \in \mathscr{N}_i} P_n^d \frac{1}{1 - \Omega_{\min}} \qquad \forall i \in \mathscr{H}. \tag{3.4.3}$$

The modification treats imported and exported power as changes to the total generation. Since β_ℓ can be positive or negative, the subtracted term in (3.4.3) could in fact represent a net *import* of power.

Algorithm 9 Algorithm for splitting transmission grid graph topology into zones.

procedure FORM ZONES($G(\mathscr{N}, \mathscr{L})$,$N_{\max}$,$N_{\min}$)
  $\mathscr{H} \leftarrow \{G\}$
  while $N_{\max} < \max_{i \in \mathscr{H}} |V(i)|$ **do** ▷ $V(i)$ is set of nodes for subgraph i
    $S \leftarrow \arg\max_{i \in \mathscr{H}} |V(i)|$
    $\mathscr{H} \leftarrow \mathscr{H} \setminus S$
    Get Fiedler vector, v_F of S
    Form S^+, S^-, with nodes corresponding to positive/negative entries in v_F, respectively.
    $\mathscr{H} \leftarrow \mathscr{H} \cup \{S^+, S^-\}$
    for $i \in \mathscr{H}$ **do**
      if $|V(i)| < N_{\min}$ **then**
        Combine i with a neighboring subgraph in $\mathscr{H}$
      end if
    end for
  end while
  return $\mathscr{H}$
end procedure

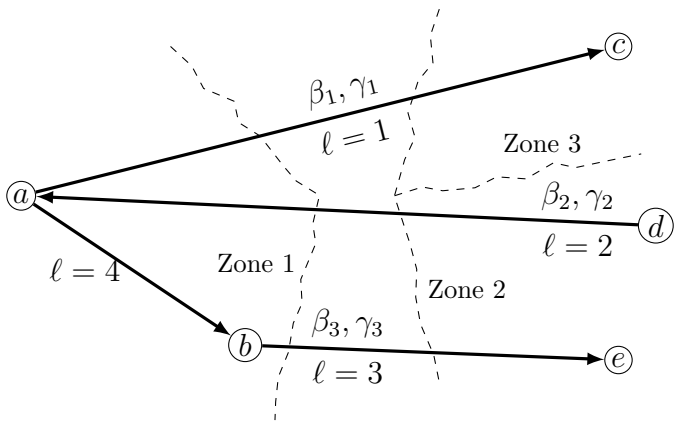

Figure 3.4.2: Illustration of boundary flow and zone definitions. Using the defined notation:
$\mathscr{H} = \{1, 2, 3\}$, $\mathscr{N}_2 = \{d, e\}$, $\mathscr{L}_1 = \{4\}$,
$\mathscr{E}_{1,2} = \{2, 3\}$, $\mathscr{E}_{2,1} = \emptyset$, $\gamma^2_{\mathscr{E}_{1,2}} = \{\gamma^2_2, \gamma^2_3\}$, $\beta^1_{\mathscr{E}_{1,2}} = \{\beta^1_2, \beta^1_3\}$,
$\mathscr{E}_1 = \{1, 2\}$, $t^{-1}(a) \cap \mathscr{E}_1 = \{2\}$, and $f^{-1}(a) \cap \mathscr{E}_1 = \{1\}$.

Let $\beta = \{\beta^i : i \in \mathscr{H}\}$, $\gamma = \{\gamma^i : i \in \mathscr{H}\}$, and $x = \{x^i : i \in \mathscr{H}\}$, where x^i is the set of all variables *local* to zone i,

$$x^i = \big\{ Z_{\mathscr{L}_i, \mathscr{L}_i}, \Pi_{\mathscr{N}_i, \mathscr{N}_i}, \theta_{\mathscr{N}_i}, u_{\mathscr{N}_i}, P^g_{\mathscr{N}_i}, Q^g_{\mathscr{N}_i}, P^f_{\mathscr{L}_i}, Q^f_{\mathscr{L}_i}, P^t_{\mathscr{L}_i}, Q^t_{\mathscr{L}_i}, q^f_{\mathscr{L}_i}, q^t_{\mathscr{L}_i}, \phi_{\mathscr{L}_i} \big\} \quad \forall i \in \mathscr{H}, \quad (3.4.4)$$

The full problem in (3.3.16) can be rewritten to include zones as:

$$\begin{aligned} \underset{x,\beta,\gamma,z,\zeta}{\textbf{Minimize}} \quad & \sum_{i \in \mathscr{H}} J(x^i) \\ \textbf{subject to} \quad & \beta^i_\ell - z_\ell = 0 \quad \forall i \in \mathscr{H}, \forall \ell \in \mathscr{E}_i \\ & \gamma^i_\ell - \zeta_\ell = 0 \quad \forall i \in \mathscr{H}, \forall \ell \in \mathscr{E}_i \\ & \text{constraints (3.4.2), (3.3.7)–(3.3.10), (3.4.3), (3.3.12) and (3.3.13).} \end{aligned} \quad (3.4.5)$$

Here z and ζ are the *true* values of boundary flows β and γ respectively. The aim is to decompose (3.4.5) so that each zone could be solved separately. Boundary reactive

flows γ (and ζ) are neglected in the subsequent derivation for clarity; their treatment is identical to β (and z).

Relaxing the new set of equality constraints, the Augmented Lagrangian function is,

$$L_p(x,\beta,z,\omega) = \sum_{i\in\mathscr{H}} \Big(J(x^i) + (\omega^i)^T(\beta^i - z) + \frac{\rho}{2}\|\beta^i - z\|_2^2 \Big) \tag{3.4.6}$$

From here, the Alternating Direction Method of Multipliers (ADMM) algorithm is used [Boyd *et al.*(2011)]:

$$\beta^i[t+1] := \underset{x^i,\beta^i}{\arg\min}\, J(x^i) + (\omega^i)^T(\beta^i - z[t]) + \frac{\rho}{2}\|\beta^i - z[t]\|_2^2 \qquad \forall i \in \mathscr{H} \tag{3.4.7}$$

$$z[t+1] := \underset{z}{\arg\min}\, L_p(\beta^1,\ldots,\beta^{|\mathscr{H}|}[t+1], z, \omega[t]) \tag{3.4.8}$$

$$\omega^i[t+1] := \omega^i[t] + \rho\left(\beta^i[t+1] - z[t+1]\right) \qquad \forall i \in \mathscr{H}. \tag{3.4.9}$$

Following [Boyd *et al.*(2011)], the dual variable ω is shown to be zero in expectation over the zones, leading to $z = \bar{\beta}$, where $\bar{y}$ denotes averaging over $\forall i \in \mathscr{H}$. Equation (3.4.8) is solvable in closed form,

$$z[t+1] = \bar{\beta}[t+1] + \frac{1}{\rho}\bar{\omega}[t]. \tag{3.4.10}$$

Averaging (3.4.9) over $\mathscr{H}$,

$$\bar{\omega}[t+1] = \bar{\omega}[t] + \rho\left(\bar{\beta}[t+1] - z[t+1]\right), \tag{3.4.11}$$

and substituting (3.4.10) in (3.4.11) reveals that $\bar{\omega}[t+1] = 0$, and therefore, $z[t] = \bar{\beta}[t]$.

Letting ν be the dual variable associated with γ (as ω is to β), and collecting all boundary variables,

$$y^i = \{\beta^i, \gamma^i\},\ \lambda^i = \{\omega^i, \nu^i\} \quad \forall i \in \mathscr{H}, \tag{3.4.12}$$

define,

$$g(y^i;\lambda^i[t]) = (\omega^i_{\mathscr{E}_i}[t])^T\beta^i_{\mathscr{E}_i} + (\nu^i_{\mathscr{E}_i}[t])^T\gamma^i_{\mathscr{E}_i} + \frac{\rho}{2}\left(\|\beta^i_{\mathscr{E}_i} - \bar{\beta}_{\mathscr{E}_i}[t]\|_2^2 + \|\gamma^i_{\mathscr{E}_i} - \bar{\gamma}_{\mathscr{E}_i}[t]\|_2^2\right). \tag{3.4.13}$$

The ADMM primal step, (3.4.7), formulation for zone i at iteration t is:

$$\begin{aligned} \underset{x^i, y^i}{\textbf{Minimize}} \quad & J(x^i) + g(y^i; \lambda^i[t]) \\ \textbf{subject to} \quad & \text{constraints (3.4.2), (3.3.7)–(3.3.10),} \\ & \text{(3.4.3), and (3.3.12)–(3.3.13).} \end{aligned} \tag{3.4.14}$$

For the dual update, (3.4.9), the elements of $z[t+1] = \bar{\beta}[t+1]$ are calculated,

$$\bar{\beta}_{\mathscr{E}_{ij}}[t+1] = \frac{\beta^i_{\mathscr{E}_{ij}}[t+1] + \beta^j_{\mathscr{E}_{ij}}[t+1]}{2}, \tag{3.4.15}$$

and similarly for the ν, γ pair.

This consensus form of ADMM is very similar to Progressive Hedging, which has been proposed in some power system applications [Watson and Woodruff(2011)]. The decomposition approach is a bit different from other ADMM formulations for power systems in literature, such as [Erseghe(2014)], since branch, rather than node, variables are communicated. An advantage of this approach is that the number of copies is always two, since a single branch cannot connect more than two different regions. This comes at the cost of effectively neglecting losses on border edges.

3.4.3 Evolutionary Algorithm

Initial results confirm that the decomposition produces similar results to the full solution on the 118-bus case. However, even the smaller subproblems proved to be too large to solve on a larger system (e.g. the Polish case)[9]. A key issue are the disjunctive constraints in (3.3.7) induced by Z.

In an effort to alleviate this issue, solutions for Z and Π are separated into two steps. An EA [Eiben and Smith(2015)] inspired approach is adopted for Z. The EA

[9]For this reason, it is not practical to provide a time comparison between the full MILP formulation and the EA approach introduced here.

algorithm eliminates the binaries associated with Z in favor of an iterative approach where problem copies, each with a different possible realization of branch permutations, are used. Disjunctive constraints (3.3.7) are simplified as discussed in the following section, and the number of binary variables is cut by more than half, making the problem easier to solve. Finally, working with ensembles of individuals (called generations) is appealing, given the original goal of producing sets of cases. Certain convergence guarantees of MILP formulations are sacrificed, however.

Algorithm 10, gives an overview of the EA approach, which consists of three main steps. The SOLVE step on line 5 determines Π given a fixed Z. Since binaries are still involved, the LPF formulation remains necessary. In the SELECTION step, the best κ individuals are chosen as progenitors for the next generation. The MUTATE step, creates a new generation, Ψ_i, of K individuals, by selecting an individuals from Ψ_{i-1} and swapping columns and rows in their Z matrix with probability p_m[10].

Since initial permutations of Z are liable to be not particularly good, slack vari-

[10]If no previous generation exists, i.e. Ψ_{-1}, K random permutations of Z are created.

Algorithm 10 EA: runs for n_G generations, at the end of which. κ best individuals are selected to from K new ones via mutation. Mutation entails swapping columns and rows of the Z matrix with probability p_m.

```
1: procedure EA(n_G, K, κ)
2:     for i ∈ {0, 1, ..., n_G − 1} do
3:         Ψ_i ← MUTATE(Ψ_{i−1}, K, p_m)
4:         for ψ ∈ Ψ_i do
5:             SOLVE (3.4.23) given Z(ψ) .
6:         end for
7:         Ψ_i ← SELECTION(Ψ_i ∪ Ψ_{i−1}, κ)
8:     end for
9:     return Ψ_i
10: end procedure
```

ables are added to several of the constraints to avoid infeasibility. High cost associated with slacks implies that individuals utilizing less are far more likely to become progenitors for the subsequent generation.

3.4.3.1 Constraint Modification

Fixing Z alters or eliminates some of the original constraints. Constraint set (3.3.7) becomes,

$$-(r_\ell + s^r_\ell) \leq P^{f,t}_\ell, Q^{f,t}_\ell \leq r_\ell + s^r_\ell \qquad \forall \ell \in \mathscr{L} \qquad (3.4.16a)$$

$$P^f_\ell - g^{ff}_\ell(1 + u_{f(\ell)}) - g^{ft}_\ell(1 - \phi_\ell + u_{t(\ell)}) - b^{ft}_\ell \theta_{ft(\ell)} = 0 \qquad \forall \ell \in \mathscr{L}. \qquad (3.4.16b)$$

Constraints (3.3.7c)–(3.3.7e) are handled exactly like (3.4.16b) and are importantly no longer disjunctive. Slack variable, $s^r \geq 0$, is added in (3.4.16a), and (3.3.9) is similarly relaxed using slack variables $s^\delta_\ell, s^u_n \geq 0$:

$$-(\Delta\theta_{\max} + s^\delta_\ell) \leq \theta_{ft(\ell)} \leq \Delta\theta_{\max} + s^\delta_\ell \qquad \forall \ell \in \mathscr{L} \qquad (3.4.17a)$$

$$u_{\min} - s^u_n \leq u_n \leq u_{\max} + s^u_n \qquad \forall n \in \mathscr{N}. \qquad (3.4.17b)$$

Finally, all constraints involving Z in (3.3.10) are removed.

3.4.3.2 Further Modeling

New possibilities are also opened, now that all branch parameters are fixed during the MILP optimization. Knowledge of line parameters allows, for example, to consider L_s as described in Section 3.1 directly in the formulation.

In per unit, the SIL rating, which equals $V^2_{\text{rated}}/Z^c_\ell$, becomes $1/Z^c_\ell$, with,

$$Z^c_\ell = \sqrt{\frac{r_\ell + jx_\ell}{g^0_\ell + jb^0_\ell}}, \qquad (3.4.18)$$

where, r and x are the branch π-model series components, and g^0 and b^0 the line charging shunts. Constraint set (3.4.19) is added to target average loading value L_s^μ:

$$c_s \sum_{\ell \in \mathscr{S}} Z_\ell^c p_\ell^f - s_{\text{sil}} \leq L_s^\mu \tag{3.4.19a}$$

$$p_\ell^f + P_\ell^f \geq 0, \quad p_\ell^f - P_\ell^f \geq 0 \qquad \forall \ell \in \mathscr{L}. \tag{3.4.19b}$$

Variable $p^f \geq 0$, similar to q^f, tracks the absolute value of real power flows, and parameter c_s compensates for the error associated with using real, instead of apparent, power magnitude:

$$c_s = \frac{\sum\limits_{\ell \in \mathscr{S}} \sqrt{(P_\ell^f)^2 + (Q_\ell^f)^2}}{\sum\limits_{\ell \in \mathscr{S}} p_\ell^f}. \tag{3.4.20}$$

Choice of c_s could be done by evaluating (3.4.20) for a reference case, or by any other reasonable method. Summation in (3.4.19a) is over set $\mathscr{S}$, containing all power lines, i.e., non-transformer branches, where SIL is a sensible quantity[11]. Finally, $s_{\text{sil}} \geq 0$ is another slack variable, allowing violations of (3.4.19a) at a cost.

3.4.3.3 EA Formulation

Redefining x as,

$$x = \left\{\Pi, \theta, u, P^g, Q^g, P^f, Q^f, P^t, Q^t, q^f, q^t, \phi, s^r, s^\delta, s^u, s^{\text{sil}}\right\}, \tag{3.4.21}$$

the objective function is modified to,

$$J(x) = \sum_{n \in \mathscr{N}} (P_n^g + w_u s_n^u) + w_{\text{sil}} s^{\text{sil}} + \sum_{\ell \in \mathscr{L}} \left(\phi_\ell + q_\ell^f + q_\ell^t + p_\ell^f + w_r s_\ell^r + w_\delta s_\ell^\delta\right), \tag{3.4.22}$$

[11]Branches in $\mathscr{S}$ must also have some line charging susceptance ($b_\ell^0 \neq 0$), otherwise Z_ℓ^c and therefore L_s are not defined.

where w_u, w_r, w_δ, and w_{sil} are tunable weights designed to discourage relaxing limits whenever possible.

With consideration for all the modifications, the formulation solved by each individual, ψ, in Algorithm 10 is,

$$\begin{aligned} \textbf{Minimize}_{x} \quad & J(x) \\ \textbf{Subject to} \quad & \text{constraints (3.3.6), (3.4.16), (3.3.8),} \\ & \text{(3.4.17), (3.3.10)–(3.3.13), and (3.4.19).} \end{aligned} \tag{3.4.23}$$

Alternatively, a decomposed formulation as discussed in Section 3.4.2 can be used by swapping constraints (3.3.6) and (3.3.11) for (3.4.2) and (3.4.3), and adding (3.4.13) to each zone's objective.

3.4.4 Convergence

A few considerations related to convergence are needed before results are presented. A MILP will eventually converge to an optimal solution, however, given time constraints a so-called MIP gap is given that is considered good enough. A fairly loose MIP gap of 15% is used, partially to help speed up the solution process, but also because feasibility is more of interest than optimality for the given problem.

Since MILP is not convex, ADMM does not guarantee convergence to the global optimum, but to a fixed point[12]. Again, as feasibility is the main concern, termination is based only on primal feasibility, i.e the norm of the error between variable copies[13]. Furthermore, due to time constraints, a limit of five ADMM iterations is imposed. The results are thus close to feasible but may not be entirely so. Following all ADMM iterations, (3.3.16) with both Z and Π fixed is solved on the complete system for a

[12] Assuming reasonable handling of step size.

[13] Also similar to Progressive Hedging.

cohesive solution.

3.4.5 Additional Adjustments

Once a case has been created by mapping node properties w_n and branch properties w_ℓ onto $G(\mathscr{N}, \mathscr{L})$, a few post-processing steps are carried out to enhance the synthetic case, ensure its AC feasibility, and get a final dispatch solution. A key tool used in these steps is the `softlimits` functionality in MATPOWER[14], which was substantially expanded as part of this effort. The improved `softlimits` relax any of the OPF limits (generation, flows, voltage, etc.) at a high linear cost. They are therefore able to pinpoint where violations are occurring and just how large they are. For synthetic cases, this is particularly useful, since this information can be generally used to modify the case and overcome violations.

A notable omission thus far are shunt elements for reactive power support. These are added in a post-processing step similar to [Birchfield *et al.*(2018)], where generators with infinite reactive limits are placed at all buses and then iteratively removed until a satisfactory solution is obtained, whereupon the generators are "converted" to shunt admittances providing the same reactive power. Instead, the solution used places generators at all nodes with real and reactive limits of zero. Enabling `softlimits` for reactive limits, the AC-OPF is solved in MATPOWER. Due to the high cost of the `softlimits`, only generators at nodes that *require* the reactive support show violations. These are then converted to shunt admittances. Some additional shunts are also added to further help minimize reactive flows using sensitivities calculated from the power flow solution. A more detailed formulation can be found in Appendix B.4.

Finally, to ensure that the final operating point is not overly restricted, binding

[14] `https://github.com/MATPOWER/matpower`

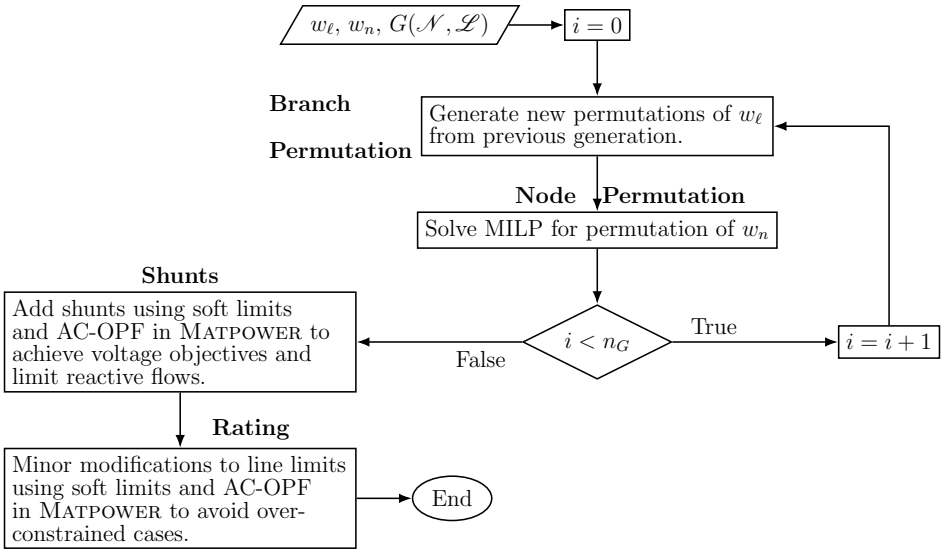

Figure 3.4.3: Full synthetic generation method, from inputs to AC power flow operable set of case. The multiple cases arise from the fact that the "Branch Permutation" step returns multiple solutions, that solve for their own node permutation. The loop starting from "Branch Permutation" is described in pseudocode in Algorithm 10.

line ratings are increased by the smaller of 5 MVA, or 5% of the original rating. In practice these are just a handful, and the statistics are negligibly influenced. Line rating statistics are further discussed in Section 3.5.4.

A flowchart of the entire synthetic generation process, from inputs to a set of AC power flow operable cases, is shown in Figure 3.4.3.

3.5 Numerical Results

3.5.1 Decomposition Results

The procedure from the previous section (see. Figure 3.4.3) is tested using the Polish 2383-bus winter peak system, available in MATPOWER, as reference. In constraint (3.4.19a), $c_s = 1.1$, and $L_s^\mu = 0.77$ based on results from the reference case.

Table 3.8: Range for D_H between real and synthetic polish 2383wp cases

	D_H		
Quantity	min	avg	max
$\theta_{ft(\ell)}$ [°]	0.123	0.129	0.137
P_ℓ^f [MW]	0.143	0.151	0.159
Q_ℓ^f [MVAr]	0.112	0.123	0.130
$\lvert S_\ell^f \rvert$ [MVA]	0.097	0.109	0.118
L_s	0.151	0.172	0.186

Also from the data, $v_{\max} = 1.12$[15]. Remaining constraint parameters are the same as in Section 3.3.3. The algorithm runs for 5 generations ($n_G = 5$) of 15 individuals ($K = 15$), out of whom the best 7 ($\kappa = 7$) are selected. Solutions are saved as MATPOWER cases, and reactive power planning and final dispatch are calculated as in Section 3.4.5. During this stage, voltage limits are tightened to the more typical range: $[0.95, 1.05]$.

The range of D_H between the synthetic cases and the reference are reported in Table 3.8. These are better than results for the 118-bus case in Table 3.7, which is attributed to reduced statistical noise due to larger sample size. Quantile plots of all *seven* synthetic variants are labeled as "case set 1" in Figure 3.5.1. Visual inspection reinforces the numerical evidence that the synthetic results match the reference fairly well.

It should be stressed that *multiple* similar yet distinct cases are created, since at each iteration of the EA algorithm seven individuals are retained. Different lines of the same color are *not* different snapshots of the same case, but rather completely

[15]This is an atypically high value but is kept to match the reference case. More typical voltage levels are enforced during the post-processing steps.

different cases, similar only in that the same inputs were passed to the algorithm that produced them.

3.5.2 Sensitivity to Topological Properties

Automatic creation of multiple, *solvable*, power flow cases, makes new types of analysis possible. Where previous literature focused on classifying the topology of the power system [Pagani and Aiello(2013)], this tool can investigate *how* different topological features might impact power system operations. In a sense, it is an expansion of the modification from Section 3.2. Whereas the modifications required a solved power flow case as an initialization, solutions to the placement problem allow to deal with solvability *after* other desirable manipulations have been carried out.

Six case sets, summarized in Table 3.9, are considered for demonstration. All have 2383 nodes and are differentiated only by topology model and average nodal degree, $\bar{k}$. Case set 1 comes from Section 3.5.1 using the reference topology, case sets 2–3 are RTnested-SmallWorld (RT) topologies [Wang *et al.*(2010a)], and case sets 4–6 are modified ER random graphs. All other EA algorithm parameters (c.f. Algorithm 10) are kept the same. Where case set 1 is, loosely speaking, a permutation of the reference case[16], case sets 2–6 are even "more" synthetic, in the sense that the topology too is fictitious.

In an ER graph with n nodes, each of the possible $n(n-1)/2$ edges is selected with probability p, resulting in an expected number of edges $\mathbb{E}(m) = n(n-1)p/2$. Therefore, $\mathbb{E}(\bar{k}) = 2\,\mathbb{E}(m)/n = p(n-1)$. Given a desired $\bar{k}$, p is selected as $\bar{k}/(n-1)$. ER graphs famously require $\bar{k}$ to scale at least as $\ln(n)$ to be almost surely connected [Erdős and Rényi(1959)], which is much larger than the desired $\bar{k}$ for power system applications. To ensure that the graph is 1) connected and 2) has the desired $\bar{k}$, the

[16] Although the w_ℓ and w_n sets are *not* the same.

Table 3.9: Synthetic Case Legend

Case #	Topology	$\bar{k}$
1	Polish 2383 bus	2.43
2	RTnested-SmallWorld[2]	2.43
3	RTnested-SmallWorld	2.86
4	ER[1,2]	2.43
5	ER[1,2]	2.86
6	ER[1,2]	3.20

[1] Modification 1 performed.

[2] Modification 2 performed.

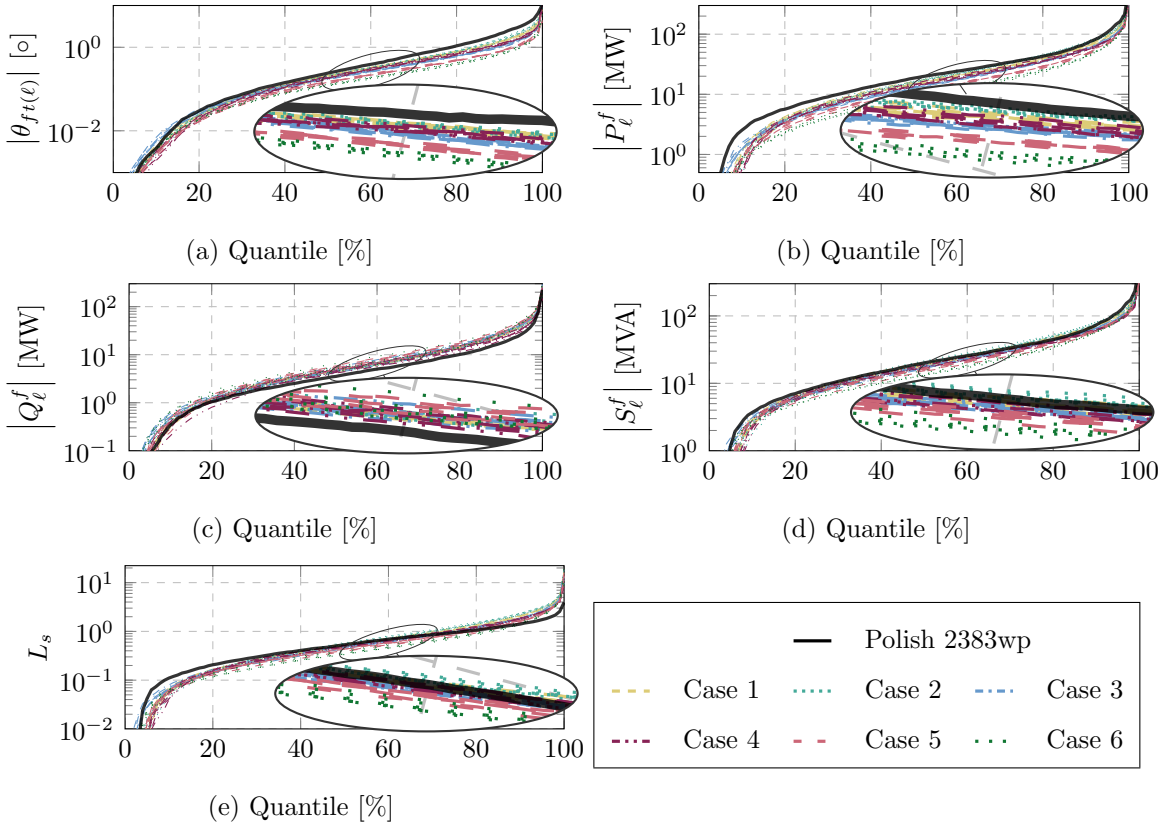

(a) Quantile [%]

(b) Quantile [%]

(c) Quantile [%]

(d) Quantile [%]

(e) Quantile [%]

Figure 3.5.1: Results for case sets in Table 3.9 compared to reference Polish 2383wp case. Each case contains 7 individual results. Zoomed in portions highlight stratification based on case in some properties, and lack thereof in others.

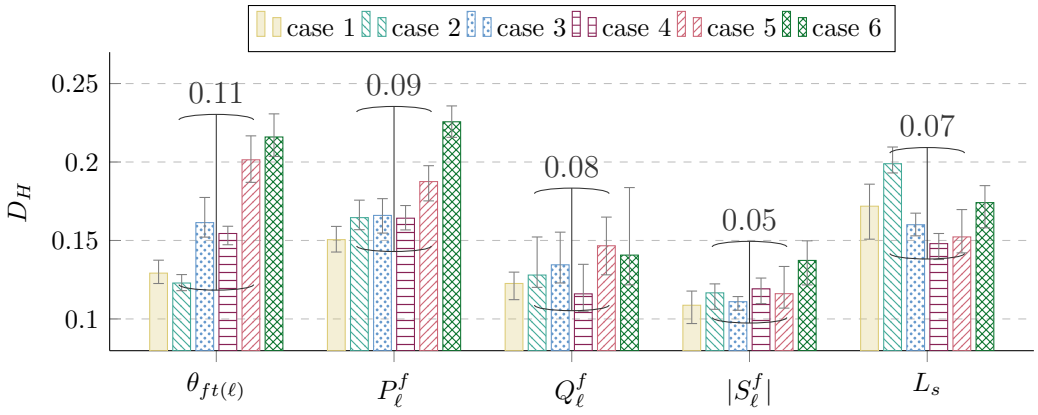

Figure 3.5.2: D_H for cases in Table 3.9 and the various properties considered. Color bars go to average values and gray error bars, $\mapsto$, show the range per case. Black brackets, $\leftrightarrow$, highlight the range over all case sets.

following modifications are adopted:

1. If multiple connected components exist, they are randomly joined with additional edges.
2. Edges are randomly removed, preserving biconnectivity, until the desired $\bar{k}$ is achieved.

Modification 2 is also used on case 2, while case 3 has the default RT inputs.

Quantile plots for all individuals in all case sets are shown in Figure 3.5.1, and D_H results for each quantity and case set are depicted in Figure 3.5.2. The two figures tell an interesting story about the impact of topology on power flow solutions.

3.5.2.1 Effect of average degree $\bar{k}$

First consider real power flow, P_ℓ^f, and the closely related $\theta_{fl(\ell)}$. In general, the cases are stratified by set, seen in Figure 3.5.1 by clear groupings. All cases from sets with $\bar{k}$ equal to the reference (1, 2, and 4) lie closer to it, and perform better according to Figure 3.5.2. Furthermore, case sets 4–6, show how increasing $\bar{k}$ reduces

overall loading on the lines, which is quite intuitive. Higher $\bar{k}$ implies more edges, which means more parallel paths, or current division. One reason why even case set 1 appears to lie a bit below the reference in Figure 3.5.1b, is that its loading is a bit lower than the reference. Slightly lower total load implies slightly reduced flows.

In contrast to P_ℓ^f, there is no clear stratification in Q_ℓ^f (cf. Figure 3.5.1c). Since reactive power is a much more local property, it makes sense that increasing the graph connectivity will not alter its flow much.

Finally, since S_ℓ^f incorporates both P_ℓ^f and Q_ℓ^f, and L_s incorporates S_ℓ^f, both properties show a mixed response to variation in $\bar{k}$. Both have a somewhat smaller range of D_H, similar to Q_ℓ^f as seen in Figure 3.5.2, but exhibit similar stratification to P_ℓ^f in Figure 3.5.1.

3.5.2.2 Effect of Topology Model

Focusing on real power and angle difference, where the topology appears to be most impactful, and comparing case set 4 (ER) to case sets 2 and 3 (RT), provides further insight on how topology influences operating conditions. With the assumption that the RT model is better than ER for power systems, case set 4 is compared to 2 and 3 in Table 3.10. Poorer $\bar{k}$ seems to outweigh a better topology model, since case set 4 outperforms case set 3. However, with equal $\bar{k}$, the RT model has superior performance with respect to P_ℓ^f and $\theta_{ft(\ell)}$, since considering the D_H for both, case set 2 outperforms case set 4.

3.5.3 OPF Related Considerations

The OPF community has expressed interest in synthetic cases, as these are critical to testing different formulations. While the objective for the synthetic cases present thus far is a realistic power flow solution, a couple OPF related results are discussed to

Table 3.10: Topology Model Comparison

case set 4	Better		
vs. case set	top. model	$\bar{k}$	avg. D_H
2	case set 2	—	case set 2
3	case set 3	case set 4	case set 4

highlight the new analysis tools available, as well as point towards further development discussed in Section 3.6. For clarity, all mention of OPF in the following always refers to AC-OPF.

Two sets of OPF solutions are considered. In one, all generators have a uniform price—arbitrarily chosen as \$10 /MW—as assumed in the placement formulation. In the other, cost information is mapped from the reference case to the synthetic cases, and these varied costs are used.

3.5.3.1 Solution Time

OPF solution time is considered first. All solutions reported in the following were solved with MATPOWER using the IPOPT solver from PARDISO [Kourounis *et al.*(2018)] on a MacBook Air, with a 2.2 GHz Intel Core i7 processor, and 8 GB of Memory. Time itself, however, is not the main focus but rather the relative times between case sets. Solution time for the reference case, as well as average times for the six case sets are shown in Figure 3.5.3.

Varied generation cost cases are a bit slower, but do not alter the trend between case sets. Namely, case sets 5 and 6 are notably slower. This can be partially explained by the fact that these have higher $\bar{k}$ and therefore more edges, which contribute to a larger number of non-linear constraints. However, case sets 5 and 3 have the same

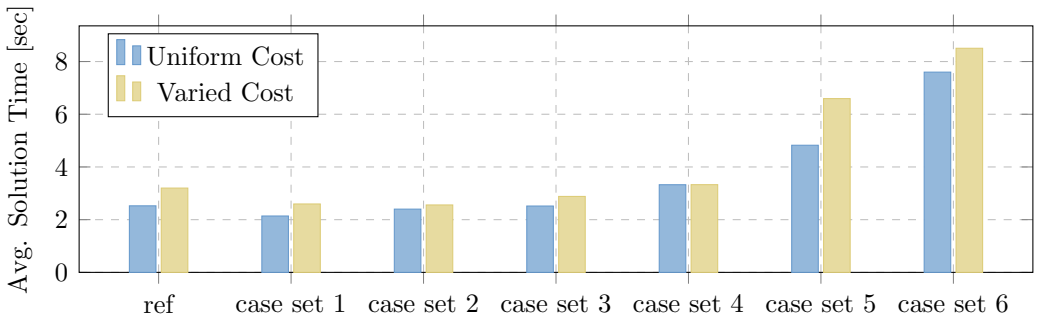

Figure 3.5.3: Comparison of average OPF solution times for the cases in Table 3.9. The solution time for the reference Polish 2383wp case is also shown with the label 'ref'.

number of edges, yet cases in set 3 solve in half the time. This suggests that the system topology—the main difference between case sets 3 and 5—may play a role in OPF solution times. Future studies could investigate whether different strategies might be more or less beneficial depending on observed topological features.

It has been reported in literature that convex relaxations return exact solutions for radial systems [Low(2014b)]. In this specific situation, a strong connection exists between system topology and solution approach performance. Synthetic cases proposed here may help in further numerical investigation of these relaxations on more general networks.

3.5.3.2 Locational Marginal Prices

LMPs are considered next. Figure 3.5.4 shows the minimum, maximum, average, and standard deviation of LMPs for all case sets. The minimum and maximum values are taken over all seven examples in each case set. For the average and standard deviation values, the mean and standard deviation is calculated for each example within a case set and those seven results are then averaged together.

Figure 3.5.4 contains some good and some not so good news. Average LMPs are similar to the reference in all cases, even when varied generation costs are added.

The spread of values is more complicated. With uniform cost, the standard deviation for several case sets is very similar to the reference. When the real generation costs are considered however, the standard deviation is somewhat less than half of the reference. Similar behavior is seen in [Xu *et al.*(2017)], where costs are assigned to the ACTIVSg2k-bus case [TAMU Electric Grid Test Cases(2017)]. Xu *et al.* design cost functions for the generators, and while the average is met by one of the approaches, the standard deviation is a third of the reference ERCOT case. In comparison, the error in standard deviation in Figure 3.5.4b is actually better.

The most troubling part of Figure 3.5.4b are the negative LMPs. While negative LMPs do occur, they are sufficiently rare that their prevalence in almost all the case sets requires further investigation. Note, however, that the number of nodes with negative LMP is small, and that not all cases exhibit them. For each case set, the number of individuals with any negative LMPs is:

Case Set	1	2	3	4	5	6
# of Inds. with Neg. LMPs	2	4	6	5	7	3

This points to a possible explanation and future work to address it. Negative LMPs occur when a cheap generator cannot operate at its maximum due to congestion, and increasing load at a node would help alleviate that congestion by creating counter flows. Systems are designed to normally have sufficient transmission paths between large loads and large generation. These results suggest that, with respect to price, the placement returned from the mathematical program presented does not achieve this quite to the degree of a real system. This is not too surprising, since generation costs are not considered in the optimization, and explains why the uniform cost results in Figure 3.5.4a are far better. Unfortunately, including generation cost in the current framework would make the objective function bilinear, since the

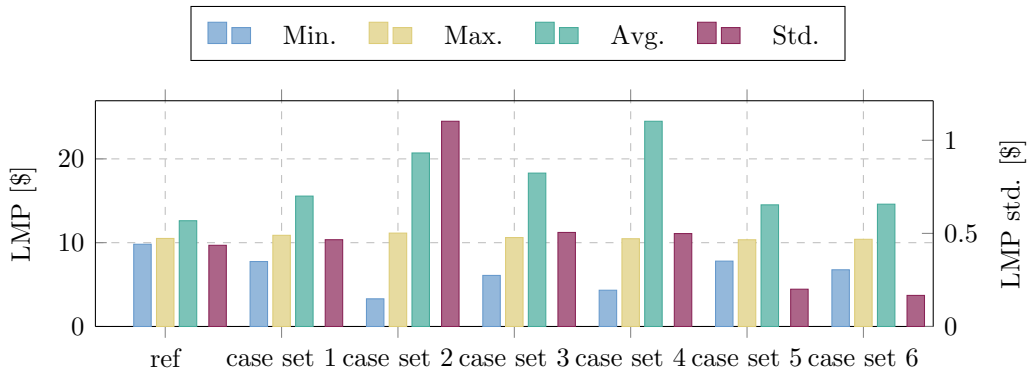

(a) Uniform generation cost

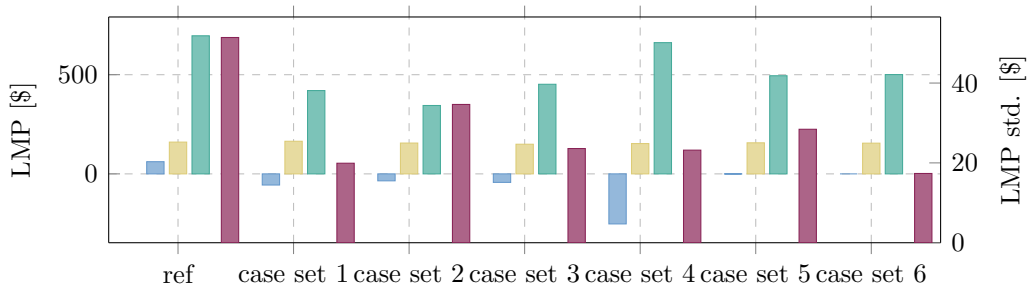

(b) Varied generation cost

Figure 3.5.4: Comparison of LMPs for the case sets in Table 3.9. Note that standard deviation values are on the right hand y-axis. Min and max values are over all seven examples in each set. For average and standard deviation, the calculation is first performed on each example in a set and then averaged over the seven examples. Values for the reference Polish 2383wp case are shown with label 'ref'.

costs must permute with matrix Π. Section 3.6 tackles this problem by switching to an EA algorithm for permutations of Π as well as Z, thus sacrificing accuracy and convergence guarantees for more flexible and detailed modeling.

3.5.4 Example Model Expansion

Power system cases are used for a variety of simulations and studies. To accommodate this variety, synthetic cases must be elaborated upon. As an example, the $N-1$ criterion with respect to generator failure is briefly considered. A detailed

study of contingency management is outside the current scope, and is left for future work. The following is intended as a proof of concept, for one way to expand the synthetic cases created with the proposed method. Simple fixed zonal reserves are used as implemented in MATPOWER's `toggle_reserves` set of callback functions. These are formulated as:

$$0 \leq R_i \leq R_i^{\max} \qquad \forall i \in \mathscr{G} \tag{3.5.1a}$$

$$P_i^g + R_i \leq P_i^{\max} \qquad \forall i \in \mathscr{G} \tag{3.5.1b}$$

$$\sum_{i \in \mathscr{G}_k} R_i \geq R_k^{\text{req}} \qquad \forall k \in \mathscr{H}, \tag{3.5.1c}$$

where $\mathscr{G}$ is the set of all generators, $\mathscr{H}$ is the set of zones, R_i are the reserves for generator i, and R_k^{req} are the required reserves for zone k. For this example, $\mathscr{H}$ consists of 3 zones, and R_k^{req} is the capacity of the largest generator in each zone. Additionally, the maximum reserve for any one generator, $R_i^{\max}$, is required to be no greater than 25% of its zones requirement:

$$R_i^{\max} = \min(P_i^{\max}, 0.25 R_k^{\text{req}}) \qquad \forall k \in \mathscr{H}, \forall i \in \mathscr{G}_k. \tag{3.5.2}$$

Note that ramp rates are neglected, partially for simplicity, and partially because they are not available in the data.

After reserves are allocated, contingencies are tested by removing reserve constraints (3.5.1), setting, $P_i^{\max} = P_i^g + R_i$, removing generators one-at-a-time and re-solving the OPF. Soft limits, summarized in Table 3.11, are used to model emergency ratings and possible second stage decisions. The voltage range is relaxed to $[0.9, 1.1]$, and line ratings may be exceeded by up to 20%. Additionally, reactive shunts can shift from their current value toward zero, for a crude model of possible STATCOM or synchronous condenser action. Although these limits *may* be violated, the high linear cost of violation encourages a solution *within* the original limits whenever possible. Before describing how the synthetic cases are minimally adjusted to

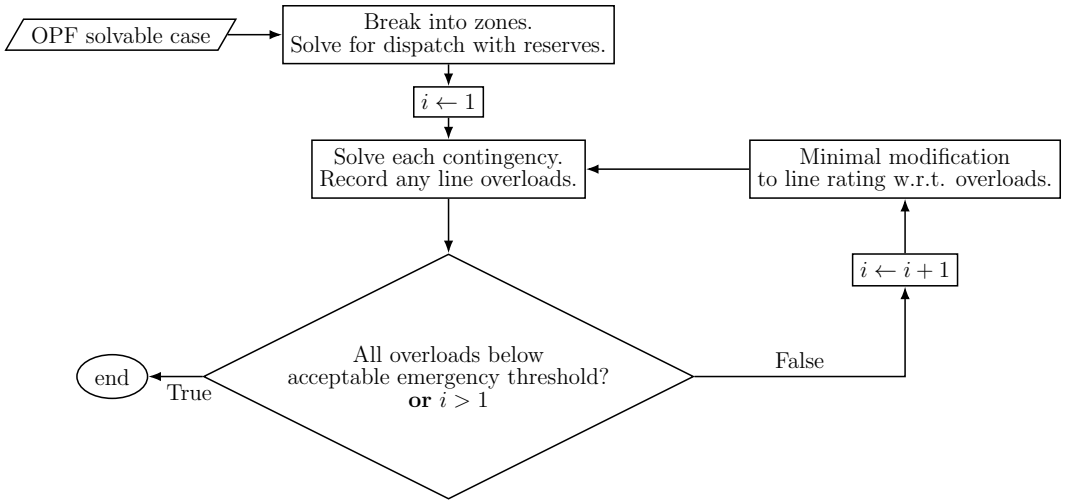

Figure 3.5.5: Example model expansion. This flowchart illustrates how the base model can be built upon to incorporate generator contingencies.

Table 3.11: Relaxed Contingency Limits

Limit	contingency limit	soft limit s
$v_{\min}$	$v_i + s_i \geq 0.95$	$0 \leq s_i \leq 0.05$
$v_{\max}$	$v_i - s_i \leq 1.05$	$0 \leq s_i \leq 0.05$
r_ℓ	$\sqrt{(P_\ell^{f,t})^2 + (Q_\ell^{f,t})^2} - s_\ell \leq r_\ell$	$0 \leq s_\ell \leq 0.2 r_\ell$
"shunt" generators	$Q_n^g - s_n = 0$	$0 \leq \text{sgn}(B^{sh}) s_g \leq \lvert B^{sh} \rvert$

accommodate generation contingencies, it should be noted that one contingency failed in the reference case under the modeling structure described.

Figure 3.5.5 provides an overview of how the synthetic cases are tested for generator contingency compliance, and minimally modified if need be. First, reserves are added to the dispatch according to (3.5.1). In a first pass, the 20% line limit violation bound is removed, and violations are recorded. If all line violations are below the prescribed threshold, then all contingencies have been satisfied. If some overloads are greater than the threshold, line ratings are minimally modified to get them within the

tolerable limit, and all contingencies are tested again. The second pass is in fact more of a check, since the modifications should resolve any issues *related to line ratings*.

The expansion module is tested on the examples in case set 1. All contingencies pass for five out of the seven synthetic examples, in one two contingencies fail, and in another a single contingency fails. Thus the ensemble results are consistent with the reference case.

A critical reader may be justifiably concerned that such modification will impact the statistics of the original inputs. To ensure that altering line limit does not adversely impact the case statistics, the two-sample Kolmogorov-Smirnov (KS) test is used on the synthetic line rating samples and the reference case samples. The KS test fails if the probability of seeing a test statistic as extreme as the one observed when two samples are in fact from the same distribution is below a level of significance α. For all but one of the examples described, the KS test passes at the traditional $\alpha = 5\%$ significance level. Where the test fails, the unmodified case fails as well, meaning that the underlying sample is somewhat further from the reference case. It is, therefore, reasonable to say that the line rating statistics are not adversely impacted by the modifications proposed. Furthermore, only about 1–2% of the lines are modified at all.

This simple example shows how the base case created by the proposed method can be expanded to other types of analysis. Due to its simplicity, it incidentally highlights another benefit of conducting analysis on ensembles of test cases. As stated on numerous occasions, the individual examples within a case set are similar yet distinct. While the proposed simple modification served to make most of the individuals $N-1$ secure with respect to generator failure, it did not succeed on all. As a comparison, the shunt placement algorithm from Section 3.4.5 successfully achieved the desired voltage profile for *all* cases. Algorithms can be better evaluated simply by

running them on ensembles. The reactive planning algorithm is quite robust, while the generator contingency algorithm requires more tweaking before it can be relied upon consistently. That is the advantage of ensemble techniques: exceptions are more likely to be found. In this case, voltage violations appear to be the reason for failure, and a more robust $N-1$ module should be considered in future work.

3.6 Non-MILP Solution

In light of the problems with the LMPs observed in Section 3.5.3.2, a solution that allows for generator prices to be considered is desired. To do so, the integer valued permutation matrices should be removed. The following describes work done as part of `syngrid`, an extension planned for MATPOWER, that will provide built in synthetic grid generation. Figure 3.6.1 provides an overview of the main program flow, which is very similar to Figure 3.4.3. The key difference is that each block contains heuristics for on how the permutations are implemented, so that no binary variables are necessary.

Additionally, each permutation block in Figure 3.6.1 can itself be a loop, where each loop produces one child individual per parent individual. For this reason, some pruning is performed after each permutation block to prevent the number of individuals from exploding. The reactive planning block at the end of Figure 3.6.1 is very similar to Section 3.4.5 except that the flow limiting shunt calculation (see Appendix B.4.2) is neglected. For this reason, it is not discussed further in the following. The initialization and two permutation blocks are presented next, as well as some sample results.

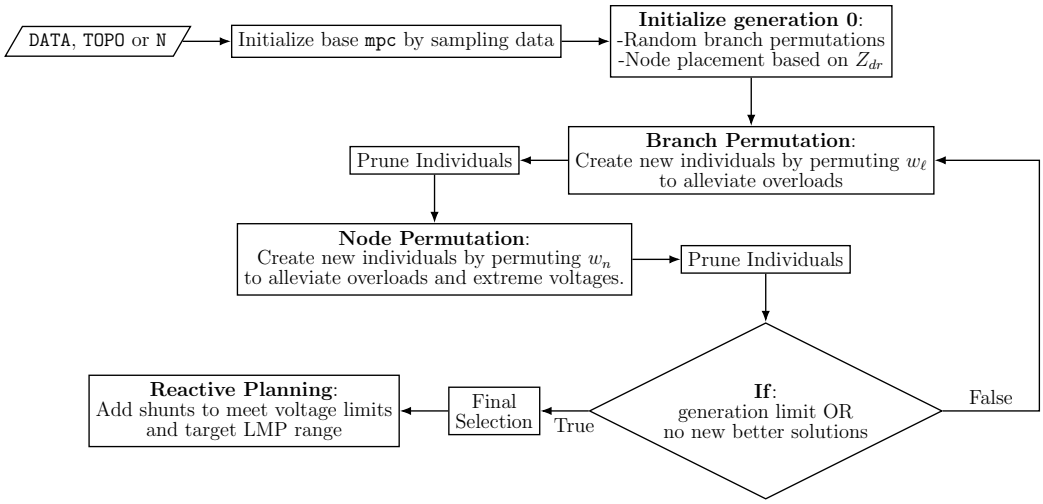

Figure 3.6.1: Flowchart overview of the placement problem solution implementation in `syngrid`.

3.6.1 Initialization

Permutation of branch parameters, w_ℓ, is in initialized randomly, at which point a preliminary Y_{bus} matrix can be constructed. The initial permutation of node parameters, w_n, derives from observations in [Schweitzer *et al.*(2016)] regarding nodes with generators and their driving point impedances, Z_{dr}, which are the diagonals of the Z_{bus} matrix. In general, it is observed that generators are located at buses with larger $|Z_{\text{dr}}|$. Within the set of buses with generators, however, there is an inverse correlation between generator size and $|Z_{\text{dr}}|$.

To achieve a similar initial relationship the smallest generator should be assigned to the largest $|Z_{\text{dr}}|$, the second smallest generator to the next biggest $|Z_{\text{dr}}|$, and so forth. However, placing all generators at the largest $|Z_{\text{dr}}|$, is a bit too extreme. Instead the fact that the kth order statistic of the Uniform distribution is distributed as $\text{Beta}(k, n-k+1)$, is used to distribute samples. Here, n is the number of samples and $\text{Beta}(\cdot)$ is the Beta distribution from (2.2.5).

Since for large n the distribution becomes quite narrow, $n = 10$ is fixed and

the 8th order statistic is chosen. Indices into a sorted array of $|Z_{\text{dr}}|$ are chosen as round$(s \cdot |\mathscr{N}|)$, where $s \sim \text{Beta}(8, 3)$. Out of these, the ones with larger $|Z_{\text{dr}}|$ are matched with the smaller generators. After the sampled buses have been assigned parameters out of w_n corresponding to generators, the remaining elements are assigned uniformly at random.

3.6.2 Branch Permutation

3.6.2.1 General Formulation

Given an operating point, the branch permutation problem can be though of as a search for permutation Z of the branch ratings, r, and impedance, $R + jX$, that minimizes overload flows. In the formulation, flows $|S_\ell^f|$ are assumed to remain constant. As the new impedances approach the old ones the likelihood of dramatic changes in flows decreases. Therefore, the difference between the old and new impedances should be minimized. The problem can be formulated as:

$$\underset{t,t^r,t^x,Z}{\textbf{Minimize}} \quad \sum_{\ell \in \mathscr{L}} (t_\ell + t_\ell^r + t_\ell^x) \tag{3.6.1a}$$

$$\textbf{Subject to} \quad t_\ell + \sum_{\ell' \in \mathscr{L}} Z_{\ell,\ell'} r_{\ell'} - |S_\ell^f| \geq 0 \qquad \forall \ell \in \mathscr{L} \tag{3.6.1b}$$

$$\begin{aligned} -t_\ell^r &\leq \sum_{\ell' \in \mathscr{L}} Z_{\ell,\ell'} R_{\ell'} - R_\ell \leq t_\ell^r \\ -t_\ell^x &\leq \sum_{\ell' \in \mathscr{L}} Z_{\ell,\ell'} X_{\ell'} - X_\ell \leq t_\ell^x \end{aligned} \qquad \forall \ell \in \mathscr{L} \tag{3.6.1c}$$

$$Z\mathbf{1} = \mathbf{1}, \quad \mathbf{1}^T Z = \mathbf{1}^T \tag{3.6.1d}$$

$$t, t_r, t_x \geq 0, \quad Z \in \{0, 1\} \tag{3.6.1e}$$

If $|S_\ell^f|$ is greater than rating $[Zr]_\ell$, constraint (3.6.1b) in conjunction with $t \geq 0$ forces t_ℓ to assume the difference magnitude and thus discourages overloads. Constraints

(3.6.1c) penalize deviation from the original impedance.

As already discussed, this problem suffers greatly from dimensionality, since Z is a $|\mathscr{L}| \times |\mathscr{L}|$ matrix. A greedy heuristic approach is therefore adopted in the following.

3.6.2.2 Greedy Permutation Approach

First, set $\mathcal{B}$ of all overloaded branches that require attention is identified:

$$\mathcal{B} = \left\{ \ell : \frac{|S_\ell^f|}{r_\ell} > \tau \quad \forall \ell \in \mathscr{L} \right\}, \tag{3.6.2}$$

where $|S_\ell^f|$ and r_ℓ are the flow and rating of branch ℓ, and τ is some ratio. Initially τ might be 1 to find only truly overloaded branches. However, it can be useful to allow τ to dip below 1, which effectively seeks capacity margins on all the branches.

For each element $\ell \in \mathcal{B}$ there is a candidate set $\mathcal{C}_\ell$ of possible branches with which to swap properties,

$$\mathcal{C}_\ell = \left\{ \ell' : r_{\ell'}\tau \geq |S_\ell^f|, |S_{\ell'}^f| \leq r_\ell \tau, \ell' \in \mathscr{L} \right\}. \tag{3.6.3}$$

That is, the set of branches whose ratings are *large* enough to support the flow on branch ℓ, and whose flows are *small* enough to be supported by branch ℓ's rating.

The remaining task is to select one candidate, $\ell^\star$, out of $\mathcal{C}_\ell$ to swap with branch ℓ. Three tests are used to determine the quality of each candidate:

Impedance Test Measures the distance between the impedance of each branch $\ell' \in \mathcal{C}_\ell$ and ℓ:

$$z_\ell(\ell') = (R_{\ell'} - R_\ell)^2 + (X_{\ell'} - X_\ell)^2. \tag{3.6.4}$$

Rating Test A Seeks the largest margin between the flow on branch ℓ and the ratings on branches $\ell' \in \mathcal{C}_\ell$:

$$m_\ell^a(\ell') = |S_\ell^f| - r_{\ell'} \tag{3.6.5}$$

Rating Test B Seeks the largest margin between the flow on each branch $\ell' \in \mathcal{C}_\ell$ and the rating of branch ℓ:

$$m_\ell^b(\ell') = |S_{\ell'}^f| - r_\ell \tag{3.6.6}$$

Lower values for all three tests are desirable and therefore, the final selection can be formalized as:

$$\ell^\star = \arg\min_{\ell' \in \mathcal{C}_\ell} w_z(\ell') z_\ell(\ell') + w_a(\ell') m_\ell^a(\ell') + w_b(\ell') m_\ell^b(\ell'), \tag{3.6.7}$$

where w_z, w_a, and w_b are used to weights to the different tests.

Letting $\text{ord}_t(\ell')$ return the order statistic of element $\ell' \in \mathcal{C}_\ell$ for test t, so that if $t(\ell')$ is the smallest $\text{ord}_t(\ell') = 1$, second smallest $\text{ord}(\ell') = 2$ etc., then the implemented weighting scheme is:

$$w_z(\ell') = \frac{\text{ord}_{z_\ell}(\ell')}{z_\ell(\ell')}, \tag{3.6.8}$$

and similarly for $w_a(\ell')$ and $w_b(\ell')$.

3.6.3 Node Permutation

The node permutation problem is solved in two steps:

1. A desired injection change, ΔP and ΔQ is sought, which, given several assumptions, should minimize overloads and stabilize the voltage profile.

2. A permutation vector π is sought that best achieves the desired change in injection calculated in Step 1.

3.6.3.1 Desired Injection Change

Bus and branch effects of changing injections, ΔP and ΔQ, are captures by linearizing the power flow around the given operating point. Voltage effects are related via the

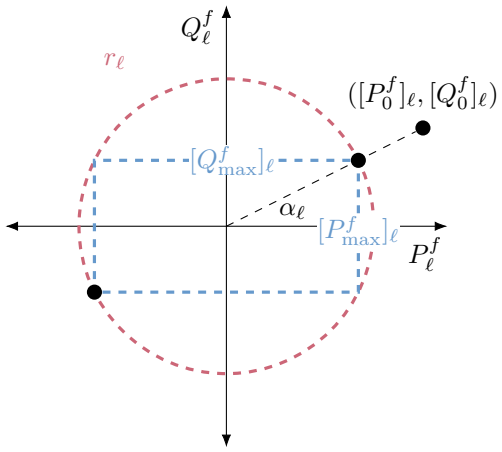

Figure 3.6.2: Geometrical depiction of how line limits are set during the node permutation procedure.

columns of the system Jacobian associated with the voltage magnitude,

$$\begin{pmatrix} \Delta P \\ \Delta Q \end{pmatrix} = J_v \Delta v, \tag{3.6.9}$$

and the branch flow effects are captured using AC-Power Transfer Distribution Factors (PTDFs),

$$\begin{pmatrix} \Delta P^f \\ \Delta Q^f \end{pmatrix} = H^f \begin{pmatrix} \Delta P \\ \Delta Q \end{pmatrix}, \tag{3.6.10}$$

where Δv, is the change in voltage magnitude, and ΔP^f and ΔQ^f are changes in real and reactive line flows. Appendix B.3 provides a derivation of the AC-PTDFs.

To create linear constraints on branch flows, the angle of flow on line ℓ,

$$\alpha = \begin{cases} \arctan\left(\frac{Q^f_\ell}{P^f_\ell}\right) & P^f_\ell \geq 0 \\ \pi - \arctan\left(\frac{Q^f_\ell}{P^f_\ell}\right) & P^f_\ell < 0, \end{cases} \tag{3.6.11}$$

is considered. New flows are only allowed to vary inside the box defined by the intersection points of the rays with angle α and $-\alpha$ and the limit circle of radius r_ℓ as shown in Figure 3.6.2. The effective limits are thus,

$$[P^f_{\max}]_\ell = r_\ell \cos(\alpha_\ell), \quad [Q^f_{\max}]_\ell = r_\ell \sin(\alpha_\ell). \tag{3.6.12}$$

With, P_0^f, Q_0^f, and v_0 as the initial real and reactive flows, and voltage magnitude, the desired injection change is formulated as the solution to:

$$\underset{\Delta P, \Delta Q, \Delta v}{\textbf{Minimize}} \quad \|\Delta P\|_1 + \|\Delta Q\|_1 + w_p^T s_p + w_q^T s_q + w_v \cdot s_v \tag{3.6.13a}$$

$$\textbf{Subject to} \quad \begin{pmatrix} \Delta P \\ \Delta Q \end{pmatrix} - J_v \Delta v = 0 \tag{3.6.13b}$$

$$v_{\min} - v_0 - s_v \leq \Delta v \leq v_{\max} - v_0 + s_v \tag{3.6.13c}$$

$$-\begin{pmatrix} P_{\max}^f + s_p \\ Q_{\max}^f + s_q \end{pmatrix} \leq \begin{pmatrix} P_0^f \\ Q_0^f \end{pmatrix} + H^f \begin{pmatrix} \Delta P \\ \Delta Q \end{pmatrix} \leq \begin{pmatrix} P_{\max}^f + s_p \\ Q_{\max}^f + s_q \end{pmatrix} \tag{3.6.13d}$$

$$\mathbf{1}^T \Delta P = 0, \quad \mathbf{1}^T \Delta Q = 0 \tag{3.6.13e}$$

$$-\Delta P_{\max} \leq \Delta P \leq \Delta P_{\max}, \quad -\Delta Q_{\max} \leq \Delta Q \leq \Delta Q_{\max} \tag{3.6.13f}$$

Constraint (3.6.13e) forces the net change to be zero, since in the end a permutation is sought, and the limits in (3.6.13f) are simply the range of the initial injections vector. Additionally, slack variables are added to allow feasibility even in the event that some violations cannot be avoided.

Finally, the desired new nodal injections, $P^\star$ and $Q^\star$ are defined as:

$$\begin{pmatrix} P^\star \\ Q^\star \end{pmatrix} \triangleq \begin{pmatrix} P^0 \\ Q^0 \end{pmatrix} + \begin{pmatrix} \Delta P \\ \Delta Q \end{pmatrix}, \tag{3.6.14}$$

where, P^0 and Q^0 are the initial injection vectors. The next section seeks a permutation to achieve the desired injections.

3.6.3.2 Greedy Permutation Approach

The "errors" in real and reactive injection are defined as,

$$\begin{aligned} \epsilon_p &= P^\star - P^0 \\ \epsilon_q &= Q^\star - Q^0, \end{aligned} \tag{3.6.15}$$

and the total magnitude error is,

$$\epsilon = \sqrt{\epsilon_p^2 - \epsilon_q^2}. \tag{3.6.16}$$

The greedy node permutation approach fixes each error sequentially, beginning with the largest. That is, vectors $P^\star$, P^0, $Q^\star$, Q^0 are sorted such that $\epsilon_1 \geq \epsilon_2 \geq \ldots \geq \epsilon_{|\mathscr{N}|}$. Then Algorithm 11 returns the desired permutation vector π. Iterating over all buses, the nearest injection to the desired injection at bus i is found in set x. The selected bus is then removed from the set so that the final result will be a true permutation.

Algorithm 11 Greedy Node Permutation

procedure GREEDY NODE PERMUTE($P^\star$, P^0, $Q^\star$, Q^0)
  $x \leftarrow \{1, 2, \ldots, |\mathscr{N}|\}$
  for $i \in \{1, 2, \ldots, |\mathscr{N}|\}$ **do**
    $\pi(i) \leftarrow \arg\min_{j \in x} \left|P_i^\star - P_j^0\right| + \left|Q_i^\star - Q_j^0\right|$
    $x \leftarrow x \setminus \{\pi(i)\}$
  end for
  return π
end procedure

3.6.4 Sample Results

As a demonstration that the approach described improves on the LMP results from Section 3.5.3.2, a test using the ACTIVSg2k case [TAMU Electric Grid Test Cases(2017)] as the seed to the sampling block in Figure 3.6.1 is performed. Five cases are selected at the end of the EA iterations and passed to the reactive planning

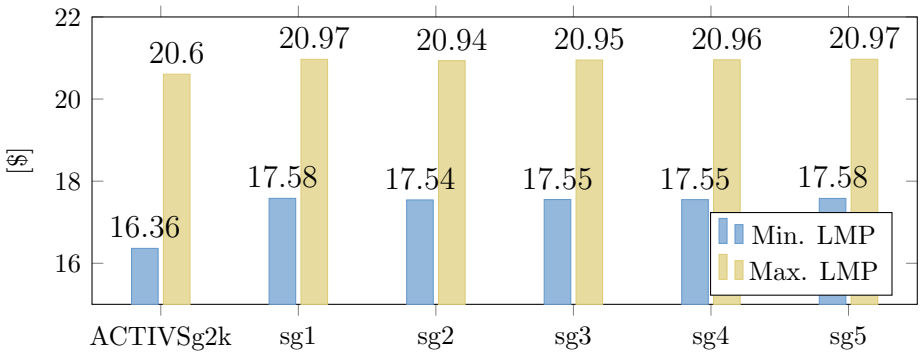

Figure 3.6.3: Range of LMPs for 5 synthetic cases 'sg1'–'sg5' created compared to their seed reference case, the ACTIVSg2k case.

stage. The LMP ranges for the original ACTIVSg2k-bus case, as well as the five synthetic samples are shown in Figure 3.6.3.

First, no negative LMPs exist, which was the primary target for improvement. Second, the ranges are quite similar. The slight differences can be attributed to multiple factors, not least among them is that the synthetic cases do not have the same generation fleet as the ACTIVSg2k and therefore, the cost distribution is understandably not quite the same.

3.7 Related Publications

Work relating to analysis and validation presented largely in Sections 3.1 and 3.2 is published in [Schweitzer *et al.*(2017b)] and [Schweitzer *et al.*(2018d)]. A DC only version of the placement problem is published in [Schweitzer *et al.*(2018c)], and the fuller AC development comes from [Schweitzer and Scaglione(2018)]. The analysis leading to the placement initialization based on Z_{dr} comes from [Schweitzer *et al.*(2016)].

— PART II —

Using Synthetic Power System Models

CHAPTER 4

TRANSMISSION & DISTRIBUTION CO-SIMULATION

A conceptual description of the problem addressed in this chapter is shown in Figure 4.0.1. While specific TnD solvers are named in the figure, these are simply the ones used in the following; the modeling principles hold irrespective of solver. The main contribution is to combine [Huang and Vittal(2016)] and [Sun *et al.*(2015)], allowing for three-sequence treatment of the transmission system, as well as closed loops through distribution. It further expands on the work in [Sun *et al.*(2015)], by explicitly deriving how an equivalent branch can be calculated, and validating against a complete transmission and distribution model. In addition, the impact of equipment configurations, specifically the distribution transformer, on co-simulation modeling choices is considered.

While most distribution circuits operate radially, the ability to include distribution

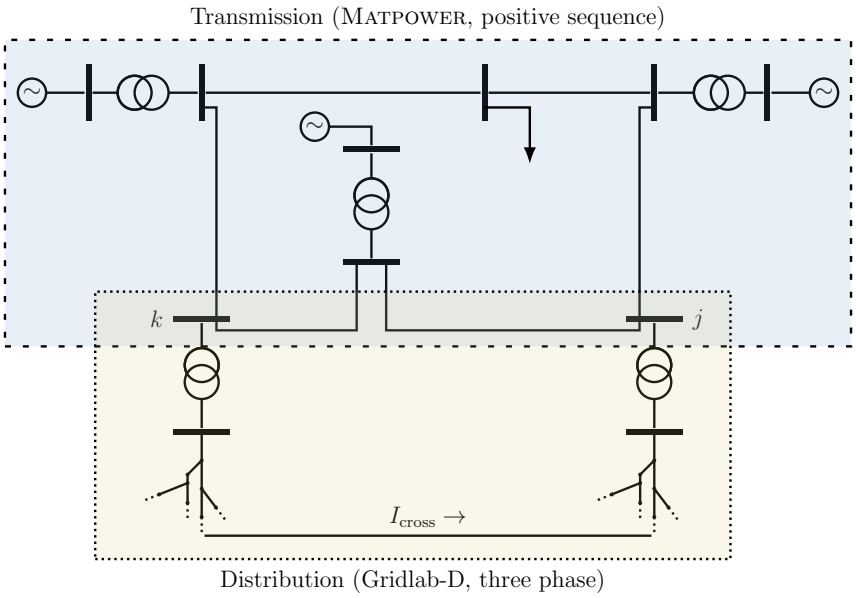

Figure 4.0.1: Conceptual set-up for the TnD co-simulation problem.

loops adds value in certain cases:

- Whenever sub-transmission is modeled along with low voltage feeders in three phase detail, several transmission substations are coupled by the model.
- Meshed distribution systems are found in denser urban areas.
- Future operation concepts could be explored with the aid of co-simulation tools, as to whether relaxing the radial constraint is advantageous for distribution feeders under certain conditions (e.g. high solar penetration).
- Depending on the particular scheme and speed of operation, current loops via distribution may temporarily exist during a reconfiguration action.

The rest of the chapter is organized as follows. Section 4.1 develops the co-simulation model. Section 4.2 shows results to both validate the model, and highlight the impact of decisions on the solution quality, and Section 4.3 further discusses possible explanations for those impacts.

4.1 Model Description

The complete co-simulation procedure is shown in Figure 4.1.1. Highlighted blocks are described in detail in the subsequent subsections.

4.1.1 Equivalent Impedance

The flow between transmission buses via the distribution system is captured by equivalent branches that are added to the transmission model similar to [Sun *et al.*(2015)]. Since [Sun *et al.*(2015)] does not explain how the equivalent model is calculated, a solution method is described here. Connections between any pair of transmission nodes through distribution, are modeled using the Thévenin equivalent

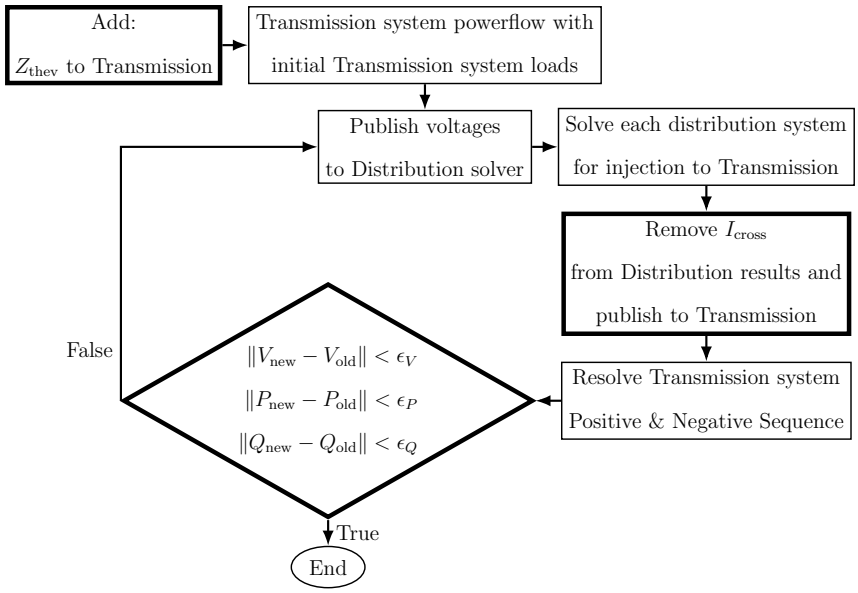

Figure 4.1.1: Flow chart for coupled TnD co-simulation. Highlighted nodes are elaborated on in subsections 4.1.1–4.1.3.

impedance, Z_{thev}, of the distribution system connecting the pair. Since the distribution model is three-phase, Z_{thev} is a 3×3 matrix. The following expands to block matrices classic derivations from [Grainger and Stevenson(1994), Chapter 8].

The relationship between voltages at buses k and j with respect to a current injected at bus k and withdrawn at bus j , absent other injections, is desired, as illustrated in Figure 4.1.2. Letting V_i^{abc} and I_i^{abc} be 3×1 vectors of complex nodal voltage and current at bus i, $Z_{m,n}$ are 3×3 matrices of complex impedance, and $\mathbf{0}$ a matrix of zeros of appropriate size, this relationship is expressed as

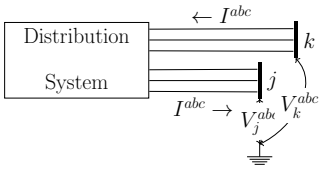

Figure 4.1.2: Circuit for Thévenin calculation.

$$\begin{bmatrix} \vdots \\ V_k^{abc} \\ \vdots \\ V_j^{abc} \\ \vdots \end{bmatrix} = \begin{bmatrix} & & \\ Z_{kk} & \dots & Z_{kj} \\ \vdots & & \vdots \\ Z_{jk} & \dots & Z_{jj} \\ & & \end{bmatrix} \begin{bmatrix} \mathbf{0} \\ I^{abc} \\ \mathbf{0} \\ -I^{abc} \\ \mathbf{0} \end{bmatrix} \tag{4.1.1}$$

$$V_k^{abc} - V_j^{abc} = \underbrace{\left(Z_{kk} + Z_{jj} - Z_{kj} - Z_{jk}\right)}_{Z_{\text{thev},kj}} I^{abc}.$$

The desired components of the Z matrix can be calculated from the triangular factors of the admittance matrix, whose inverse is multiplied by a banded matrix,

$$\begin{array}{c} \begin{array}{ccccccc} I_k^a & I_k^b & I_k^c & & I_j^a & I_j^b & I_j^c \end{array}^T \\ \begin{pmatrix} 1 & & & & -1 & & \\ & 1 & & & & -1 & \\ & & 1 & & & & -1 \\ \mathbf{0} & & & \mathbf{0} & & & \mathbf{0} \end{pmatrix} \end{array} . \tag{4.1.2}$$

The result are the columns of Z corresponding to bus j subtracted from those corresponding to bus k. Therefore, the bus k *rows* contain $Z_{kk} - Z_{kj}$, while the bus j *rows* contain $Z_{jk} - Z_{jj}$. Subtracting the latter from the former gives the desired result: $Z_{\text{thev},kj} = Z_{kk} + Z_{jj} - Z_{kj} - Z_{jk}$.

An equivalent branch is added between each pair of transmission system nodes coupled through distribution. First, the three-phase, real-units matrix is converted to sequence, per-unit values. The $(1,1)$, $(2,2)$, and $(3,3)$ entries of the inverse are

taken as the zero, positive, and negative sequence admittances and added to their respective transmission models.

4.1.2 Accounting for Cross Currents

Since the distribution system under consideration creates a current path between transmission nodes, a current, I_{cross}, will flow *in* one node and *out* another rather than be consumed as load. An admittance matrix, Y_{eq}, of all the equivalent branches is constructed to calculate I_{cross} using the full 3×3 primitives rather than just the diagonal entries as described in the previous section. For example, when only two nodes, k and j, are coupled through distribution, Y_{eq} will be a 6×6 matrix,

$$\begin{bmatrix} Y_{\text{thev},kj} & -Y_{\text{thev},kj} \\ -Y_{\text{thev},jk} & Y_{\text{thev},jk} \end{bmatrix}. \tag{4.1.3}$$

Letting the *known* transmission voltages be V_{coupled}, the currents between them due to voltage differences are

$$I_{\text{cross}} = Y_{eq} V_{\text{coupled}}. \tag{4.1.4}$$

These are subtracted from the injected currents, I_{inj}, to give the final load current,

$$I_{\text{load},k} = I_{\text{inj},k} - I_{\text{cross},k}. \tag{4.1.5}$$

In a similar manner to [Huang and Vittal(2016)], I_{load} is passed back to the transmission system as three sequence load. The complex, positive sequence load at bus k is calculated using the positive sequence current, $I_k^{(+)}$, and positive sequence voltage $V_k^{(+)}$:

$$S_k = 3V_k^{(+)} \left(I_k^{(+)}\right)^*. \tag{4.1.6}$$

Negative and zero sequence currents, are used directly to solve

$$I^{(0)} = Y^{(0)} V^{(0)} \quad \text{and} \quad I^{(-)} = Y^{(-)} V^{(-)}. \tag{4.1.7}$$

4.1.3 Iteration Termination

Most algorithms in literature use a voltage-based criteria to terminate iteration between federates, i.e., when transmission node voltages change less than some threshold, ϵ_V, between subsequent iterations. As shown in Figure 4.1.1 similar thresholds are imposed for real and reactive loads, ϵ_P and ϵ_Q, in addition to the voltage-based criterion. These criteria are needed since the coupled connection redistributes load between the feeders. While transmission voltage is quite stiff, the exact load magnitude is occasionally more sensitive.

4.2 Results

To test the proposed approach, simulations connecting PNNL prototypical taxonomy feeders [Schneider *et al.*(2008)] modeled in GridLAB-D [GridLAB-D(2018)] to the IEEE 118-bus case modeled in MATPOWER [Zimmerman *et al.*(2011)] are performed. Feeders are connected to transmission buses whose load best matches the total feeder load[1]. All termination thresholds are set to 0.1% change between consecutive iterations. As described in the previous section, at each iteration the transmission system sends voltages at coupled nodes to the distribution systems, who return loads. Other transmission cases have been tested with similar results but are omitted for presentation clarity. The method described is quiet general and can model multiple loops, however, again for presentation clarity only two feeders at a time are modeled, unless otherwise stated.

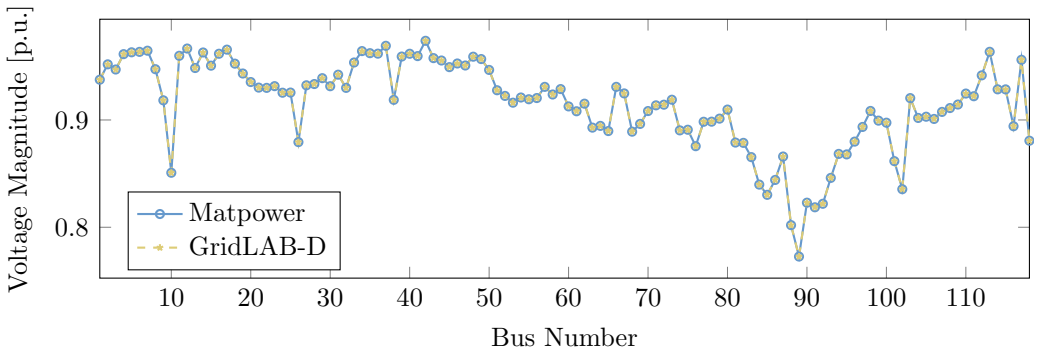

Figure 4.2.1: Node voltages for the 118-bus case in MATPOWER and GridLAB-D, showing a good translation of the model.

4.2.1 Validation Method

Co-simulation results are validated against a full, three-phase model of the combined TnD system constructed in GridLAB-D, which is taken as ground-truth. "Error" in the co-simulation therefore means deviations from the full model solution. Surprisingly, such validation is lacking from [Sun *et al.*(2015)], which only compares the co-simulation result to independent transmission and distribution solutions.

Given the differences between the MATPOWER and GridLAB-D data models, translation is needed. Figure 4.2.1 demonstrate that solutions in both solvers are sufficiently similar, validating the translation. The code for translating the model is provided in Appendix C.1.

4.2.2 Main result

Forty five tests are constructed by selecting a different pair of taxonomy feeders out of a library of nine (pairs of the same feeder are allowed). Since a common Δ-Y substation transformer configuration is used, zero sequence currents are neglected in

[1]Several nodes in the IEEE 118-bus system have smaller loads ($< 20\,\text{MW}$) that closely match the PNNL prototypical feeders.

the transmission model, as they cannot exit the delta connection. After running both co-simulation and full simulation for each case, phase voltages and currents at a few key spots are compared:

Voltages
- Distribution coupled transmission nodes.
- Distribution nodes at the coupling switch.

Currents
- Substation step down transformers.
- Feeders' coupling switch.

Figure 4.2.2 shows the maximum percent errors in each phase for the 45 cases. Current error on phase A, for example, is

$$\text{percent current error} = 100 \times \frac{|I_{A,\text{co-simulation}} - I_{A,\text{full}}|}{|I_{A,\text{full}}|}. \tag{4.2.1}$$

While all the voltage errors are quite small, there are a few somewhat larger current errors. The reason for these larger percent errors is due to a smaller denominator, rather than poorer performance. This is highlighted by the overlaid points in Figure 4.2.2a showing the magnitude of the current in the full simulation. Errors exceeding 5% are out of 15 A or less. In this respect current errors are also very reasonable.

The impact of a few modeling choices are considered next by focusing on a single case, the first from the series in Figure 4.2.2.

4.2.3 Convergence

Since [Huang *et al.*(2017)] shows that co-simulation without iteration between federates is possible, the convergence characteristics in these tests is considered. To that end an additional test is introduced, where another feeder is connected, so that three substations in the 118-bus system are coupled via distribution feeders. Figure 4.2.3 shows how the real and reactive powers converge to their final quantities at bus 23 of the transmission system.

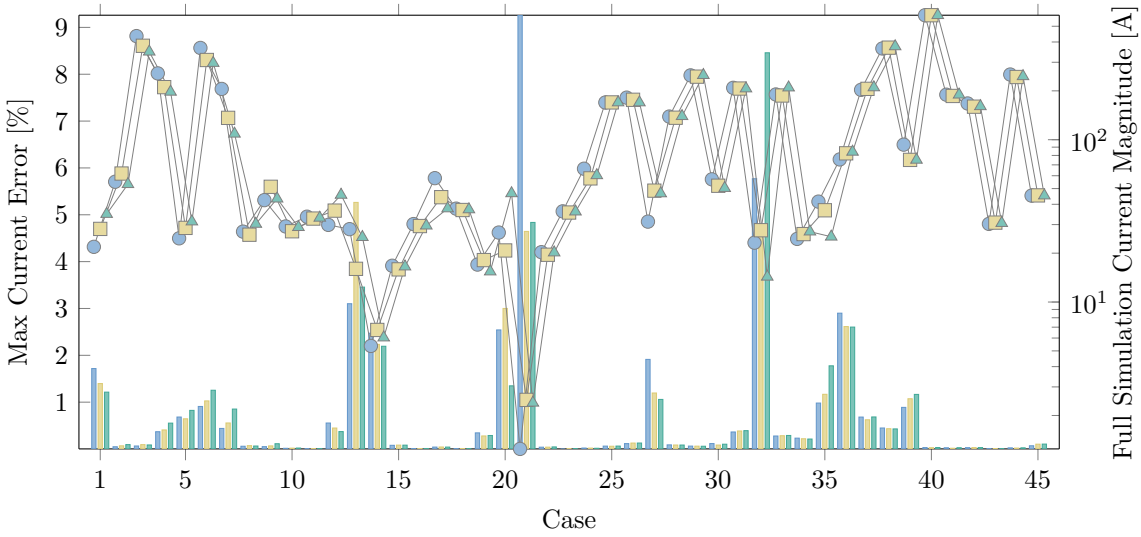

(a) Per-phase current error (bars) and magnitude (markers). Phase colors are consistent between bars and markers.

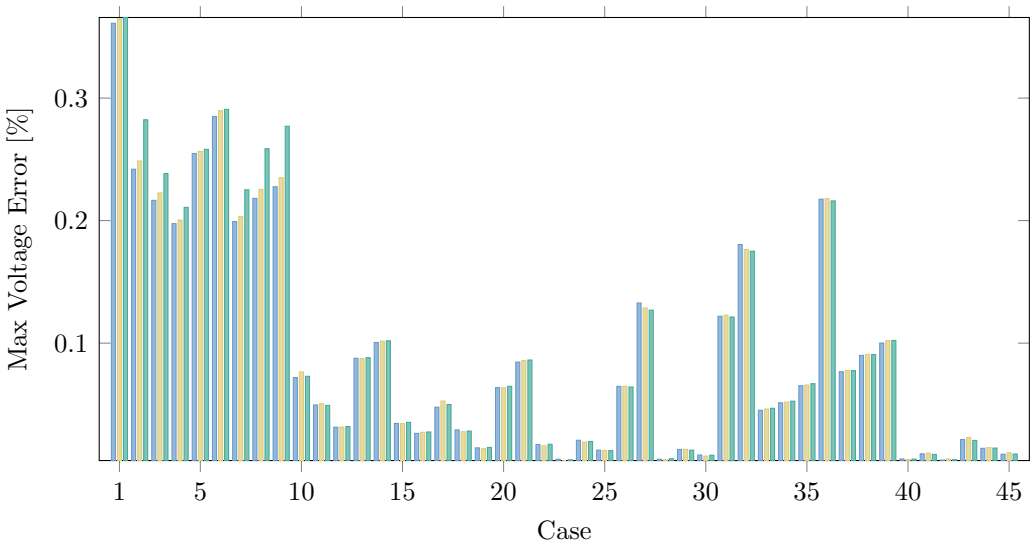

(b) Voltage error

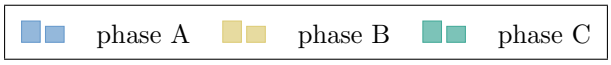

Figure 4.2.2: Maximum percent errors between co-simulated results and full case.

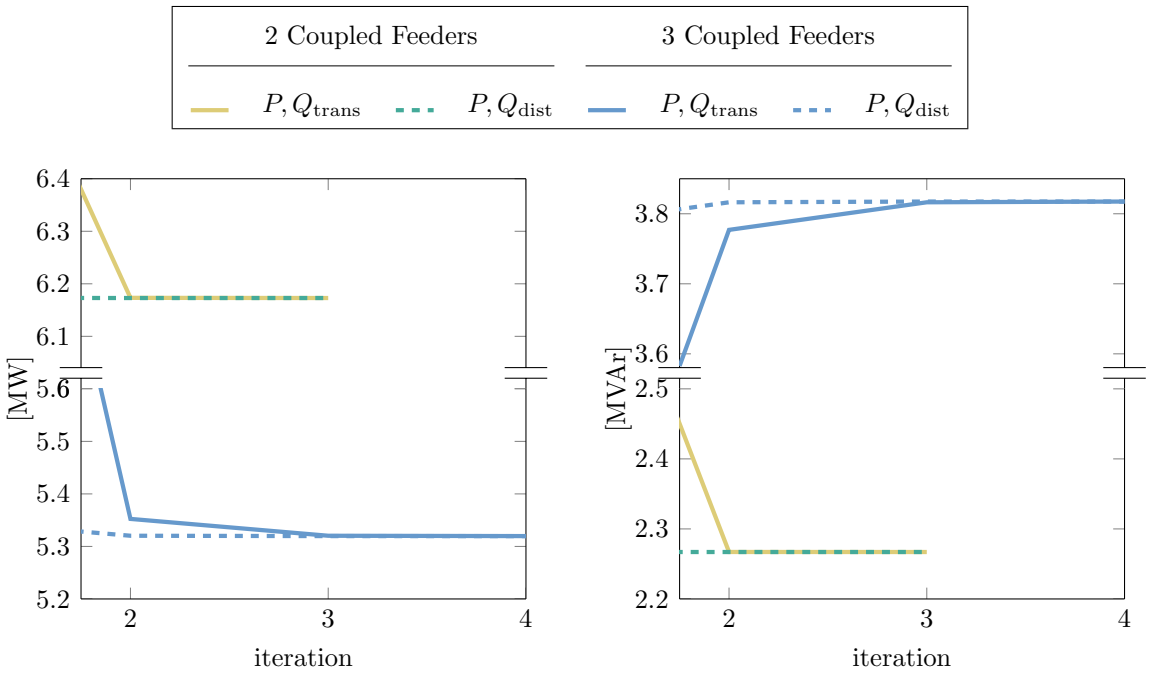

(a) Positive Sequence Real Power Convergence (b) Positive Sequence Reactive Power Convergence

Figure 4.2.3: Convergence of load termination criteria for Case 1 in Figure 4.2.2, as well as a modification where an additional third feeder is added.

Some of the change between iterations 1 and 2 is due to initial model mismatch, which is why Figure 4.2.3 begins at iteration two. Better initial matching should somewhat minimize these jumps. A portion, however, is load rebalancing between the feeders due to the coupling. This is highlighted by the slower convergence in the altered case with three coupled substations.

Quick convergence in for the original case seems to support the findings in [Huang *et al.*(2017)] that re-iteration is unnecessary. However, as the degree of coupling increases so does the necessity for iteration. These results also highlight the need for convergence criteria beyond voltage. Voltages traces are not shown since they are practically straight lines. Even very small voltage changes, however, result in more noticeable impacts in distribution loads, which should be taken into account.

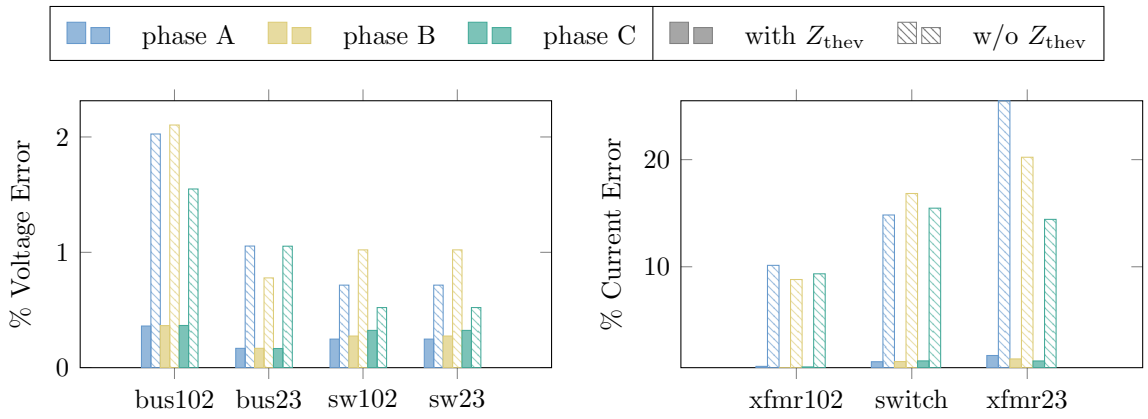

(a) Voltage Error

(b) Current Error

Figure 4.2.4: Impact of equivalent impedance branch addition to the transmission model on co-simulation errors. Label 'sw23' refers to the node at the coupling switch on the side of transmission bus 23's feeder.

4.2.4 Impact of Equivalent Branch

The impact of adding equivalent branches to the transmission model as first suggested by [Sun *et al.*(2015)] is investigated in this section. Using the setup from Section 4.2.2 the co-simulation is run twice: with and without the equivalent branch. In both cases, however, Z_{thev} is still calculated and used to determine I_{cross} as in Section 4.1.2. Figure 4.2.4 shows that the case *with* the equivalent branch (solid bars) has significantly smaller errors, suggesting that modifying the transmission model is critical.

4.2.5 Impact of Including Sequence Models

Finally, the benefits of using negative and zero sequence models in transmission, as done in [Huang and Vittal(2016)], are considered. The co-simulation is performed three times, where transmission is modeled with: 1) only positive sequence, 2) positive and negative sequence, and 3) all three. Additionally, both Δ-Y and Y-Y step-down

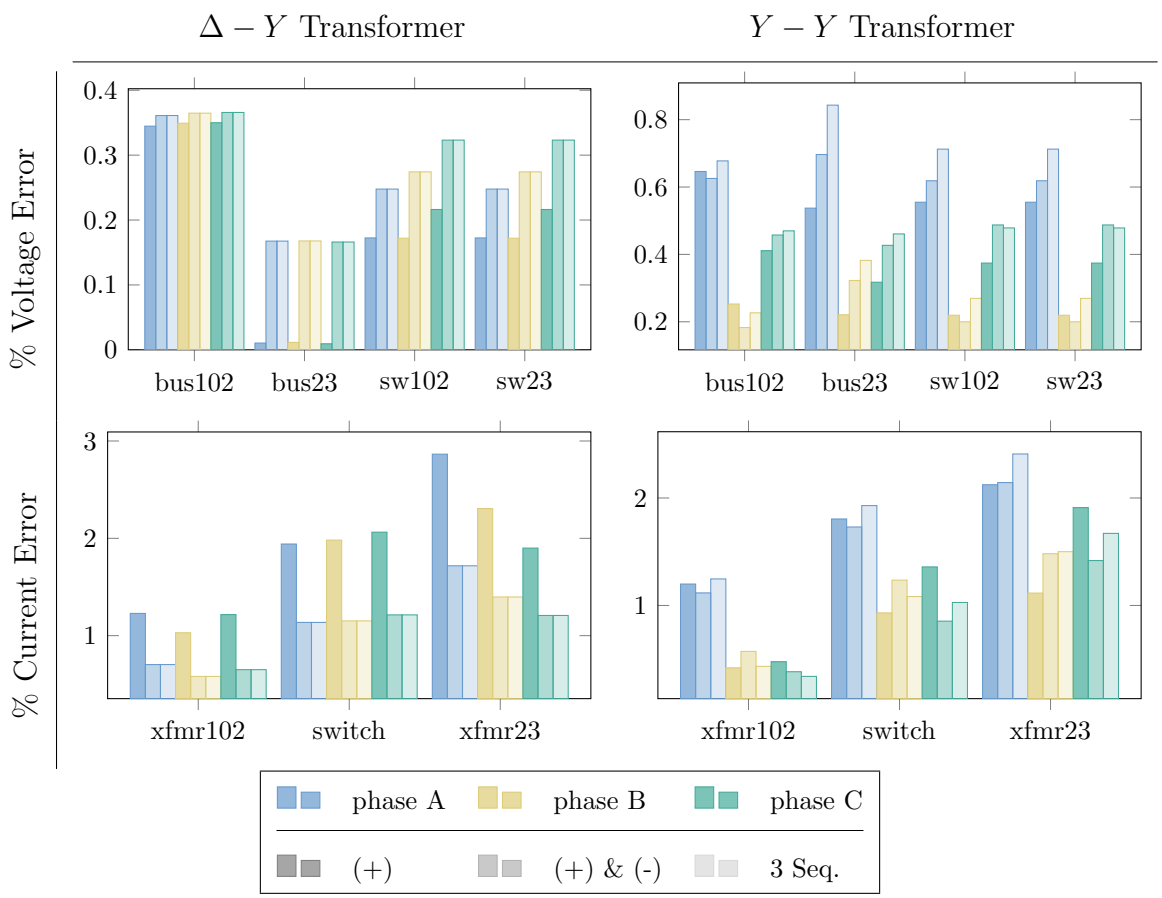

Figure 4.2.5: Impact of additional sequences, as well as different step-down transformer models on co-simulation errors.

transformer configurations are tested.

Figure 4.2.5 summarizes the results. As expected, there is no impact of including zero sequence with the Δ-Y transformer. Surprisingly, voltage error almost always *increases* with additional sequences, while current errors, form a more complicated picture. Performance improves for Δ-Y transformers, while with Y-Y it is unclear.

This analysis suggests that variable solution approaches may be desirable, depending on system configuration. It is worth emphasizing however, that errors are small in all cases.

Table 4.1: Comparison between Z_{thev} with Δ-Y and Y-Y connected step-down transformers.

$Z_{\text{thev},\Delta-Y}$ [p.u.]			$Z_{\text{thev},Y-Y}$ [p.u.]		
0.00	0	0	$2.02+4.98j$	$\mathbf{0.19-0.09j}$	$-0.04+0.01j$
0	$1.04+2.02j$	$0.08+0.04j$	$-0.05+0.01j$	$1.04+2.03j$	$0.08-0.05j$
0	$0+0.02j$	$1.04+2.02j$	$\mathbf{0.19-0.09j}$	$-0.02+0.00j$	$1.04+2.02j$

4.3 Discussion

Section 4.2.5 suggests that including additional sequence models could be *disadvantageous*. This unexpected result merits further discussion. Essentially, the errors arise from the transmission model assumption that sequences are decoupled.

The Thévenin equivalent impedances from the previous section are shown in Table 4.1 for both Δ-Y and Y-Y connected step-down transformers. Non-zero off-diagonals represent the degree of coupling between the sequences. In co-simulation, the transmission model neglects the coupling, while the distribution model does not.

When transmission sequence voltages are translated to three-phase at the substation nodes, mismatch errors occur due to the decoupled assumption. These, errors propagate through the distribution system, resulting in current errors. As seen in Figure 4.3.1a, negative sequence voltage errors are greater at the substation buses (102 and 23) than at the switch nodes (sw102 and sw23), which are further down the feeder. Conversely, negative sequence current errors are much more pronounced in the switch than in the substation transformers (cf. 4.3.1b). Larger coupling terms in $Z_{\text{thev},Y-Y}$ compared with $Z_{\text{thev},\Delta-Y}$ in Table 4.1 help explain why errors increase more in Figure 4.2.5 when additional sequences are added to the Y-Y configuration than the Δ-Y one. Incorporating additional sequences in transmission is thus a balancing act between extra information and the related approximation errors.

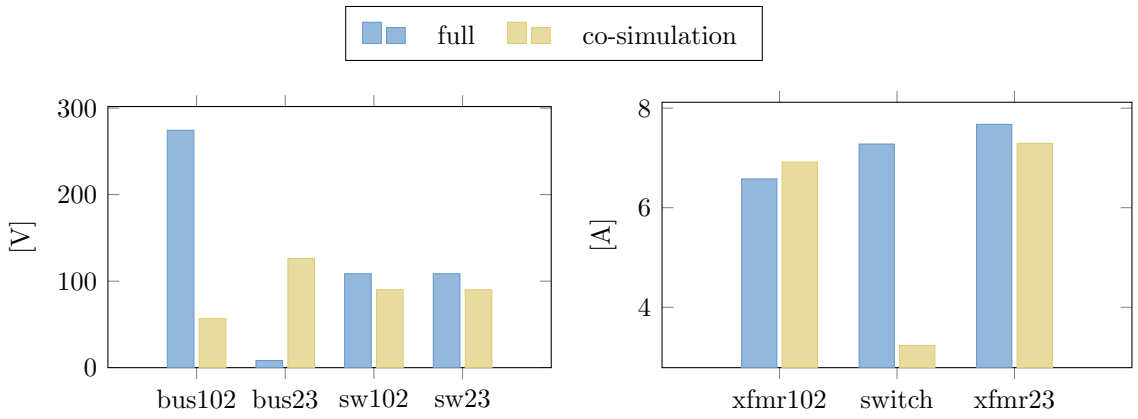

(a) Negative Sequence Voltage Magnitudes

(b) Negative Sequence Current Magnitudes

Figure 4.3.1: Negative sequence errors with Δ-Y step-down transformers.

4.4 Related Publications

This work was first published as [Schweitzer *et al.*(2018a)] in the 2018 proceedings of the IEEE's Power and Energy Society, where it was named one of four best papers.

CHAPTER 5

LOSSY DISTFLOW

Where the previous chapter uses synthetic feeders to create a larger TnD co-simulation case, this chapter uses synthetic data to help train and validate an algorithm. The DistFlow formulation, and specifically its linear, lossless variant, has recently been used to study how inverter VAr control settings could be determined in a decentralized manner [Zhu and Liu(2016), Baker *et al.*(2018)]. Motivation is drawn from these efforts to maintain the mathematical properties of lossless DistFlow, useful for analysis, while improving accuracy. Single and multiphase formulations are developed as matrix-vector equations with similarities noted between the two derivations. The parametrization to approximate line losses and reduce error is performed numerically utilizing synthetic feeders from Chapter 2.

5.1 Single Phase Balanced

Balanced systems are considered first in their single phase representation. As such, in this section, all Φ_j are singletons, making V_j, I_ℓ, and z_ℓ scalars. Real and reactive load and flows are also handled separately, e.g. $s_j^Y = p_j + jq_j$.

5.1.1 Matrix-Vector Formulation

The classic DistFlow [Baran and Wu(1989)] equations are,

$$P_\ell = p_j + r_\ell c_\ell^2 + \sum_{\ell' \in f^{-1}(j)} P_{\ell'} \tag{5.1.1a}$$

$$Q_\ell = q_j + x_\ell c_\ell^2 + \sum_{\ell' \in f^{-1}(j)} Q_{\ell'} \tag{5.1.1b}$$

$$v_i^2 - v_j^2 = 2(r_\ell P_\ell + x_\ell Q_\ell) - (r_\ell^2 + x_\ell^2) c_\ell^2, \tag{5.1.1c}$$

where $(f(\ell), t(\ell)) = (i, j)$, $c_\ell^2 = |I_\ell|^2$, and P_ℓ and Q_ℓ are the *sending* end real and reactive power flows on branch ℓ, such that,

$$v_i^2 c_\ell^2 = P_\ell^2 + Q_\ell^2. \tag{5.1.2}$$

Define the following $|\mathscr{L}| \times |\mathscr{N}|$ connection matrices,

$$\begin{aligned} [\boldsymbol{F}]_{\ell,i} &= \begin{cases} 1 & f(\ell) = i,\ \ell \in \mathscr{L}, i \in \mathscr{N} \\ 0 & \text{otherwise} \end{cases} \\ [\boldsymbol{T}]_{\ell,j} &= \begin{cases} 1 & t(\ell) = j,\ \ell \in \mathscr{L}, j \in \mathscr{N} \\ 0 & \text{otherwise.} \end{cases} \end{aligned} \tag{5.1.3a}$$

Matrix $\boldsymbol{F}$ maps vectors of bus properties to the branches for whom those buses are the *from* end. Its transpose sums branch properties at their *from* bus. Furthermore, incidence matrix $\boldsymbol{M}_0$ is defined as,

$$\boldsymbol{M}_0 = \boldsymbol{F} - \boldsymbol{T} = [m_0\ \boldsymbol{M}], \tag{5.1.3b}$$

where m_0 is the column corresponding the the slack node. Using these definitions, equations (5.1.1) can be combined as,

$$\boldsymbol{P} = \boldsymbol{T}\boldsymbol{p} + \mathrm{D}(\boldsymbol{r})\boldsymbol{c}^2 + \boldsymbol{T}\boldsymbol{F}^T\boldsymbol{P} \tag{5.1.4a}$$

$$\boldsymbol{Q} = \boldsymbol{T}\boldsymbol{q} + \mathrm{D}(\boldsymbol{x})\boldsymbol{c}^2 + \boldsymbol{T}\boldsymbol{F}^T\boldsymbol{Q} \tag{5.1.4b}$$

$$\boldsymbol{M}(\boldsymbol{v}^2 - v_0^2\mathbf{1}_{|\mathscr{L}|}) = 2(\mathrm{D}(\boldsymbol{r})\boldsymbol{P} + \mathrm{D}(\boldsymbol{x})\boldsymbol{Q}) - \mathrm{D}(\boldsymbol{r}^2 + \boldsymbol{x}^2)\boldsymbol{c}^2, \tag{5.1.4c}$$

where $\boldsymbol{v}^2$ is the $|\mathscr{L}| \times 1$ vector of all bus v^2s except the source bus, whose squared voltage magnitude is v_0^2. Solving for $\boldsymbol{P}$ and $\boldsymbol{Q}$, and substituting, the matrix-vector form of DistFlow is:

$$\boxed{\boldsymbol{M}\boldsymbol{v}^2 = \boldsymbol{M}v_0^2\mathbf{1}_{|\mathscr{L}|} + 2\left[\mathrm{D}(\boldsymbol{r})\boldsymbol{B}\boldsymbol{T}\boldsymbol{p} + \mathrm{D}(\boldsymbol{x})\boldsymbol{B}\boldsymbol{T}\boldsymbol{q}\right] + \boldsymbol{C}\boldsymbol{c}^2,} \tag{5.1.5}$$

where,

$$\begin{aligned}\boldsymbol{B} &= (\mathbb{I} - \boldsymbol{T}\boldsymbol{F}^T)^{-1} \\ \boldsymbol{C} &= 2(\mathrm{D}(\boldsymbol{r})\boldsymbol{B}\,\mathrm{D}(\boldsymbol{r}) + \mathrm{D}(\boldsymbol{x})\boldsymbol{B}\,\mathrm{D}(\boldsymbol{x})) - \mathrm{D}(\boldsymbol{r}^2 + \boldsymbol{x}^2).\end{aligned} \tag{5.1.6}$$

A typical assumption, e.g. [Baran and Wu(1989), Method 1], is to neglect the quadratic current term, $\boldsymbol{c}^2$, which accounts for losses, in which case (5.1.5) becomes linear in $\boldsymbol{v}^2$. This is referred to as lossless DistFlow in the following.

5.1.2 Approximating Losses

An approximation for losses term $\boldsymbol{c}^2$ is developed next, controlled by parameter $\alpha \in [0, 1]$. Section 5.2 discusses how this parametrization is carried out.

The quadratic current term in (5.1.1) can be expanded as follows:

$$\begin{aligned}c_\ell^2 = I_\ell I_\ell^* &= \frac{V_i - V_j}{r_\ell + jx_\ell} \cdot \frac{V_i^* - V_j^*}{r_\ell - jx_\ell} \\ &= \frac{v_i^2 + v_j^2 - 2v_i v_j \cos(\theta_{ij})}{r_\ell^2 + x_\ell^2},\end{aligned} \tag{5.1.7}$$

where, $(f(\ell), t(\ell)) = (i, j)$ and $\theta_{ij} = \theta_i - \theta_j$.

Approximation: Using the small angle assumption, $\cos(\theta_{ij}) \approx 1$, the mixed term is approximated as a convex combination of the two end voltage magnitudes squared,

$$v_i v_j \approx \alpha_\ell (v_i^2 - v_j^2) + v_j^2, \qquad 0 \le \alpha_\ell \le 1 \tag{5.1.8}$$

Substituting (5.1.8) in (5.1.7),

$$c_\ell^2 \approx (1 - 2\alpha_\ell)\frac{v_i^2 - v_j^2}{r_\ell^2 + x_\ell^2}, \tag{5.1.9}$$

and in vector form,

$$\boldsymbol{c}^2 \approx \mathrm{D}(\boldsymbol{r}^2 + \boldsymbol{x}^2)^{-1}\left[\mathbb{I} - 2\,\mathrm{D}(\boldsymbol{\alpha})\right]\boldsymbol{M}(\boldsymbol{v}^2 - v_0^2\mathbf{1}_{|\mathscr{L}|}). \tag{5.1.10}$$

Defining,

$$\begin{aligned}\boldsymbol{\mathcal{A}}(\boldsymbol{\alpha}) &= \mathbb{I} - \boldsymbol{C}\,\mathrm{D}(\boldsymbol{r}^2+\boldsymbol{x}^2)^{-1}\left[\mathbb{I}-2\,\mathrm{D}(\boldsymbol{\alpha})\right]\\ \boldsymbol{R} &= 2\boldsymbol{M}^{-1}\boldsymbol{\mathcal{A}}(\boldsymbol{\alpha})^{-1}\,\mathrm{D}(\boldsymbol{r})\boldsymbol{B}\boldsymbol{T}\\ \boldsymbol{X} &= 2\boldsymbol{M}^{-1}\boldsymbol{\mathcal{A}}(\boldsymbol{\alpha})^{-1}\,\mathrm{D}(\boldsymbol{x})\boldsymbol{B}\boldsymbol{T},\end{aligned} \tag{5.1.11}$$

the lossy DistFlow formulation is:

$$\boldsymbol{v}^2 = v_0^2\mathbf{1}_{|\mathscr{L}|} + \boldsymbol{R}\boldsymbol{p} + \boldsymbol{X}\boldsymbol{q} \tag{5.1.12}$$

Remark: When $\boldsymbol{\alpha} = 0.5\cdot\mathbf{1}_{|\mathscr{L}|}$, $\boldsymbol{\mathcal{A}}(\boldsymbol{\alpha}) = \mathbb{I}$, and the lossless approximation, $\boldsymbol{c}^2 \to 0$ in (5.1.5), is recovered.

Letting, $\boldsymbol{Z} = \frac{1}{2}(\boldsymbol{R} + j\boldsymbol{X})$ and $\boldsymbol{s} = \boldsymbol{p} + j\boldsymbol{q}$, (5.1.12) can also be written,

$$\boldsymbol{v}^2 = v_0^2\mathbf{1}_{|\mathscr{L}|} + \boldsymbol{Z}^*\boldsymbol{s} + \boldsymbol{Z}\boldsymbol{s}^*. \tag{5.1.13}$$

This form mirrors the later derived multiphase result in Secton 5.3.6.

5.1.3 Connection to DC Power Flow in Meshed Systems

The following is a small detour to show how the DistFlow formulation relates to the DC power flow. When considering a meshed system, (5.1.1a) becomes,

$$\sum_{\ell\in t^{-1}(j)}\left(P_\ell - r_\ell c_\ell^2\right) = p_j + \sum_{\ell\in f^{-1}(j)} P_\ell. \tag{5.1.14}$$

Since set $t^{-1}(j)$ is not always a singleton, unlike a radial system, the summation is needed. Using connection matrices (5.1.3), the matrix-vector form for active and reactive flows is,

$$-\boldsymbol{M}_0^T\boldsymbol{P} = \boldsymbol{p} + \boldsymbol{T}^T\,\mathrm{D}(\boldsymbol{r})\boldsymbol{c}^2 \tag{5.1.15a}$$

$$-\boldsymbol{M}_0^T\boldsymbol{Q} = \boldsymbol{q} + \boldsymbol{T}^T\,\mathrm{D}(\boldsymbol{x})\boldsymbol{c}^2. \tag{5.1.15b}$$

Under the typical assumptions for control of P_ℓ in transmission systems [Glover *et al.*(2012), Chapter 6.7] with $(f(\ell), t(\ell)) = (i, j)$, and the classic DC power flow assumptions [Stott *et al.*(2009)],

$$P_\ell \approx \frac{v_i v_j \sin(\theta_{ij})}{x_\ell} \Rightarrow \boldsymbol{P} \approx \mathrm{D}(\boldsymbol{x})^{-1} \boldsymbol{M}_0 \boldsymbol{\theta}_0, \tag{5.1.16}$$

and (5.1.15a) becomes,

$$-\boldsymbol{M}_0^T \mathrm{D}(\boldsymbol{x})^{-1} \boldsymbol{M}_0 \boldsymbol{\theta}_0 = \boldsymbol{p} + \boldsymbol{T}^T \mathrm{D}(\boldsymbol{r}) \boldsymbol{c}^2, \tag{5.1.17}$$

where $\boldsymbol{\theta}_0$ is the vector of all bus angles including the slack bus. Equation (5.1.4c) can also be solved for $\boldsymbol{Q}$, and (5.1.15b) becomes,

$$\begin{aligned} -\frac{1}{2} \boldsymbol{M}_0^T \mathrm{D}(\boldsymbol{x})^{-1} \boldsymbol{M}_0 \boldsymbol{v}_0^2 = \boldsymbol{q} - \boldsymbol{M}_0^T \mathrm{D}(\boldsymbol{r}) \mathrm{D}(\boldsymbol{x})^{-2} \boldsymbol{M}_0 \boldsymbol{\theta_0} \\ + \left[\boldsymbol{T}^T \mathrm{D}(\boldsymbol{x}) - \frac{1}{2} \boldsymbol{M}_0^T \mathrm{D}(\boldsymbol{x})^{-1} \mathrm{D}(\boldsymbol{r}^2 + \boldsymbol{x}^2) \right] \boldsymbol{c}^2. \end{aligned} \tag{5.1.18}$$

If losses, $\boldsymbol{c}^2$, are neglected, (5.1.17) reduces to the DC power flow, where $\boldsymbol{M}_0^T \mathrm{D}(\boldsymbol{x})^{-1} \boldsymbol{M}_0$ is the well known susceptance "B" matrix. Equation (5.1.18) derives a link between squared voltage magnitude, reactive power, *and* voltage angles.

Future work could consider whether and how approximation (5.1.10) could be applied:

$$-\boldsymbol{M}_0^T \mathrm{D}(\boldsymbol{x})^{-1} \boldsymbol{M}_0 \boldsymbol{\theta}_0 = \boldsymbol{p} + \boldsymbol{T}^T \mathrm{D}(\boldsymbol{r}) \mathrm{D}(\boldsymbol{r}^2 + \boldsymbol{x}^2)^{-1} \left[\mathbb{I} - 2 \mathrm{D}(\boldsymbol{\alpha}) \right] \boldsymbol{M}_0 \boldsymbol{v}_0^2 \tag{5.1.19a}$$

$$\begin{aligned} -\boldsymbol{M}_0^T \mathrm{D}(\boldsymbol{x})^{-1} \mathrm{D}(\boldsymbol{\alpha}) \boldsymbol{M}_0 \boldsymbol{v}_0^2 - \boldsymbol{T}^T \mathrm{D}(\boldsymbol{x}) \mathrm{D}(\boldsymbol{r}^2 + \boldsymbol{x}^2)^{-1} (\mathbb{I} - 2 \mathrm{D}(\boldsymbol{\alpha})) \boldsymbol{M}_0 \boldsymbol{v}_0^2 \\ = \boldsymbol{q} - \boldsymbol{M}_0^T \mathrm{D}(\boldsymbol{r}) \mathrm{D}(\boldsymbol{x})^{-2} \boldsymbol{M}_0 \boldsymbol{\theta_0}. \end{aligned} \tag{5.1.19b}$$

Note that all matrices are Laplacian, except for those involving $\boldsymbol{\alpha}$. Even these have a somewhat similar structure only that $\boldsymbol{M}_0^T$ is replaced by $\boldsymbol{T}^T$. Future work might investigate whether synthetic grids generated in some automated manner, as in Chapter 3, could be used in a manner similar to the synthetic feeders in the next section, to explore good choices for setting $\boldsymbol{\alpha}$.

5.2 Single Phase Numerical Results

Parameters α_ℓ attempt to correct the relationship between voltages on both ends of a branch due to losses. This is the classic non-linear, non-convex problem in power flow solutions. This section demonstrates how synthetic test case generation from Chapter 2 can be applied to appropriately choose α_ℓ values.

5.2.1 Parametrization via Test Data

The value of α_ℓ is informed by branch ℓ's characteristics, as branch losses depend on impedance as well as the current flow. Combining (5.1.2) and (5.1.9) and rearranging,

$$\alpha_\ell \approx \frac{1}{2} - \frac{(P_\ell^2 + Q_\ell^2)(r_\ell^2 + x_\ell^2)}{2v_i^2(v_i^2 - v_j^2)}, \tag{5.2.1}$$

where again $(f(\ell), t(\ell)) = (i, j)$. $P_\ell^2 + Q_\ell^2$ can be estimated by neglecting losses and simply summing up all downstream powers. This this can be put in a general form:

$$\alpha_\ell = -m_\ell \cdot h(\ell) + \frac{1}{2}, \tag{5.2.2}$$

where $h(\ell)$ is some function of branch ℓ and m_ℓ captures the influence of the voltage difference.

Keeping distinct m_ℓ for each branch does not simplify the problem formulation as there are still $|\mathscr{L}|$ parameters to determine. Instead, reasoning that voltage drops vary over a small range, assume that $m_\ell = m \; \forall \ell$, and allow the intercept to shift from 1/2 to further assist the linearization. Given a range $\alpha_\ell \in [\underline{\alpha}, \overline{\alpha}]$, α_ℓ is parametrized as,

$$\alpha_\ell = -m \cdot h(\ell) + b, \tag{5.2.3}$$

where $h(\ell)$ is some function of branch ℓ and,

$$\begin{aligned} m &= \frac{\overline{\alpha} - \underline{\alpha}}{\max_{\ell \in \mathscr{L}} h(\ell) - \min_{\ell \in \mathscr{L}} h(\ell)} \\ b &= \overline{\alpha} + m \cdot \min_{\ell \in \mathscr{L}} h(\ell). \end{aligned} \tag{5.2.4}$$

Equation (5.2.3) linearly maps the parametrization function $h(\ell)$ onto the specified α_ℓ range. Beyond the choice of $h(\ell) = (P_\ell^2 + Q_\ell^2)(r_\ell^2 + x_\ell^2)$, several other parametrization are explored. Given the chain of assumptions in approximating α_ℓ and m_ℓ, it stands to reason that the sensitivity may not behave exactly according to (5.2.1).

Using the synthetic feeder generation capability from Chapter 2 a large space of possible feeders can be explored to determine good α_ℓ ranges. Feeders of size $|\mathscr{N}| = \{10, 20, \ldots 600\}$ are generated. For each size, $k = 100$ samples are generated, for a total test set of almost 6000 feeders[1]. A grid search is performed for all combinations of ranges for $\underline{\alpha}, \overline{\alpha} \in [0.4, 0.6]$ in steps of 0.001. Combinations where $\underline{\alpha} > \overline{\alpha}$ are allowed, which amounts to switching the sign of m in (5.2.3)[2]. The lossless DistFlow is implicitly considered, since $\underline{\alpha} = \overline{\alpha} = 0.5$ is among the options.

Each solution error is measured as,

$$\epsilon = \frac{1}{\sqrt{|\mathscr{L}|}} \left(\|\boldsymbol{v}^{\text{nr}} - \boldsymbol{v}\|_2 + \|\boldsymbol{P}^{\text{nr}} - \boldsymbol{P}\|_2 + \|\boldsymbol{Q}^{\text{nr}} - \boldsymbol{Q}\|_2 \right), \tag{5.2.5}$$

where superscript 'nr' denotes MATPOWER's Newton-Raphson solutions, taken as ground truth. All values are in per unit, and the division by $\sqrt{|\mathscr{L}|}$ provides a root mean square measure. Error, ϵ, can be seen as a function of four parameters:

1. $|\mathscr{N}|$: the size of the feeder.

2. k: the sample number for feeder set of size $|\mathscr{N}|$.

[1]Occasionally, the power flow for a synthetic feeder fails to converge in which case it is simply removed from the set. Therefore, there are actually only 5995 in the total test set rather than 6000.

[2]Note that as long as there are no reverse flows $v_i > v_j$ and based on (5.2.1) $m_\ell > 0 \; \forall \ell$.

Table 5.1: Optimal α Ranges Per Parametrization Option

$h(\ell)$	$\underline{\alpha}$	$\overline{\alpha}$	$\sum_{\lvert\mathscr{N}\rvert}\sum_k \epsilon$	$\bar{\epsilon}$	$\frac{\bar{\epsilon}_{\text{lossless}}-\bar{\epsilon}_{h(\ell)}}{\bar{\epsilon}_{\text{lossless}}}$
$(P_\ell^2+Q_\ell^2)(r_\ell^2+x_\ell^2)$	0.483	0.499	62.73	$1.046\cdot10^{-2}$	0.58
$\sqrt{(P_\ell^2+Q_\ell^2)(r_\ell^2+x_\ell^2)}$	0.486	0.500	69.38	$1.157\cdot10^{-2}$	0.54
$(P_\ell^2+Q_\ell^2)$	0.490	0.499	75.58	$1.261\cdot10^{-2}$	0.5
$\sqrt{P_\ell^2+Q_\ell^2}$	0.494	0.499	78.76	$1.314\cdot10^{-2}$	0.48
$\sqrt{r_\ell^2+x_\ell^2}$	0.492	0.499	90.99	$1.518\cdot10^{-2}$	0.4
$(r_\ell^2+x_\ell^2)$	0.485	0.499	93.21	$1.555\cdot10^{-2}$	0.38
lossless	0.500	0.500	150.74	$2.514\cdot10^{-2}$	0

3. i: an index into all possible pairings of $(\underline{\alpha},\overline{\alpha})$.

4. $h(\ell)$: the parametrization method.

The numerically obtained optimal range and method is,

$$(i^\star,h^\star(\ell))=\underset{i,h(\ell)}{\arg\min}\sum_{|\mathscr{N}|}\sum_k\epsilon(|\mathscr{N}|,k,i,h(\ell)). \tag{5.2.6}$$

Table 5.1 shows the optimal ranges found for six parametrization functions, $h(\ell)$, as well as the lossless DistFlow. Parameterizations are sorted from best to worst based on the average error, $\bar{\epsilon}$. The heuristic parametrization based on (5.2.1) indeed performs the best. All parametrization methods perform 38% or better than lossless DistFlow, including those that only use topology parameters.

This final observation merits further comment. In an OPF setting where injections are changing, α_ℓ could become variable and (5.1.12) ceases to be linear. The results in Table 5.1 suggest that fixing α_ℓ based on the branch impedance still improves accuracy, while preserving linearity.

Since the optimal range from Table 5.1 is selected considering many feeders of different sizes, it is likely that for particular size sets the optimal range may differ. Restricting further analysis to $h^\star(\ell)$ from Table 5.1, there is some optimal range for each feeder size set:

$$i^\star_{|\mathscr{N}|} = \arg\min_i \sum_k \epsilon(|\mathscr{N}|, k, i, h^\star(\ell)), \tag{5.2.7}$$

where each $i^\star_{|\mathscr{N}|}$ might not correspond to the range in Table 5.1. For each $|\mathscr{N}|$, define the minimum cumulative error, $\epsilon^\star_{|\mathscr{N}|}$, as,

$$\epsilon^\star_{|\mathscr{N}|} = \sum_k \epsilon(|\mathscr{N}|, k, i^\star_{|\mathscr{N}|}, h^\star(\ell)). \tag{5.2.8}$$

Similarly, let $\epsilon_{|\mathscr{N}|}$ be the cumulative error for feeders of size $|\mathscr{N}|$, when using $i^\star$ corresponding to the range in Table 5.1:

$$\epsilon_{|\mathscr{N}|} = \sum_k \epsilon(|\mathscr{N}|, k, i^\star, h^\star(\ell)). \tag{5.2.9}$$

If the increase in error from $\epsilon^\star_{|\mathscr{N}|}$ to $\epsilon_{|\mathscr{N}|}$ is not significant, it is far more practical to keep the parametrization fixed. This consideration is evaluated with results expressed in Figure 5.2.1 showing the increased percent error,

$$100 \times \frac{\epsilon_{|\mathscr{N}|} - \epsilon^\star_{|\mathscr{N}|}}{\epsilon^\star_{|\mathscr{N}|}}, \tag{5.2.10}$$

for each feeder set, as well as the average over all feeder sizes. Small errors support using the α values in Table 5.1.

5.2.2 Numerical Parametrization Validation

To test how well lossy DistFlow with the chosen parametrization of α_ℓ performs in comparison to other method, a new and *different* set, C, of 4996 feeders with sizes between 6 and 880 is created. The size and loading of each feeder is chosen by sampling a KDE as in Section 2.4.2, except that only load is present on the feeders.

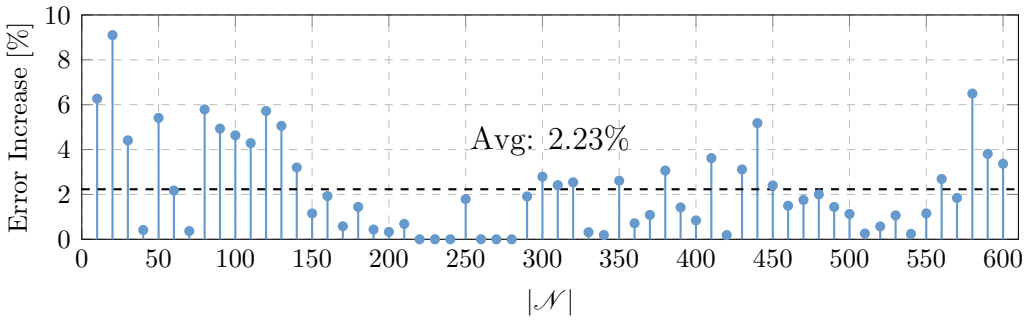

Figure 5.2.1: Added percent error when using the α range in Table 5.1 compared with the minimum error achieved for each size group.

The logarithmic voltage transformation approach from [Li *et al.*(2017)], denoted with $\log(v)$, as well as the approach from [Fatemi *et al.*(2015)], denoted with 'ftm', are considered in addition to the lossless and lossy DistFlow methods, denoted with 'df' and 'ldf', Voltage, real, and reactive errors are calculated for each sample i:

$$\Delta \boldsymbol{x}_i^t = \boldsymbol{x}_i^{\text{nr}} - \boldsymbol{x}_i^t \quad \boldsymbol{x} \in \{\boldsymbol{v}, \boldsymbol{P}, \boldsymbol{Q}\},\ t \in \{\text{df, ldf, log}(v)\text{, ftm}\}. \tag{5.2.11}$$

The root-mean-square and absolute maximum errors (infinity norm) for each sample are calculated as,

$$\begin{aligned} [\boldsymbol{\epsilon}_{\text{rms}}^x]_i &= \frac{1}{\sqrt{|\mathscr{L}_i|}} \|\Delta \boldsymbol{x}\|_2 \\ [\boldsymbol{\epsilon}_{\infty}^x]_i &= \|\Delta \boldsymbol{x}\|_\infty, \end{aligned} \tag{5.2.12}$$

and their histograms are show in Figure 5.2.2. Cumulative statistics are additionally shown in Figure 5.2.3 and reported in Table 5.2. Errors for the 'ftm' method are significantly worse than the other three methods and are therefore left out of plots for presentation clarity.

Six radial feeders available in MATPOWER are also tested. These are quite small, ranging from 18 to 141 buses. Cumulative statistics are also presented in Table 5.2, and are generally similar in trend to the synthetic feeder set.

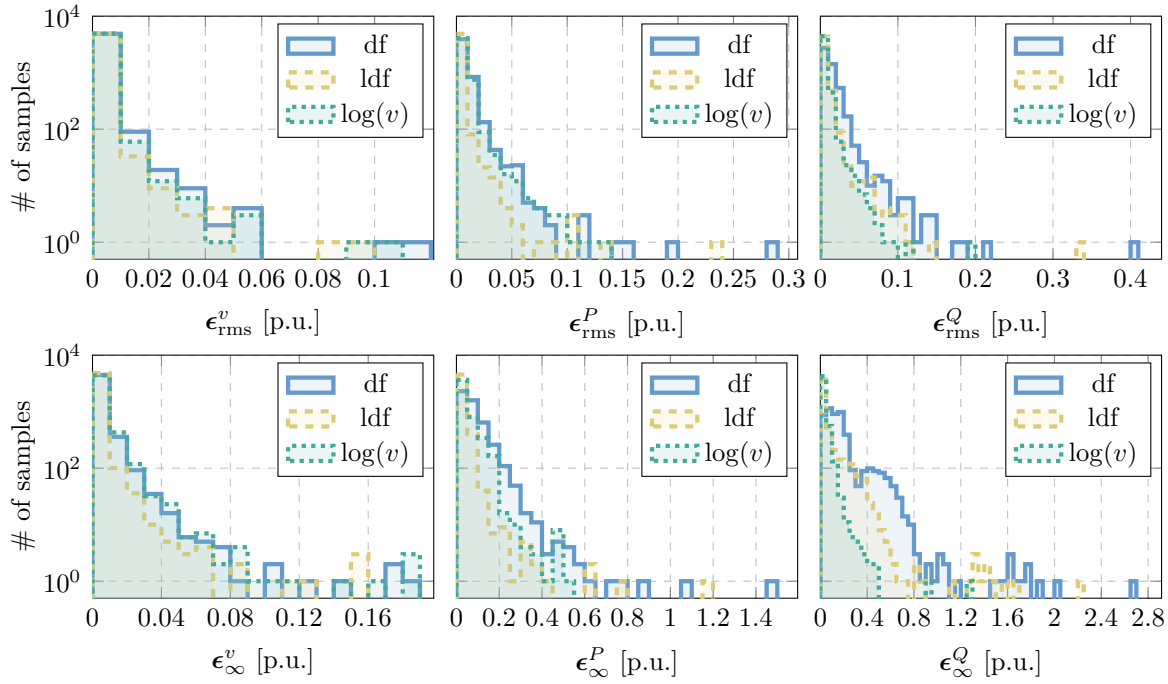

Figure 5.2.2: Error histograms for 4996 synthetic feeders.

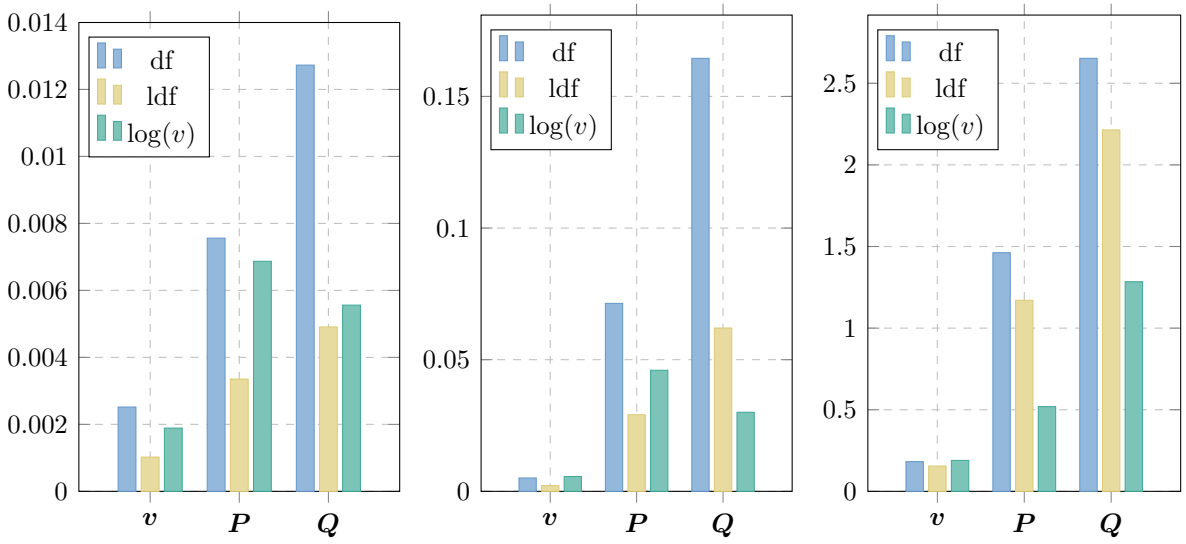

(a) $\frac{1}{|C|}\sum_{i\in C}[\boldsymbol{\epsilon}^x_{\text{rms}}]_i$ (b) $\frac{1}{|C|}\sum_{i\in C}[\boldsymbol{\epsilon}^x_{\infty}]_i$ (c) $\max_{i\in C}[\boldsymbol{\epsilon}^x_{\infty}]_i$

Figure 5.2.3: Cumulative errors, average ϵ_{rms}, average ϵ_∞, and maximum ϵ_∞, for lossless, lossy DistFlow, as well as $\log(v)$ method.

Table 5.2: Cumulative Error Statistics for Lossy DistFlow Validation

		Synthetic Feeders $\lvert C\rvert = 4996$				MATPOWER Cases $\lvert C\rvert = 6$	
	$\boldsymbol{x}$ [p.u.]	df	ldf	$\log(v)$	ftm	df	ldf
$\frac{1}{\lvert C\rvert}\sum_{i\in C}\left[\boldsymbol{\epsilon}^x_{\text{rms}}\right]_i$	$\boldsymbol{v}$	0.0025	0.0010	0.0019	0.0221	0.0095	0.0104
	$\boldsymbol{P}$	0.0076	0.0034	0.0069	0.0575	0.0294	0.0223
	$\boldsymbol{Q}$	0.0127	0.0049	0.0056	0.0777	0.1265	0.0806
$\frac{1}{\lvert C\rvert}\sum_{i\in C}\left[\boldsymbol{\epsilon}^x_{\infty}\right]_i$	$\boldsymbol{v}$	0.0051	0.0022	0.0056	0.0471	0.0110	0.0112
	$\boldsymbol{P}$	0.0714	0.0291	0.0460	0.2986	0.0861	0.0737
	$\boldsymbol{Q}$	0.1644	0.0620	0.0300	0.6570	0.3736	0.2430
$\max_{i\in C}\left[\boldsymbol{\epsilon}^x_{\infty}\right]_i$	$\boldsymbol{v}$	0.1820	0.1550	0.1896	0.3619	0.0500	0.0500
	$\boldsymbol{P}$	1.4620	1.1705	0.5191	3.1926	0.3958	0.2574
	$\boldsymbol{Q}$	2.6527	2.2143	1.2842	3.7284	2.1626	1.3306

Figures 5.2.2 and 5.2.3, as well as Table 5.2 support the argument that lossy DistFlow outperforms the lossless version, and in general is an improvement over other methods. Some interpretation is required, however, with respect to the $\log v$ method as well as the MATPOWER cases. In terms of $\boldsymbol{\epsilon}_{\text{rms}}$, lossy DistFlow outperforms $\log v$ in all cases, as seen in Figure 5.2.3a. The $\log(v)$ method does perform better in terms of average $\boldsymbol{\epsilon}^Q_{\infty}$ ($\sim 107\%$), as seen in Figure 5.2.3b. However, this is offset by the outperformance of lossy DistFlow in $\boldsymbol{\epsilon}^P_{\infty}$ ($\sim 37\%$), $\boldsymbol{\epsilon}^v_{\infty}$ ($\sim 61\%$), and $\boldsymbol{\epsilon}^Q_{\text{rms}}$ ($\sim 12\%$). The maximum $\boldsymbol{\epsilon}_{\infty}$ in Figure 5.2.3c should not be given too much weight as they represent a single event, are thus quite rare, and their statistics are less reliable. Nonetheless, these results do suggest that if the most important consideration is

reactive power flow, the $\log(v)$ method may be a more appropriate choice. In all other cases, however, lossy DistFlow is expected to perform better overall.

Another advantage of the lossy DistFlow formulation over the $\log(v)$ method is that the solution structure remains identical to the lossless case. Therefore, stability analysis in the presence of multiple inverters performed under the lossless assumption, which originally motivated this work, is directly transferable. Switching to $\log(v)$ would alter such analyses. Finally, note that DistFlow does not calculate bus angles. Therefore, the problem actually has *half* the number of variables, which may be appealing in certain situations.

For the six MATPOWER cases, the average of both $\boldsymbol{\epsilon}^{v}_{\text{rms}}$ and $\boldsymbol{\epsilon}^{v}_{\infty}$ are slightly worse for lossy DistFlow ($\sim$10% and $\sim$2% respectively). However, the improvements in $\boldsymbol{\epsilon}^{P}_{\text{rms}}$ ($\sim$24%) and $\boldsymbol{\epsilon}^{P}_{\infty}$ ($\sim$14%), as well as $\boldsymbol{\epsilon}^{Q}_{\text{rms}}$ ($\sim$36%) and $\boldsymbol{\epsilon}^{Q}_{\infty}$ ($\sim$34%), still render the lossy DistFlow approximation more accurate. The discrepancy in voltage magnitude is likely due to the low sample number. Based on these results, the lossy DistFlow, parametrized by many synthetic trials, is concluded to be an improvement over the conventional lossless DistFlow, and broadly speaking also beats other linear approximations from literature.

It is worth noting that the lossless solutions still provide good approximations for $\boldsymbol{v}$, $\boldsymbol{P}$, and $\boldsymbol{Q}$, and thus give further validity to the linearized DistFlow model. Lossless DistFlow is an "optimistic" solution in which voltage drops due to losses are neglected in (5.2.1) yielding higher bus voltages and lower flows than the nonlinear solution. Lossy DistFlow, on the other hand, is a more "pessimistic" solution. By considering loading due to losses, it reduces the likelihood of falsely predicting normal operation in cases with violations.

5.3 Multiphase Extension

The matrix-vector formulation of DistFlow is extened to unbalanced multiphase feeders. At some abuse of notation, several symbols are redefined, to highlight the similarity to the single phase formulation in the previous sections.

5.3.1 Definitions

The use of outer products in [Gan and Low(2014)] produces squared quantities of interest. Bus j now has $|\Phi_j|^2$ indices rather than $|\Phi_j|$. Let $\Phi_j^2 = \Phi_j \times \Phi_j$ the cartesian product of the phase indices. The connection matrices become $E \times N$ with,

$$E = \sum_{\nu=1}^{3} E_\nu \nu^2 \qquad N = \sum_{\nu=1}^{3} N_\nu \nu^2, \tag{5.3.1}$$

where E_ν and N_ν are the number of branches and buses, respectively, with $\nu \in \{1, 2, 3\}$ phases. For branch-phase index pairs (ℓ, ϕ) and bus-phase index pairs (i, φ), define mappings,

$$\begin{aligned} e : (\ell, \phi) &\mapsto k \in 1, 2, \ldots, E \quad \ell \in \mathscr{L}, \phi \in \Phi_{t(\ell)}^2 \\ n : (j, \varphi) &\mapsto k \in 1, 2, \ldots, N \quad j \in \mathscr{N}, \varphi \in \Phi_j^2. \end{aligned} \tag{5.3.2}$$

Using these functions, connections matrices $\boldsymbol{T}$ and $\boldsymbol{F}$ are redefined as,

$$\begin{aligned} [\boldsymbol{T}]_{e(\ell,\phi),n(i,\varphi)} &= \begin{cases} 1 & t(\ell) = i \text{ and } \phi = \varphi \\ 0 & \text{otherwise} \end{cases} \\ [\boldsymbol{F}]_{e(\ell,\phi),n(i,\varphi)} &= \begin{cases} 1 & f(\ell) = i \text{ and } \phi = \varphi \\ 0 & \text{otherwise.} \end{cases} \end{aligned} \tag{5.3.3}$$

The source node (assumed to be the first) is by definition without predecessor, leading its columns in $\boldsymbol{T}$ to be all zero. Define $\boldsymbol{T}_E$, size $E \times E$, as $\boldsymbol{T}$ with the first all zero columns removed. Incidence matrix $\boldsymbol{M}_0$ is still defined as in (5.1.3b), except

that m_0 is now an $E \times |\Phi_0|^2$ matrix corresponding to the source bus. Similarly, $\boldsymbol{v}_0^{(2)} = [v_0^{(2)},\ \boldsymbol{v}^{(2)}]^T$, is the $N \times 1$ "squared" voltage vector (see (5.3.24) for a more precise definition), with $v_0^{(2)}$ the vector of $|\Phi_0|^2$ terms corresponding to the source bus.

Define operator, $\text{ph}(A)$, as taking matrix A, and removing rows corresponding to physically non-existing branch-phases indices. Then,

$$\boldsymbol{M}_0 \,\text{ph}(\mathbf{1}_{|\mathscr{N}|} \otimes \mathbb{I}_{|\Phi_0|}) v_0^{(2)} = \mathbf{0}, \tag{5.3.4}$$

since $\text{ph}(\mathbf{1}_{|\mathscr{N}|} \otimes \mathbb{I}_{|\Phi_0|}) v_0^{(2)}$ creates an $N \times 1$ vector, where entries $n(1,\varphi) = n(2,\varphi) = \ldots = n(|\mathscr{N}|,\varphi) = [v_0^{(2)}]_\varphi$. Letting $\mathbb{1}_0 = \text{ph}(\mathbf{1}_{|\mathscr{N}|-1} \otimes \mathbb{I}_{|\Phi_0|})$,

$$\boldsymbol{M}_0 \boldsymbol{v}_0^{(2)} = \boldsymbol{M}_0 (\boldsymbol{v}_0^{(2)} - \text{ph}(\mathbf{1}_{|\mathscr{N}|} \otimes \mathbb{I}_{|\Phi_0|}) v_0^{(2)}) = \boldsymbol{M}(\boldsymbol{v}^{(2)} - \mathbb{1}_0 v_0^{(2)}). \tag{5.3.5}$$

An example of these matrices and the $\text{ph}(\cdot)$ operator can be found in Appendix D.1. Finally, if $\boldsymbol{X}$ and $\boldsymbol{Y}$ are block diagonal matrices,

$$\boldsymbol{X} = \begin{bmatrix} X_1 & & \\ & \ddots & \\ & & X_n \end{bmatrix}, \qquad \boldsymbol{Y} = \begin{bmatrix} Y_1 & & \\ & \ddots & \\ & & Y_n \end{bmatrix}, \tag{5.3.6}$$

then define the product $\boldsymbol{X} \,\square\, \boldsymbol{Y}$ as,

$$\boldsymbol{X} \,\square\, \boldsymbol{Y} = \begin{bmatrix} X_1 \otimes Y_1 & & \\ & \ddots & \\ & & X_n \otimes Y_n \end{bmatrix}. \tag{5.3.7}$$

5.3.2 Constant Impedance Loads

The current flowing *out* of node j due to a wye connected constant impedance loads is:

$$I_j^0 = y_j^0 V_j, \tag{5.3.8}$$

where y_j^0 is a $|\Phi_j| \times |\Phi_j|$ matrix. Shunt capacitances of lines could also be included in this term, in which case y_j^0 would *not* be diagonal. From (5.3.8) the power flowing *out* of node j due to a wye connected constant impedance load is:

$$\mathrm{d}(V_j(I_j^0)^H) = \mathrm{d}(V_j V_j^H (y_j^0)^H). \tag{5.3.9}$$

For delta connected loads, incidence matrix $\mathbf{\Delta}$ is defined as in [Zhao *et al.*(2017)] and [Bernstein *et al.*(2018)],

$$\mathbf{\Delta} = \begin{bmatrix} 1 & -1 & \\ & 1 & -1 \\ -1 & & 1 \end{bmatrix}. \tag{5.3.10}$$

Additionally, letting $\mathbf{\Delta}_j$ be the $3 \times |\Phi_j|$ matrix with the columns corresponding to $\nu \in \Phi_j$, the currents flowing in the delta branches are,

$$I_j^\Delta = \mathbf{\Delta}_j^T \,\mathrm{D}(y_j^\Delta)\mathbf{\Delta}_j V_j, \tag{5.3.11}$$

where y_j^Δ is a 3×1 vector of load admittances. The power *out* of each phase node is therefore,

$$\mathrm{d}(V_j(I_j^\Delta)^H) = \mathrm{d}(V_j V_j^H \mathbf{\Delta}_j^T \,\mathrm{D}(y_j^\Delta)^H \mathbf{\Delta}_j). \tag{5.3.12}$$

Letting $l_j^H = (y_j^0)^H + \mathbf{\Delta}_j^T \,\mathrm{D}(y_j^\Delta)^H \mathbf{\Delta}_j$, the total power withdrawal due to constant impedance loads is,

$$s_j^z = \mathrm{d}(V_j V_j^H l_j^H). \tag{5.3.13}$$

5.3.3 Constant Power Delta Loads

Unlike wye-connected loads, changing line-to-line currents couple phase voltages in delta connected loads. In per unit and at nominal voltage, constant power load is equal to admittance conjugate. Therefore, constant power delta loads are modeled similarly to (5.3.12) as,

$$\sqrt{3} \cdot \mathrm{d}(\mathbf{\Delta}_j^T \,\mathrm{D}(s_j^\Delta)\mathbf{\Delta}_j), \tag{5.3.14}$$

where s_j^{Δ} is the 3×1 vector of delta connected constant power loads, and the $\sqrt{3}$ factor accounts for the difference between line-to-line and line-to-neutral voltages. This modeling choice differs from [Zhao *et al.*(2017)], however, over the limited number of test cases used it is numerically found to better match nonlinear power flow solutions.

5.3.4 Power Balance

Following the development in [Gan and Low(2014)] for a branch ℓ with $(f(\ell), t(\ell)) = (i, j)$, Ohm's law states,

$$V_j = V_i^{\Phi_j} - z_\ell I_\ell. \tag{5.3.15}$$

The power at the *receiving* end of ℓ is,

$$V_j I_\ell^H = S_\ell - z_\ell c_\ell^2. \tag{5.3.16}$$

with redefinitions $c_\ell^2 = I_\ell I_\ell^H$, and $S_\ell = V_i^{\Phi_j} I_\ell^H$. The nodal power balance equation at the receiving end is:

$$\mathrm{d}(S_\ell - z_\ell c_\ell^2) = s_j + s_j^z + \sum_{\ell' \in f^{-1}(j)} \mathrm{d}(S_{\ell'}^{\Phi_j^2}). \tag{5.3.17}$$

Using $\mathrm{d}(A - B) = \mathrm{d}(A) - \mathrm{d}(B)$,

$$\mathrm{d}(S_\ell) = s_j + s_j^z + \mathrm{d}(z_\ell c_\ell^2) + \sum_{\ell' \in f^{-1}(j)} \mathrm{d}(S_{\ell'}^{\Phi_j^2}), \tag{5.3.18}$$

and substituting for s_j^z from (5.3.13),

$$\mathrm{d}(S_\ell) = s_j + \mathrm{d}\left(V_j V_j^H l_j^H\right) + \mathrm{d}(z_\ell c_\ell^2) + \sum_{\ell' \in f^{-1}(j)} \mathrm{d}(S_{\ell'}^{\Phi_j^2}), \tag{5.3.19}$$

where $s_j = s_j^Y + \sqrt{3} \cdot \mathrm{d}(\mathbf{\Delta}_j^T \, \mathrm{D}(s_j^{\Delta}) \mathbf{\Delta}_j)$, is the $|\Phi_j| \times 1$ constant power load vector.

Instead of $\mathrm{d}(S_j)$, an equation in S_j is needed to substitute into the voltage difference relation to come. Excluding s_j, all elements in (5.3.19) are inside the $\mathrm{d}(\cdot)$ function. The goal is thus, to take the "inverse" of the $\mathrm{d}(\cdot)$ function, $\mathrm{d}^{-1}(\cdot)$, to get

the, more constrained, full matrix equation. For this, the meaning of $\mathrm{d}^{-1}(s_j)$ needs to be studied.

Assumption 1: Following [Gan and Low(2014)], assume the phase voltages are balanced, i.e. $V_j^a/V_j^b \approx V_j^b/V_j^c \approx V_j^c/V_j^a = e^{j2\pi/3}$.

Using Assumption 1, the complex power is approximated as,

$$S_\ell = V_i^{\Phi_j} I_\ell^H \approx \gamma^{\Phi_j^2} \mathrm{D}(\mathrm{d}(S_\ell)). \tag{5.3.20}$$

Where,

$$\gamma = \begin{bmatrix} 1 & a^2 & a \\ a & 1 & a^2 \\ a^2 & a & 1 \end{bmatrix}, \tag{5.3.21}$$

with $a = e^{-j2\pi/3}$. This suggests that $\mathrm{d}^{-1}(s_j)$ can be approximated with $\gamma\,\mathrm{D}(s_j)$, and (5.3.19) becomes,

$$S_\ell = \gamma^{\Phi_j^2} \mathrm{D}(s_j) + V_j V_j^H l_j^H + z_\ell c_\ell^2 + \sum_{\ell' \in f^{-1}(j)} S_{\ell'}^{\Phi_j^2}. \tag{5.3.22}$$

The conjugate transpose of (5.3.22) will also be needed,

$$S_j^H = \mathrm{D}(s_j^*)\gamma^{\Phi_j^2} + l_j V_j V_j^H + c_\ell^2 z_\ell^H + \sum_{\ell' \in f^{-1}(j)} (S_{\ell'}^{\Phi_j^2})^H, \tag{5.3.23}$$

noting that c_j^2, and γ are hermitian matrices.

The matrix-matrix equations are next converted to matrix-vector form using the

vec$(\cdot)$ operation. Define[3],

$$\begin{aligned}
\sigma_j &= \mathrm{vec}(\mathrm{D}(s_j)) \in \mathbb{C}^{|\Phi_j|^2\times 1},\\
(v_i^{(2)})^{\Phi_j^2} &= \mathrm{vec}(V_i^{\Phi_j}(V_i^{\Phi_j})^H) \in \mathbb{C}^{|\Phi_j|^2\times 1},\\
\xi_\ell &= \mathrm{vec}(c_\ell^2) \in \mathbb{C}^{|\Phi_{t(\ell)}|^2\times 1},\\
\psi_\ell^{\Phi_j} &= \mathrm{vec}(S_\ell^{\Phi_j^2}) \in \mathbb{C}^{|\Phi_j|^2\times 1},\\
\tilde{\psi}_\ell^{\Phi_j} &= \mathrm{vec}((S_\ell^{\Phi_j^2})^H) \in \mathbb{C}^{|\Phi_j|^2\times 1}.
\end{aligned} \tag{5.3.24}$$

Using $\mathrm{vec}(AXB) = (B^T \otimes A)\,\mathrm{vec}(X)$, Equations (5.3.22) and (5.3.23) become,

$$\psi_\ell^{\Phi_j^2} = (\mathbb{I}\otimes\gamma^{\Phi_j^2})\sigma_j + (l_j^*\otimes\mathbb{I})v_j^{(2)} + (\mathbb{I}\otimes z_\ell)\xi_\ell + \sum_{\ell'\in f^{-1}(j)}\psi_{\ell'}^{\Phi_j^2}, \tag{5.3.25}$$

$$\tilde{\psi}_\ell^{\Phi_j^2} = \left[(\gamma^{\Phi_j^2})^*\otimes\mathbb{I}\right]\sigma_j^* + (\mathbb{I}\otimes l_j)v_j^{(2)} + (z_\ell^*\otimes\mathbb{I})\xi_\ell + \sum_{\ell'\in f^{-1}(j)}\tilde{\psi}_{\ell'}^{\Phi_j^2}. \tag{5.3.26}$$

With the definitions in Section 5.3.1, the combined matrix-vector equations are,

$$\boldsymbol{\psi} = \boldsymbol{B}\left[\boldsymbol{T}_E(\mathbb{I}\square\boldsymbol{\Gamma})\boldsymbol{\sigma} + \boldsymbol{T}_E(\boldsymbol{L}^*\square\mathbb{I})\boldsymbol{v}^{(2)} + (\mathbb{I}\square\boldsymbol{Z})\boldsymbol{\xi}\right] \tag{5.3.27}$$

$$\tilde{\boldsymbol{\psi}} = \boldsymbol{B}\left[\boldsymbol{T}_E(\boldsymbol{\Gamma}^*\square\mathbb{I})\boldsymbol{\sigma}^* + \boldsymbol{T}_E(\mathbb{I}\square\boldsymbol{L})\boldsymbol{v}^{(2)} + (\boldsymbol{Z}^*\square\mathbb{I})\boldsymbol{\xi}\right], \tag{5.3.28}$$

where, $\boldsymbol{B} = (\mathbb{I}_E - \boldsymbol{T}\boldsymbol{F}^T)^{-1}$, $\boldsymbol{\sigma}$ and $\boldsymbol{v}^{(2)}$ are the stacked σ_j and $v_j^{(2)}$ for all nodes *except* the source node, and matrices $\boldsymbol{\Gamma}$, $\boldsymbol{\Gamma}^*$, $\boldsymbol{L}$, $\boldsymbol{L}^*$, $\boldsymbol{Z}$, and $\boldsymbol{Z}^*$ are block diagonal matrices with blocks $\gamma^{\Phi_j^2}$, $(\gamma^{\Phi_j^2})^*$, l_j, l_j^*, z_j, and z_j^* respectively.

5.3.5 Squared Voltage Difference

Multiplying (5.3.15) by its complex conjugate and rearranging,

$$V_i^{\Phi_j}(V_i^{\Phi_j})^H - V_jV_j^H = S_\ell z_\ell^H + z_\ell S_\ell^H - z_\ell c_\ell^2 z_\ell^H, \tag{5.3.29}$$

the vectorized form is,

$$(v_i^{(2)})^{\Phi_j^2} - v_j^{(2)} = (z_\ell^*\otimes\mathbb{I})\psi_\ell^{\Phi_j^2} + (\mathbb{I}\otimes z_\ell)\tilde{\psi}_\ell^{\Phi_j^2} - (z_\ell^*\otimes z_\ell)\xi_\ell, \tag{5.3.30}$$

[3]Note that $v_i^{(2)}$ has complex valued entries, only the diagonals are strictly real.

and the full matrix-vector formulation using (5.3.5) is,

$$\boldsymbol{M}(\boldsymbol{v}^{(2)} - \mathbb{1}_0 v_0^{(2)}) = (\boldsymbol{Z}^* \square \mathbb{I})\boldsymbol{\psi} + (\mathbb{I} \square \boldsymbol{Z})\tilde{\boldsymbol{\psi}} - (\boldsymbol{Z}^* \square \boldsymbol{Z})\boldsymbol{\xi}. \tag{5.3.31}$$

Plugging (5.3.27) and (5.3.28) into (5.3.31), noting that,

$$\begin{aligned}(\boldsymbol{Z}^* \square \mathbb{I})(\mathbb{I} \square \boldsymbol{Z}) &= \boldsymbol{Z}^* \square \boldsymbol{Z} \\ (\mathbb{I} \square \boldsymbol{Z})(\boldsymbol{Z}^* \square \mathbb{I}) &= \boldsymbol{Z}^* \square \boldsymbol{Z},\end{aligned} \tag{5.3.32}$$

and defining,

$$\begin{aligned}\tilde{\boldsymbol{\mathcal{Z}}} &= (\boldsymbol{Z}^* \square \mathbb{I})\boldsymbol{B}\boldsymbol{T}_E(\mathbb{I} \square \boldsymbol{\Gamma}), \\ \boldsymbol{\mathcal{Z}} &= (\mathbb{I} \square \boldsymbol{Z})\boldsymbol{B}\boldsymbol{T}_E(\boldsymbol{\Gamma}^* \square \mathbb{I}), \\ \boldsymbol{K} &= (\boldsymbol{Z}^* \square \mathbb{I})\boldsymbol{B}\boldsymbol{T}_E(\boldsymbol{L}^* \square \mathbb{I}) + (\mathbb{I} \square \boldsymbol{Z})\boldsymbol{B}\boldsymbol{T}_E(\mathbb{I} \square \boldsymbol{L}), \\ \boldsymbol{C} &= (\boldsymbol{Z}^* \square \mathbb{I})\boldsymbol{B}(\mathbb{I} \square \boldsymbol{Z}) + (\mathbb{I} \square \boldsymbol{Z})\boldsymbol{B}(\boldsymbol{Z}^* \square \mathbb{I}) - (\boldsymbol{Z}^* \square \boldsymbol{Z}),\end{aligned} \tag{5.3.33}$$

the multiphase DistFlow equation is:

$$(\boldsymbol{M} - \boldsymbol{K})\boldsymbol{v}^{(2)} = \boldsymbol{M}\mathbb{1}_0 v_0^{(2)} + \tilde{\boldsymbol{\mathcal{Z}}}\boldsymbol{\sigma} + \boldsymbol{\mathcal{Z}}\boldsymbol{\sigma}^* + \boldsymbol{C}\boldsymbol{\xi}. \tag{5.3.34}$$

Remark: When $\boldsymbol{\xi} \to \boldsymbol{0}$, (5.3.34) is a matrix-vector representation of the linearized solution in [Gan and Low(2014)], with the added impact of constant impedance loads, captured in the $\boldsymbol{K}$ matrix, and constant power delta loads.

5.3.6 Approximating Losses

Solving (5.3.15) for I_ℓ, with $y_\ell = z_\ell^{-1}$, the quadratic current term on branch ℓ with $(f(\ell), t(\ell)) = (i, j)$ can be written as,

$$c_\ell^2 = I_\ell I_\ell^H = y_\ell[V_i^{\Phi_j} - V_j][(V_i^{\Phi_j})^H - V_j^H]y_\ell^H. \tag{5.3.35}$$

Assumption 2: Angle differences across distribution branches are fairly small. Therefore, in a similar spirit as (5.1.8), the mixed term voltage outer products are

approximated as convex combinations of the two end nodes:

$$V_i^{\Phi_j} V_j^H \approx \mathrm{D}(\alpha_\ell)(V_i^{\Phi_j}(V_i^{\Phi_j})^H - V_j V_j^H) + V_j V_j^H, \tag{5.3.36}$$

where α_ℓ is redefined as a $|\Phi_j| \times 1$ parameter vector with each entry $0 \leq [\alpha_\ell]_\nu \leq 1$.

Substituting (5.3.36) and its conjugate transpose into (5.3.35), collecting terms, and letting $\mathrm{D}(\alpha_\ell^{\mathsf{c}}) = \mathbb{I}_{|\Phi_j|} - \mathrm{D}(\alpha_\ell)$,

$$c_\ell^2 \approx y_\ell \left[\mathrm{D}(\alpha_\ell^{\mathsf{c}})[V_i^{\Phi_j}(V_i^{\Phi_j})^H - V_j V_j^H] - [V_i^{\Phi_j}(V_i^{\Phi_j})^H - V_j V_j^H]\,\mathrm{D}(\alpha_\ell)\right] y_\ell^H. \tag{5.3.37}$$

Vectorizing,

$$\xi_\ell \approx (y_\ell^* \otimes [y_\ell\,\mathrm{D}(\alpha_\ell^{\mathsf{c}})] - [y_\ell^*\,\mathrm{D}(\alpha_\ell)] \otimes y_\ell)\,[(v_i^{(2)})^{\Phi_j^2} - v_j^{(2)}], \tag{5.3.38}$$

and stacking all branches,

$$\boldsymbol{\xi} \approx \left[\boldsymbol{Y}^* \,\square (\boldsymbol{Y}\,\mathrm{D}(\boldsymbol{\alpha}^{\mathsf{c}})) - (\boldsymbol{Y}^*\,\mathrm{D}(\boldsymbol{\alpha})) \,\square\, \boldsymbol{Y}\right] \boldsymbol{M}(\boldsymbol{v}^{(2)} - \mathbb{1}_0 v_0^{(2)}), \tag{5.3.39}$$

where $\boldsymbol{Y}$, $\boldsymbol{Y}^*$, $\mathrm{D}(\boldsymbol{\alpha}^{\mathsf{c}})$, and $\mathrm{D}(\boldsymbol{\alpha})$ are block diagonal matrices with blocks, y_ℓ, y_ℓ^*, $\mathrm{D}(\alpha_\ell^{\mathsf{c}})$, and $\mathrm{D}(\alpha_\ell)$. Substituting back into (5.3.34) and letting,

$$\boldsymbol{\mathcal{A}}(\boldsymbol{\alpha}) = \mathbb{I}_E - \boldsymbol{C}\left[\boldsymbol{Y}^* \,\square (\boldsymbol{Y}\,\mathrm{D}(\boldsymbol{\alpha}^{\mathsf{c}})) - (\boldsymbol{Y}^*\,\mathrm{D}(\boldsymbol{\alpha})) \,\square\, \boldsymbol{Y}\right], \tag{5.3.40}$$

the multiphase lossy DistFlow parametrized by $\boldsymbol{\alpha}$ is,

$$\boxed{(\boldsymbol{\mathcal{A}}(\boldsymbol{\alpha})\boldsymbol{M} - \boldsymbol{K})\,\boldsymbol{v}^{(2)} = \boldsymbol{\mathcal{A}}(\boldsymbol{\alpha})\boldsymbol{M}\,\mathbb{1}_0 v_0^{(2)} + \tilde{\boldsymbol{\mathcal{Z}}}\boldsymbol{\sigma} + \boldsymbol{\mathcal{Z}}\boldsymbol{\sigma}^*.} \tag{5.3.41}$$

Remark: When $\alpha_\ell = 0.5 \cdot \mathbf{1}_{|\Phi_{t(\ell)}|}$, $c_\ell^2 \to 0\ \forall \ell$ in (5.3.37), therefore, $\boldsymbol{\mathcal{A}}(\boldsymbol{\alpha}) = \mathbb{I}_E$, and the lossless formulation is recovered. Additionally, the formulation in (5.3.41) has essentially the same form as (5.1.13). While $\boldsymbol{\mathcal{Z}}$ and $\tilde{\boldsymbol{\mathcal{Z}}}$ are not exactly conjugates of one another, due to inter-phase terms, they are "conjugate like". On the terms corresponding to diagonal entries of the σ_j blocks, they are exactly conjugates, which yields real values for the final voltage magnitudes.

5.4 Multiphase Numerical Results

While an automatic generation tool for multiphase feeders is not available, a similar loss parametrization to Section 5.2.1 is developed, and tested on four available test feeders.

5.4.1 Multiphase Parametrization

Similar to Section 5.2.1, α_ℓ is parametrized based on properties of branch ℓ. Beginning with the definition of S_ℓ,

$$S_\ell^H S_\ell = I_\ell (V_i^{\Phi_j})^H V_i^{\Phi_i} I_\ell^H = \|V_i^{\Phi_j}\|_2^2 c_\ell^2, \tag{5.4.1}$$

where S_ℓ is estimated by summing all downstream power and premultiplying by γ as in (5.3.20). Substituting into the approximation for c_ℓ^2 in (5.3.37), and rearranging:

$$\begin{aligned}\frac{1}{\|V_i^{\Phi_j}\|_2^2}(S_\ell z_\ell^H)^H (S z_\ell^H) \approx [V_i^{\Phi_j}(V_i^{\Phi_j})^H - V_j V_j^H] \\ - \left[\mathrm{D}(\alpha_\ell)[V_i^{\Phi_j}(V_i^{\Phi_j})^H - V_j V_j^H] + [V_i^{\Phi_j}(V_i^{\Phi_j})^H - V_j V_j^H]\,\mathrm{D}(\alpha_\ell)\right].\end{aligned} \tag{5.4.2}$$

Noting that $\mathrm{d}(\mathrm{D}(\alpha)\cdot A) = \mathrm{d}(A\cdot \mathrm{D}(\alpha))$, and letting v_i^2 and v_j^2 be the diagonal entries of $V_i^{\Phi_j}(V_i^{\Phi_j})^H$ and $V_j V_j^H$ respectively,

$$\frac{1}{\mathbf{1}^T v_i^2}\,\mathrm{d}[(S_\ell z_\ell^H)^H (S z_\ell^H)] \approx [\mathbb{I} - 2\,\mathrm{D}(\alpha_\ell)](v_i^2 - v_j^2). \tag{5.4.3}$$

Using $\mathrm{D}(x)y = \mathrm{D}(y)x$, $\mathrm{d}(\mathrm{D}(x)) = x$ and rearranging,

$$\alpha_\ell \approx 0.5\cdot\mathbf{1} - \frac{1}{\mathbf{1}^T v_i^2}\,\mathrm{D}^{-1}(v_i^2 - v_j^2)\,\mathrm{d}[(S_\ell z_\ell^H)^H (S z_\ell^H)], \tag{5.4.4}$$

is the generalization of (5.2.1). The corresponding parametrization to (5.2.3) given some range $[\alpha_\ell]_\nu \in [\underline{\alpha}, \overline{\alpha}]$ is then,

$$\alpha_\ell = -\,\mathrm{D}(m^{\Phi_{t(\ell)}})\cdot h(\ell) + b^{\Phi_{t(\ell)}}, \tag{5.4.5}$$

with,

$$m_\nu = \frac{\overline{\alpha} - \underline{\alpha}}{\max_{\ell \in \mathscr{L}}[h(\ell)]_\nu - \min_{\ell \in \mathscr{L}}[h(\ell)]_\nu}, \quad \nu \in \{1,2,3\}. \tag{5.4.6}$$
$$b_\nu = \overline{\alpha} + m_\nu \cdot \min_{\ell \in \mathscr{L}}[h(\ell)]_\nu.$$

Function $h(\ell)$ could be $\mathrm{d}[(S_\ell z_\ell^H)^H (S z_\ell^H)]$ based on (5.4.4) or some other function of branch ℓ.

5.4.2 Sample Results

Unlike the single-phase case, there is currently no tool to generate very large number of multiphase feeders. The results presented here are therefore a simple proof-of-concept.

The IEEE 13, 34, 37, and 123 bus feeders from [IEEE PES Distribution Test Feeders(2018)] are used to assess the performance of the multiphase lossy DistFlow. A few modifications are made to conform to the current modeling status presented thus far:

- Voltage regulators and transformers are replaced with overhead line models.
- Shunt capacitors are disabled.
- All load models that are neither constant power nor constant impedance are converted to constant power.

Let $\boldsymbol{v}$ be the vector composed of square root of the diagonal entries of the "unvectorized" $\boldsymbol{v}^{(2)}$ vector, $\boldsymbol{P}$ and $\boldsymbol{Q}$ be the real and reactive parts of the diagonals of the "unvectorized" $\boldsymbol{\psi}$ vector, and $\tilde{E} = \sum_{\nu=1}^{3} E_\nu \nu$ with E_ν defined as in (5.3.1). The error, ϵ is measured as in (5.2.5),

$$\epsilon = \frac{1}{\sqrt{\tilde{E}}}(\|\boldsymbol{v}^{\mathrm{dss}} - \boldsymbol{v}\|_2 + \|\boldsymbol{P}^{\mathrm{dss}} - \boldsymbol{P}\|_2 + \|\boldsymbol{Q}^{\mathrm{dss}} - \boldsymbol{Q}\|_2), \tag{5.4.7}$$

Table 5.3: Multiphase Lossy DistFlow Results

$h(\ell)$	$\underline{\alpha}$	$\overline{\alpha}$	$\sum \epsilon$	$\bar{\epsilon}$
$\mathrm{d}[(S_\ell z_\ell^H)^H (S z_\ell^H)]$	0.492	0.501	0.1044	0.0261
$\mathrm{d}(z_\ell z_\ell^H)$	0.498	0.500	0.1061	0.0265
lossless	0.500	0.500	0.1065	0.0266

where 'dss' refers to the non-linear solutions obtained with OpenDSS [Electric Power Research Institute(2011), Reno and Coogan(2014)], taken as ground truth.

Table 5.3 shows results for two parametrization functions $h(\ell)$ and the lossless DistFlow. Once again, both parameterizations outperform lossless DistFlow, however, as opposed to the results in Section 5.2.1 the differences are much smaller. Since the sample size is so small, it is difficult to draw very general conclusions. Results suggest that the loss parametrization is useful if the parameters are tuned correctly. However, a larger set of cases needs to be considered before a stronger statement about preferred parametrization settings can be made. If a future multiphase incarnation of `synfeeder` is realized, the necessary larger case study will be possible.

5.5 Related Publications

The results presented in this chapter are currently under review in [Schweitzer *et al.*(2018b)]. Both the single phase and multiphase lossy DistFlow implementations are available on GitHub at: `https://github.com/eranschweitzer/distflow`.

REFERENCES

[Akinbode and Hedman(2013)] Akinbode, O. W. and K. W. Hedman, "Fictitious losses in the dcopf with a piecewise linear approximation of losses", in "Power and Energy Society General Meeting (PES), 2013 IEEE", pp. 1–5 (IEEE, 2013).

[Aksoy *et al.*(2017)] Aksoy, S. G., E. Purvine, E. Cotilla-Sanchez and M. Halappanavar, "A generative graph model for electrical infrastructure networks", arXiv preprint arXiv:1711.11098 (2017).

[Albert *et al.*(2004)] Albert, R., I. Albert and G. L. Nakarado, "Structural vulnerability of the North American power grid", Phys. Rev. E **69**, 025103 (2004).

[ARPA-E Grid Data(2017)] ARPA-E Grid Data, "ARPA-E Grid Data", URL `https://arpa-e.energy.gov/?q=arpa-e-programs/grid-data` (2017).

[Arritt and Dugan(2010)] Arritt, R. and R. Dugan, "The IEEE 8500-node test feeder", in "Transmission and Distribution Conference and Exposition, 2010 IEEE PES", pp. 1–6 (2010).

[Baker *et al.*(2018)] Baker, K., A. Bernstein, E. Dall'Anese and C. Zhao, "Network-cognizant voltage droop control for distribution grids", IEEE Transactions on Power Systems **33**, 2, 2098–2108 (2018).

[Barabási and Albert(1999)] Barabási, A.-L. and R. Albert, "Emergence of Scaling in Random Networks", Science **286**, 5439, 509–512 (1999).

[Baran and Wu(1989)] Baran, M. E. and F. F. Wu, "Network reconfiguration in distribution systems for loss reduction and load balancing", IEEE Transactions on Power Delivery **4**, 2, 1401–1407 (1989).

[Berger *et al.*(2004)] Berger, F., P. Gritzmann and S. de Vries, "Minimum cycle bases for network graphs", Algorithmica **40**, 1, 51–62 (2004).

[Bernstein *et al.*(2018)] Bernstein, A., C. Wang, E. Dall'Anese, J.-Y. Le Boudec and C. Zhao, "Load-flow in multiphase distribution networks: Existence, uniqueness, non-singularity, and linear models", IEEE Transactions on Power Systems (2018).

[Birchfield *et al.*(2016)] Birchfield, A. B., K. M. Gegner, T. Xu, K. S. Shetye and T. J. Overbye, "Statistical considerations in the creation of realistic synthetic power grids for geomagnetic disturbance studies", IEEE Transactions on Power Systems **PP**, 99, 1–1 (2016).

[Birchfield *et al.*(2017a)] Birchfield, A. B., E. Schweitzer, M. H. Athari, T. Xu, T. J. Overbye, A. Scaglione and Z. Wang, "A metric-based validation process to assess the realism of synthetic power grids", Energies **10**, 8 (2017a).

[Birchfield *et al.*(2017b)] Birchfield, A. B., T. Xu, K. M. Gegner, K. S. Shetye and T. J. Overbye, "Grid structural characteristics as validation criteria for synthetic networks", IEEE Transactions on power systems **32**, 4, 3258–3265 (2017b).

[Birchfield *et al.*(2018)] Birchfield, A. B., T. Xu and T. J. Overbye, "Power Flow Convergence and Reactive Power Planning in the Creation of Large Synthetic Grids", IEEE Transactions on Power Systems (2018).

[Boyd *et al.*(2011)] Boyd, S., N. Parikh, E. Chu, B. Peleato and J. Eckstein, "Distributed optimization and statistical learning via the alternating direction method of multipliers", Foundations and Trends® in Machine Learning **3**, 1, 1–122 (2011).

[Brameller *et al.*(1969)] Brameller, A., M. N. John and M. Scott, *Practical diakoptics for electrical networks* (CRC Press, 1969).

[Brandes(2001)] Brandes, U., "A Faster Algorithm for Betweenness Centrality", Journal of Mathematical Sociology **25**, 163–177 (2001).

[Brummitt *et al.*(2013)] Brummitt, C. D., P. D. H. Hines, I. Dobson, C. Moore and R. M. D'Souza, "Transdisciplinary electric power grid science", Proceedings of the National Academy of Sciences **110**, 30, 12159 (2013).

[Carrano *et al.*(2006)] Carrano, E. G., L. A. E. Soares, R. H. C. Takahashi, R. R. Saldanha and O. M. Neto, "Electric distribution network multiobjective design using a problem-specific genetic algorithm", IEEE Transactions on Power Delivery **21**, 2, 995–1005 (2006).

[Cloteaux(2013)] Cloteaux, B., "Limits in modeling power grid topology", in "Network Science Workshop (NSW), 2013 IEEE 2nd", pp. 16–22 (2013).

[Coffrin and Van Hentenryck(2014)] Coffrin, C. and P. Van Hentenryck, "A linear-programming approximation of ac power flows", INFORMS Journal on Computing **26**, 4, 718–734 (2014).

[Comaniciu *et al.*(2003)] Comaniciu, D., V. Ramesh and P. Meer, "Kernel-based object tracking", IEEE Transactions on Pattern Analysis and Machine Intelligence **25**, 5, 564–577 (2003).

[Cotilla-Sanchez *et al.*(2012)] Cotilla-Sanchez, E., P. Hines, C. Barrows and S. Blumsack, "Comparing the Topological and Electrical Structure of the North American Electric Power Infrastructure", IEEE Systems Journal **6**, 4, 616–626 (2012).

[Cotilla-Sanchez *et al.*(2013)] Cotilla-Sanchez, E., P. D. H. Hines, C. Barrows, S. Blumsack and M. Patel, "Multi-attribute partitioning of power networks based on electrical distance", IEEE Transactions on Power Systems **28**, 4, 4979–4987 (2013).

[Deka and Vishwanath(2013)] Deka, D. and S. Vishwanath, "Generative Growth Model for Power Grids", in "2013 International Conference on Signal-Image Technology Internet-Based Systems (SITIS)", pp. 591–598 (2013).

[Deka *et al.*(2016)] Deka, D., S. Vishwanath and R. Baldick, "Analytical models for power networks:the case of the western us and ercot grids", IEEE Transactions on Smart Grid **PP**, 99, 1–1 (2016).

[Dembo and Zeitouni(2009)] Dembo, A. and O. Zeitouni, *Large Deviations Techniques and Applications*, Stochastic Modelling and Applied Probability (Springer Berlin Heidelberg, 2009).

[Dickert *et al.*(2013)] Dickert, J., M. Domagk and P. Schegner, "Benchmark low voltage distribution networks based on cluster analysis of actual grid properties", in "2013 IEEE Grenoble PowerTech (POWERTECH)", pp. 1–6 (2013).

[Eiben and Smith(2015)] Eiben, A. E. and J. E. Smith, *Introduction to evolutionary computing* (Springer, 2015), 2 edn.

[Electric Power Research Institute(2011)] Electric Power Research Institute, "Simulation Tool – OpenDSS", URL `http://smartgrid.epri.com/SimulationTool.aspx` (2011).

[Elyas and Wang(2016a)] Elyas, S. H. and Z. Wang, "Improved synthetic power grid modeling with correlated bus type assignments", IEEE Transactions on Power Systems **PP**, 99, 1–1 (2016a).

[Elyas and Wang(2016b)] Elyas, S. H. and Z. Wang, "A multi-objective optimization algorithm for bus type assignments in random topology power grid model", in "2016 49th Hawaii International Conference on System Sciences (HICSS)", pp. 2446–2455 (2016b).

[Erdős and Rényi(1959)] Erdős, P. and A. Rényi, "On random graphs", Publicationes Mathematicae Debrecen **6**, 290–297 (1959).

[Erseghe(2014)] Erseghe, T., "Distributed optimal power flow using admm", IEEE transactions on power systems **29**, 5, 2370–2380 (2014).

[Fatemi *et al.*(2015)] Fatemi, S. M., S. Abedi, G. B. Gharehpetian, S. H. Hosseinian and M. Abedi, "Introducing a novel dc power flow method with reactive power considerations", IEEE Transactions on Power Systems **30**, 6, 3012–3023 (2015).

[Fiedler(1975)] Fiedler, M., "A property of eigenvectors of nonnegative symmetric matrices and its application to graph theory", Czechoslovak Mathematical Journal **25**, 4, 619–633 (1975).

[Fortenbacher and Demiray(2017)] Fortenbacher, P. and T. Demiray, "Linear/quadratic programming based optimal power flow using linear power flow and absolute loss approximations", arXiv preprint arXiv:1711.00317 (2017).

[Gan and Low(2014)] Gan, L. and S. H. Low, "Convex relaxations and linear approximation for optimal power flow in multiphase radial networks", in "2014 Power Systems Computation Conference (PSCC)", pp. 1–9 (IEEE, 2014).

[Garcia *et al.*(2000)] Garcia, P. A. N., J. L. R. Pereira, S. Carneiro, V. M. da Costa and N. Martins, "Three-phase power flow calculations using the current injection method", IEEE Transactions on Power Systems **15**, 2, 508–514 (2000).

[Glover *et al.*(2012)] Glover, J. D., M. Sarma and T. Overbye, *Power System Analysis & Design* (Cengage Learning, 2012).

[Grainger and Stevenson(1994)] Grainger, J. and W. Stevenson, *Power system analysis*, McGraw-Hill series in electrical and computer engineering: Power and energy (McGraw-Hill, 1994).

[GridLAB-D(2018)] GridLAB-D, "Gridlab-d", URL `www.gridlabd.org` (2018).

[Grigg *et al.*(1999)] Grigg, C., P. Wong, P. Albrecht, R. Allan, M. Bhavaraju, R. Billinton, Q. Chen, C. Fong, S. Haddad, S. Kuruganty *et al.*, "The ieee reliability test system-1996. a report prepared by the reliability test system task force of the application of probability methods subcommittee", IEEE Transactions on power systems **14**, 3, 1010–1020 (1999).

[Hellinger(1909)] Hellinger, E., "Neue begründung der theorie quadratischer formen von unendlichvielen veränderlichen.", Journal für die reine und angewandte Mathematik **136**, 210–271 (1909).

[Hines *et al.*(2010)] Hines, P., E. Cotilla-Sanchez and S. Blumsack, "Do topological models provide good information about electricity infrastructure vulnerability?", Chaos: An Interdisciplinary Journal of Nonlinear Science **20**, 3, –, URL `http://scitation.aip.org/content/aip/journal/chaos/20/3/10.1063/1.3489887` (2010).

[Hines *et al.*(2016)] Hines, P., I. Dobson and P. Rezaei, "Cascading power outages propagate locally in an influence graph that is not the actual grid topology", IEEE Transactions on Power Systems **PP**, 99, 1–1 (2016).

[Horton(1987)] Horton, J. D., "A polynomial-time algorithm to find the shortest cycle basis of a graph", SIAM Journal on Computing **16**, 2, 358–366 (1987).

[Hu *et al.*(2015)] Hu, J., L. Sankar and D. J. Mir, "Cluster-and-connect: An algorithmic approach to generating synthetic electric power network graphs", in "2015 53rd Annual Allerton Conference on Communication, Control, and Computing (Allerton)", pp. 223–230 (2015).

[Huang and Vittal(2016)] Huang, Q. and V. Vittal, "Integrated transmission and distribution system power flow and dynamic simulation using mixed three-sequence/three-phase modeling", IEEE Transactions on Power Systems **PP**, 99, 1–1 (2016).

[Huang *et al.*(2017)] Huang, R., R. Fan, J. Daily, A. Fisher and J. Fuller, "An open-source framework for power system transmission and distribution dynamics co-simulation", IET Generation, Transmission & Distribution (2017).

[IEEE PES Distribution Test Feeders(2018)] IEEE PES Distribution Test Feeders, "IEEE PES Distribution Test Feeders", URL `http://sites.ieee.org/pes-testfeeders/resources/` (2018).

[Jabr(2006)] Jabr, R. A., "Radial distribution load flow using conic programming", IEEE transactions on power systems **21**, 3, 1458–1459 (2006).

[Jain *et al.*(2016)] Jain, H., A. Parchure, R. P. Broadwater, M. Dilek and J. Woyak, "Three-phase dynamic simulation of power systems using combined transmission and distribution system models", IEEE Transactions on Power Systems **31**, 6, 4517–4524 (2016).

[Kadavil *et al.*(2016)] Kadavil, R., T. M. Hansen and S. Suryanarayanan, "An algorithmic approach for creating diverse stochastic feeder datasets for power systems co-simulations", in "2016 IEEE Power and Energy Society General Meeting", (2016).

[Kepner and Gilbert(2011)] Kepner, J. and J. Gilbert, *Graph Algorithms in the Language of Linear Algebra*, Software, Environments, Tools (Society for Industrial and Applied Mathematics, 2011).

[Kersting(2001)] Kersting, W. H., "Radial distribution test feeders", in "Power Engineering Society Winter Meeting, 2001. IEEE", vol. 2, pp. 908–912 vol.2 (2001).

[Kersting(2012)] Kersting, W. H., *Distribution system modeling and analysis* (CRC press, 2012).

[Kirchhoff(1847)] Kirchhoff, G., "Ueber die auflösung der gleichungen, auf welche man bei der untersuchung der linearen vertheilung galvanischer ströme geführt wird", Annalen der Physik **148**, 12, 497–508 (1847).

[Klein and Randić(1993)] Klein, D. J. and M. Randić, "Resistance distance", Journal of Mathematical Chemistry **12**, 1, 81–95 (1993).

[Kourounis *et al.*(2018)] Kourounis, D., A. Fuchs and O. Schenk, "Towards the next generation of multiperiod optimal power flow solvers", IEEE Transactions on Power Systems **PP**, 99, 1–10 (2018).

[Kron(1963)] Kron, G., *Diakoptics: The Piecewise Solution Of Large-Scale Systems* (London, Macdonald, 1963).

[Kullback and Leibler(1951)] Kullback, S. and R. A. Leibler, "On Information and Sufficiency", Ann. Math. Statist. **22**, 1, 79–86 (1951).

[Lewis(2009)] Lewis, T. G., *Network Science: Theory and Applications* (Wiley Publishing, 2009).

[Li *et al.*(2017)] Li, Z., J. Yu and Q. H. Wu, "Approximate linear power flow using logarithmic transform of voltage magnitudes with reactive power and power loss consideration", IEEE Transactions on Power Systems **PP**, 99, 1–1 (2017).

[Low(2014a)] Low, S. H., "Convex relaxation of optimal power flow—part i: Formulations and equivalence", IEEE Transactions on Control of Network Systems **1**, 1, 15–27 (2014a).

[Low(2014b)] Low, S. H., "Convex relaxation of optimal power flow—part ii: Exactness", IEEE Transactions on Control of Network Systems **1**, 2, 177–189 (2014b).

[Mateo *et al.*(2018)] Mateo, C., G. Prettico, T. Gómez, R. Cossent, F. Gangale, P. Frías and G. Fulli, "European representative electricity distribution networks", International Journal of Electrical Power & Energy Systems **99**, 273–280 (2018).

[Mateo *et al.*(2011)] Mateo, C., T. G. S. Roman, Á. Sanchez-Miralles, J. P. P. Gonzalez and A. C. Martinez, "A reference network model for large-scale distribution planning with automatic street map generation", IEEE Transactions on Power Systems **26**, 1, 190–197 (2011).

[Mohar(1992)] Mohar, B., "Laplace eigenvalues of graphs—a survey", Discrete Mathematics **109**, 1–3, 171 – 183, URL `http://www.sciencedirect.com/science/article/pii/0012365X9290288Q` (1992).

[National Grid(2017)] National Grid, "National grid electricity plc special condition 2k.4–transmission losses report reporting period 1 april 2016 to 31 march 2017", Tech. rep., National Grid, URL `https://www.nationalgrid.com/sites/default/files/documents/8589938427-SC2K%20Transmission%20Losses%20Report%202015_16%20v3.pdf` (2017).

[Newman(2003)] Newman, M. E. J., "The Structure and Function of Complex Networks", SIAM Review **45**, 2, 167–256, URL `http://dx.doi.org/10.1137/S003614450342480` (2003).

[Pagani and Aiello(2011)] Pagani, G. A. and M. Aiello, "Towards Decentralization: A Topological Investigation of the Medium and Low Voltage Grids", IEEE Transactions on Smart Grid **2**, 3, 538–547 (2011).

[Pagani and Aiello(2013)] Pagani, G. A. and M. Aiello, "The Power Grid as a complex network: A survey", Physica A: Statistical Mechanics and its Applications **392**, 11, 2688 – 2700 (2013).

[Power Systems Test Case Archive(2018)] Power Systems Test Case Archive, "Power Systems Test Case Archive", URL `https://www2.ee.washington.edu/research/pstca/` (2018).

[Reno and Coogan(2014)] Reno, M. J. and K. Coogan, "Grid integrated distributed pv (gridpv) version 2", Sandia National Labs SAND2014-20141 (2014).

[Rivera *et al.*(2016)] Rivera, J., J. Leimhofer and H.-A. Jacobsen, "Opengridmap: towards automatic power grid simulation model generation from crowdsourced data", Computer Science - Research and Development pp. 1–11 (2016).

[Rosas-Casals *et al.*(2015)] Rosas-Casals, M., S. Bologna, E. F. Bompard, G. D'Agostino, W. Ellens, G. A. Pagani, A. Scala and T. Verma, "Knowing power grids and understanding complexity science", International Journal of Critical Infrastructures **11**, 1, 4–14 (2015).

[Rosas-Casals *et al.*(2007)] Rosas-Casals, M., S. Valverde and R. V. Sole, "Topological vulnerability of the European power grid under errors and attacks", International Journal of Bifurcation and Chaos **17**, 7, 2465 – 2475 (2007).

[Rosato *et al.*(2007)] Rosato, V., S. Bologna and F. Tiriticco, "Topological properties of high-voltage electrical transmission networks", Electric Power Systems Research **77**, 2, 99 – 105 (2007).

[Rotering *et al.*(2011)] Rotering, N., C. Schroders, J. Kellermann and A. Moser, "Medium-voltage network planning with optimized power factor control of distributed generators", in "Power and Energy Society General Meeting, 2011 IEEE", pp. 1–8 (2011).

[Schneider *et al.*(2008)] Schneider, K. P., Y. Chen, D. P. Chassin, R. G. Pratt, D. W. Engel and S. E. Thompson, "Modern grid initiative distribution taxonomy final report", Tech. Rep. PNNL-18035, Pacific Northwest National Laboratory, Richland, WA (2008).

[Schweitzer *et al.*(2018a)] Schweitzer, E., J. Hansen and J. Fuller, "Transmission and distribution co-simulation with possible distribution loops", in "2018 IEEE Power and Energy Society General Meeting", (2018a).

[Schweitzer and Monti(2017)] Schweitzer, E. and A. Monti, "Tool development for distribution grid topology generation", Tech. rep., Flexible Elektrische Netze (FEN), URL `https://fenaachen.net/en/research/projects/seed-fund/seed-fund-projects-of-mv-consortium-2/` (2017).

[Schweitzer *et al.*(2018b)] Schweitzer, E., S. Saha, A. Scaglione, N. G. Johnson and D. Arnold, "Lossy DistFlow Formulation for Single and Multiphase Radial Feeders", (submitted) IEEE Transactions on Power Systems (2018b).

[Schweitzer and Scaglione(2018)] Schweitzer, E. and A. Scaglione, "A Mathematical Programing Solution for Automatic Generation of Synthetic Power Flow Cases", IEEE Transactions on Power Systems (2018).

[Schweitzer *et al.*(2018c)] Schweitzer, E., A. Scaglione and K. Hedman, "Assignment of electrical properties to power grid topologies", in "Proceedings of the 51st Hawaii International Conference on System Sciences", (2018c).

[Schweitzer *et al.*(2017a)] Schweitzer, E., A. Scaglione, A. Monti and G. A. Pagani, "Automated Generation Algorithm for Synthetic Medium Voltage Radial Distribution Systems", IEEE Journal on Emerging and Selected Topics In Circuits and Systems (2017a).

[Schweitzer *et al.*(2017b)] Schweitzer, E., A. Scaglione and R. Thomas, "The validation of synthetic power system cases", in "IREP'2017 Symposium", (2017b).

[Schweitzer *et al.*(2016)] Schweitzer, E., A. Scaglione, R. Thomas and T. Overbye, "Analysis of the Coupling Between Power System Topology and Operating Condition for Synthetic Test Case Validation", in "2016 Grid of the Future Symposium", (CIGRE US National Committee, 2016).

[Schweitzer *et al.*(2015)] Schweitzer, E., K. Togawa, T. Schloesser and A. Monti, "A Matlab GUI for the Generation of Distribution Grid Models", in "ETG-Fachbericht-International ETG Congress 2015", (VDE VERLAG GmbH, 2015).

[Schweitzer *et al.*(2018d)] Schweitzer, E., T. Xu, A. B. Birchfield, A. Scaglione, T. J. Overbye, R. Thomas and Z. Wang, "Towards operational validation: Mapping power system inputs to operating conditions", in "Proceedings of the 20th Power Systems Computation Conference", (2018d).

[Short(2014)] Short, T. A., *Electric power distribution handbook* (CRC press, 2014), second edn.

[SMART-DS(2018)] SMART-DS, "SMART-DS", URL `https://www.nrel.gov/grid/smart-ds.html` (2018).

[Soltan and Zussman(2015)] Soltan, S. and G. Zussman, "Generation of Synthetic Spatially Embedded Power Grid Networks", ArXiv e-prints (2015).

[Soltan and Zussman(2016)] Soltan, S. and G. Zussman, "Generation of synthetic spatially embedded power grid networks", in "Power and Energy Society General Meeting (PESGM), 2016", pp. 1–5 (IEEE, 2016).

[Stott *et al.*(2009)] Stott, B., J. Jardim and O. Alsac, "Dc power flow revisited", IEEE Transactions on Power Systems **24**, 3, 1290–1300 (2009).

[Sun *et al.*(2015)] Sun, H., Q. Guo, B. Zhang, Y. Guo, Z. Li and J. Wang, "Master-slave-splitting based distributed global power flow method for integrated transmission and distribution analysis", IEEE Transactions on Smart Grid **6**, 3, 1484–1492 (2015).

[TAMU Electric Grid Test Cases(2017)] TAMU Electric Grid Test Cases, "TAMU Electric Grid Test Cases", URL `https://electricgrids.engr.tamu.edu/` (2017).

[US-Canada Power System Outage Task Force *et al.*(2004)] US-Canada Power System Outage Task Force, S. Abraham, H. Dhaliwal, R. J. Efford, L. J. Keen, A. McLellan, J. Manley, K. Vollman, N. J. Diaz, T. Ridge *et al.*, *Final report on the august 14, 2003 blackout in the united states and canada: Causes and recommendations* (US-Canada Power System Outage Task Force, 2004).

[Wang *et al.*(2010a)] Wang, Z., A. Scaglione and R. Thomas, "Generating Statistically Correct Random Topologies for Testing Smart Grid Communication and Control Networks", IEEE Transactions on Smart Grid **1**, 1, 28–39 (2010a).

[Wang *et al.*(2010b)] Wang, Z., A. Scaglione and R. Thomas, "The Node Degree Distribution in Power Grid and Its Topology Robustness under Random and Selective Node Removals", in "2010 IEEE International Conference on Communications Workshops (ICC)", pp. 1–5 (2010b).

[Watson and Woodruff(2011)] Watson, J.-P. and D. L. Woodruff, "Progressive hedging innovations for a class of stochastic mixed-integer resource allocation problems", Computational Management Science **8**, 4, 355–370 (2011).

[Watts and Strogatz(1998)] Watts, D. J. and S. H. Strogatz, "Collective dynamics of 'small-world' networks", Nature **393**, 6684, 440–442 (1998).

[Wong(2011)] Wong, L., "A review of trasmission losses in planning studies", Tech. Rep. CEC-200-2011-009, California Energy Commission (2011).

[Wood *et al.*(2014)] Wood, A., B. Wollenberg and G. Sheblé, *Power Generation, Operation, and Control* (Wiley, 2014), 3rd edn.

[Xu *et al.*(2017)] Xu, T., A. B. Birchfield, K. M. Gegner, K. S. Shetye and T. J. Overbye, "Application of large-scale synthetic power system models for energy economic studies", in "Proceedings of the 50th Hawaii International Conference on System Sciences", (2017).

[Yang *et al.*(2018a)] Yang, Z., K. Xie, J. Yu, H. Zhong, N. Zhang and Q. Xia, "A general formulation of linear power flow models: Basic theory and error analysis", IEEE Transactions on Power Systems (2018a).

[Yang *et al.*(2018b)] Yang, Z., H. Zhong, A. Bose, T. Zheng, Q. Xia and C. Kang, "A linearized opf model with reactive power and voltage magnitude: a pathway to improve the mw-only dc opf", IEEE Transactions on Power Systems **33**, 2, 1734–1745 (2018b).

[Yang *et al.*(2017)] Yang, Z., H. Zhong, Q. Xia and C. Kang, "Solving opf using linear approximations: fundamental analysis and numerical demonstration", IET Generation, Transmission & Distribution **11**, 17, 4115–4125 (2017).

[Zhang *et al.*(2013)] Zhang, H., G. T. Heydt, V. Vittal and J. Quintero, "An improved network model for transmission expansion planning considering reactive power and network losses", IEEE Transactions on Power Systems **28**, 3, 3471–3479 (2013).

[Zhao *et al.*(2017)] Zhao, C., E. Dall'Anese and S. Low, "Convex relaxation of opf in multiphase radial networks with delta connection", in "Proceedings of the 10th Bulk Power Systems Dynamics and Control Symposium", (2017).

[Zhu and Liu(2016)] Zhu, H. and H. J. Liu, "Fast local voltage control under limited reactive power: Optimality and stability analysis", IEEE Transactions on Power Systems **31**, 5, 3794–3803 (2016).

[Zimmerman(2010)] Zimmerman, R., "Ac power flows, generalized opf costs and their derivatives using complex matrix notation", Tech. Rep. Matpower Technical Note 2, URL `http://www.pserc.cornell.edu/matpower/TN2-OPF-Derivatives.pdf` (2010).

[Zimmerman *et al.*(2011)] Zimmerman, R., C. Murillo-Sánchez and R. Thomas, "MATPOWER: Steady-State Operations, Planning, and Analysis Tools for Power Systems Research and Education", IEEE Transactions on Power Systems **26**, 1, 12–19 (2011).

APPENDIX A

RADIAL FEEDERS DETAILS

A.1 Statistical Analysis Results

Table A.1: KL-Divergences

Property	Distribution	Cumulative D_{KL}	Per Feeder D_{KL}† $< 90\%$	$< 95\%$	< 1
Hop Distance	Negative Binomial	0.0173	0.3903	2.3022	92%
No-Load					
Fraction	Beta	0.0014	—	—	—
Hop Distance	Bimodal Poisson	0.0755	—	—	—
Power Injection					
Fraction	Beta	0.0620	—	—	—
Hop Distance	Bimodal Normal	0.1706	—	—	—
Deviation From Uniform	Normal	0.0459	—	—	—
Load Deviation From Uniform	tLocationScale	0.0008	3.4103	4.5785	83%
Degree Distribution	Bimodal Gamma	0.0211	0.1457	0.2701	99%
$I_\ell^{\text{est}}/I_\ell^{\text{nom}}$	Exponential	0.0098	0.2010	0.3795	98%
Cable Length	Modified Cauchy	0.0247	0.6967	1.1387	95%
Downstream Power	Generalized Pareto	0.0111	0.6691	1.0766	94%
Voltage Drop	Generalize Pareto	0.0917	0.9961	1.5091	90%

† The number in column $< 90\%$ says that 90% of the individual feeders have a KL-Divergence with the functional law below the tabulated number, similarly for column $< 95\%$. Column < 1 reports the percent of feeders whose KL distance to the functional law is less than 1.

Table A.2: Fit Parameters

Property	Parameter Values
Hop Distance	$n = 7.46$, $p = 0.50$
No-Load	
Fraction	$\alpha = 3.03$, $\beta = 49.54$
Hop Distance	$p = 0.53$, $\mu_1 = 3.55$, $\mu_2 = 10.50$
Power Injection	
Fraction	$\alpha = 4.28$, $\beta = 246.19$
Hop Distance	$p = 0.92$, $\mu_1 = 0.12$, $\sigma_1 = 0.04$, $\mu_2 = 0.32$, $\sigma_2 = 0.32$
Deviation From Uniform	$\mu = 0$, $\sigma = 0.15$
Load Deviation From Uniform	$\mu = -0.001$, $\sigma = 0.002$, $\nu = 1.46$
Degree Distribution	$p = 0.03$, $a_1 = 5.30$, $b_1 = 1.24$, $a_2 = 9.00$, $b_2 = 0.21$
$I_\ell^{\text{est}}/I_\ell^{\text{nom}}$	$\mu = 0.17$
Cable Length	$x_0 = 0.4807$, $\gamma = 0.3595$
Downstream Power	$k = 0.27$, $\sigma = 0.015$, $\theta = 0$
Voltage Drop	$k = 0.67$, $\sigma = 4.12 \times 10^{-4}$, $\theta = 0$
Maximum Degree	$a = 23.47$, $b = -0.68$
Maximum Length	$a = 26.97$, $b = -0.13$

A.2 Cable Library

Table A.3 shows the 10 kV cables used in the feeder generation algorithm. Frequency is the fraction of cables belonging to the particular group. For example, around 20% of cables have a nominal rating of 240 A. Subscript 0 refers to the zero sequence values.

Table A.3: Library of cables with 10 kV nominal voltage used in the radial feeder algorithm

Cable Type	I_{nom} [A]	Frequency	R [Ω/km]	X [Ω/km]	C [µF/km]	R_0 [Ω/km]	X_0 [Ω/km]	[C_0 µF/km]
3x16 Cu	82	0.0948	1.1585	0.1074	0.2058	7.2969	0.1706	0.1025
3x35 Cu	135	0.1056	0.5325	0.0978	0.2707	4.9507	0.1536	0.1358
3x95 Al	185	0.3205	0.3283	0.0867	0.3840	3.0182	0.1344	0.1945
3x150 Al	240	0.1949	0.2086	0.0821	0.4505	2.4068	0.1264	0.2292
3x120 Cu	275	0.0825	0.1567	0.0843	0.4167	2.6882	0.1303	0.2115
3x240 Al	320	0.1499	0.1308	0.0776	0.5311	1.9066	0.1187	0.2714
3x240 Al	355	0.0393	0.1308	0.0776	0.5311	1.9066	0.1187	0.2714
1x240 Alrm	445	0.0069	0.1352	0.1082	0.4355	0.7096	0.0505	0.4355
1x630 Alrm	575	0.0052	0.0511	0.0927	0.6410	0.4416	0.0395	0.6410
1x630 Alrm	700	0.0005	0.0511	0.0927	0.6410	0.4416	0.0395	0.6410

A.3 Real vs. Synthetic Feeders

Figure A.3.1 is identical to Figure 2.4.1 except that the real feeder (a) is identified is identified with a frame.

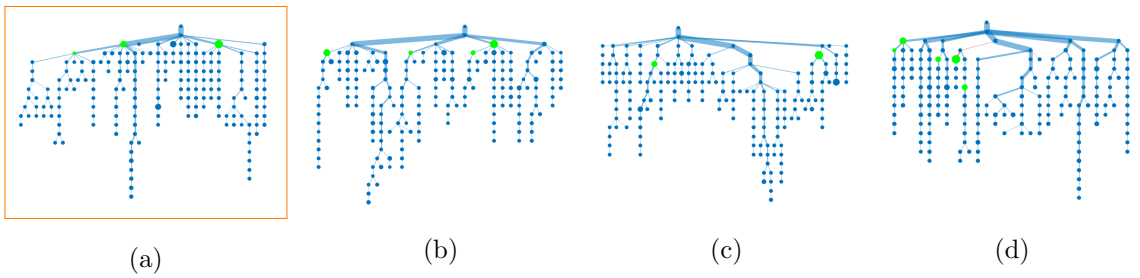

(a) (b) (c) (d)

Figure A.3.1: Three samples generated with the following inputs: $|\mathcal{N}|$: 195, Load: 23 MVA, and Generation: 3 MVA. The width of each line represents the relative real power flow magnitude. Edges with reverse flow are marked in red. The size of each node represents the relative magnitude of real load/injection. Injection nodes are identified with green.

APPENDIX B

PLACEMENT PROBLEM DETAILS

B.1 Sizing $\mathcal{M}$

Using u for both $u_{f(\ell)}$ and $u_{t(\ell)}$ since boundary values will eventually be applied, constraint (3.3.7b) is broken into two parts when $Z_{\ell,\tilde{\ell}} = 0$:

$$\mathcal{M}_{Pf} \geq -P_\ell^f + (g_\ell^{ff} + g_\ell^{ft})(1+u) - g_\ell^{ft}\phi + b_\ell^{ft}\theta_{ft(\ell)} \qquad \forall \ell \in \mathscr{L} \qquad \text{(B.1.1)}$$

$$\mathcal{M}_{Pf} \geq P_\ell^f - (g_\ell^{ff} + g_\ell^{ft})(1+u) + g_\ell^{ft}\phi - b_\ell^{ft}\theta_{ft(\ell)} \qquad \forall \ell \in \mathscr{L} \qquad \text{(B.1.2)}$$

To find the smallest possible $\mathcal{M}_{Pf}$ the right-hand side of each is maximized term by term.

Constraint (B.1.1)

1. To maximize $-P_\ell^f$ let $P_\ell^f \to -r_{\max}$, where $r_{\max} = \max_\ell r_\ell$, and the whole term becomes $r_{\max}$.

2. To maximize $(g_\ell^{ff} + g_\ell^{ft})(1+u)$ first let $x_\ell = (g_\ell^{ff} + g_\ell^{ft})$ and $y = (1+u)$, noting that $y > 0$. There are 2 cases to consider:

   (a) If $\exists \ell \in \mathscr{L} : x_\ell > 0$, then $\max_{\ell,y}(x_\ell y) = \max_\ell(x_\ell)\max(y)$

   (b) If $\nexists \ell \in \mathscr{L} : x_\ell > 0$, $\max_{\ell,y}(x_\ell y) = \max_\ell(x_\ell)\min(y)$

   There final expression is:

   $$\max\left\{\max_\ell(g_\ell^{ff} + g_\ell^{ft})(1+u_{\max}), \max_\ell(g_\ell^{ff} + g_\ell^{ft})(1+u_{\min})\right\}.$$

3. to maximize $-g_\ell^{ft}\phi$, minimize $g_\ell^{ft}\phi$, noting that $\phi \geq 0$. There are again 2 cases to consider:

   (a) If $\exists \ell \in \mathscr{L} : g_\ell^{ft} < 0$, then $\min_{\ell,\phi}(g_\ell^{ft}\phi) = \min_\ell(g_\ell^{ft})\max(\phi)$

   (b) If $\nexists \ell \in \mathscr{L} : g_\ell^{ft} < 0$, then $\min_{\ell,\phi}(g_\ell^{ft}\phi) = \min_\ell(g_\ell^{ft})\min(\phi) = 0$.

The final expression is therefore, $\min\left\{\min_\ell(g_\ell^{ft})\frac{\Delta\theta_{\max}^2}{2},\, 0\right\}$.

4. To maximize $b_\ell^{ft}\theta_{ft(\ell)}$ the maximum absolute value of b_ℓ^{ft} is multiplied by the maximum angle difference: $\max(\left|b_\ell^{ft}\right|)\Delta\theta_{\max}$.

Combining the parts:

$$\mathcal{M}_{Pf}^1 \geq r_{\max} + \max\left\{\max_\ell(g_\ell^{ff}+g_\ell^{ft})(1+u_{\max}),\, \max_\ell(g_\ell^{ff}+g_\ell^{ft})(1+u_{\min})\right\} - \min\left\{\min_\ell(g_\ell^{ft})\frac{\Delta\theta_{\max}^2}{2},\, 0\right\} + \max_\ell(\left|b_\ell^{ft}\right|)\Delta\theta_{\max} \quad \text{(B.1.3)}$$

Constraint (B.1.2)

1. To maximize P_ℓ^f let $P_\ell^f \to r_{\max}$.

2. To maximize $-(g_\ell^{ff}+g_\ell^{ft})(1+u)$, minimize $(g_\ell^{ff}+g_\ell^{ft})(1+u)$, letting $x_\ell = (g_\ell^{ff}+g_\ell^{ft})$ and $y=(1+u)$, noting that $y>0$.

   (a) If $\exists\ell\in\mathscr{L} : x_\ell<0$, then $\min_{\ell,y}(x_\ell y) = \min_\ell(x_\ell)\max(y)$.

   (b) If $\nexists\ell\in\mathscr{L} : x_\ell<0$, then $\min_{\ell,y}(x_\ell y) = \min_\ell(x_\ell)\min(y)$.

   The final expression is:

$$\min\left\{\min_\ell(g_\ell^{ff}+g_\ell^{ft})(1+u_{\max}),\, \min_\ell(g_\ell^{ff}+g_\ell^{ft})(1+u_{\min})\right\}.$$

3. To maximize $g_\ell^{ft}\phi$, noting that $\phi\geq 0$:

   (a) If $\exists\ell\in\mathscr{L} : g_\ell^{ft}>0$, then $\max_{\ell,\phi}(g_\ell^{ft}\phi) = \max_\ell(g_\ell^{ft})\max(\phi)$

   (b) If $\nexists\ell\in\mathscr{L} : g_\ell^{ft}>0$, then $\max_{\ell,\phi}(g_\ell^{ft}\phi) = \max_\ell(g_\ell^{ft})\min(\phi) = 0$.

   The final expression is therefore, $\max\left\{\max_\ell(g_\ell^{ft})\frac{\Delta\theta_{\max}^2}{2},\, 0\right\}$.

4. Maximizing $-b_\ell^{ft}\theta_{ft(\ell)}$ is the same as before due to the symmetry of $\theta_{ft(\ell)}$.

Combining the parts:

$$\mathcal{M}_{Pf}^2 \geq f_{\max} - \min\left\{\min_\ell(g_\ell^{ff} + g_\ell^{ft})(1+u_{\max}),\, \min_\ell(g_\ell^{ff} + g_\ell^{ft})(1+u_{\min})\right\} + \max\left\{\max_\ell(g_\ell^{ft})\frac{\Delta\theta_{\max}^2}{2},\, 0\right\} + \max_\ell(\left|b_\ell^{ft}\right|)\Delta\theta_{\max}. \quad \text{(B.1.4)}$$

The greater of $\mathcal{M}_{Pf}^1$ and $\mathcal{M}_{Pf}^2$ is taken is the final big multiplier:

$$\mathcal{M}_{Pf} = \max(\mathcal{M}_{Pf}^1, \mathcal{M}_{Pf}^2). \quad \text{(B.1.5)}$$

The same treatment is performed on Constraints (3.3.7c)–(3.3.7e).

Calculating $\mathcal{M}_{Qf}$

$$\mathcal{M}_{Qf}^1 \geq -Q_\ell^f - (b_\ell^{ff} + b_\ell^{ft})(1+u) + b_\ell^{ft}\phi + g_\ell^{ft}\theta_{ft(\ell)} \quad \text{(B.1.6a)}$$

$$\geq r_{\max} - \min\left\{\min_\ell(b_\ell^{ff} + b_\ell^{ft})(1+u_{\max}),\, \min_\ell(b_\ell^{ff} + b_\ell^{ft})(1+u_{\min})\right\} + \max\left\{\max_\ell(b_\ell^{ft})\frac{\Delta\theta_{\max}^2}{2},\, 0\right\} + \max_\ell(\left|g^{ft}\right|)\Delta\theta_{\max}$$

$$\mathcal{M}_{Qf}^2 \geq +Q_\ell^f + (b_\ell^{ff} + b_\ell^{ft})(1+u) - b_\ell^{ft}\phi - g_\ell^{ft}\theta_{ft(\ell)} \quad \text{(B.1.6b)}$$

$$\geq r_{\max} + \max\left\{\max_\ell(b_\ell^{ff} + g_\ell^{ft})(1+u_{\max}), \max_\ell(b_\ell^{ff} + b_\ell^{ft})(1+u_{\min})\right\} - \min\left\{\min_\ell(b_\ell^{ft})\frac{\Delta\theta_{\max}^2}{2},\, 0\right\} + \max_\ell(\left|g^{ft}\right|)\Delta\theta_{\max}$$

$$\mathcal{M}_{Qf} = \max(\mathcal{M}_{Qf}^1, \mathcal{M}_{Qf}^2) \quad \text{(B.1.6c)}$$

Calculating $\mathcal{M}_{P^t}$

$$\mathcal{M}^1_{P^t} \geq -P^t_\ell + (g^{tt}_\ell + g^{tf}_\ell)(1+u) - g^{tf}_\ell \phi - b^{tf}_\ell \theta_{ft(\ell)} \tag{B.1.7a}$$

$$\begin{aligned} &\geq r_{\max} + \max\left\{\max_\ell(g^{tt}_\ell + g^{tf}_\ell)(1+u_{\max}), \max_\ell(g^{tt}_\ell + g^{tf}_\ell)(1+u_{\min})\right\} \\ &\qquad - \min\left\{\min_\ell(g^{tf}_\ell)\frac{\Delta\theta^2_{\max}}{2},\, 0\right\} + \max_\ell(\left|b^{tf}_\ell\right|)\Delta\theta_{\max} \end{aligned}$$

$$\mathcal{M}^2_{P^t} \geq +P^t_\ell - (g^{tt}_\ell + g^{tf}_\ell)(1+u) + g^{tf}_\ell \phi + b^{tf}_\ell \theta_{ft(\ell)} \tag{B.1.7b}$$

$$\begin{aligned} &\geq r_{\max} - \min\left\{\min_\ell(g^{tt}_\ell + g^{tf}_\ell)(1+u_{\max}),\, \min_\ell(g^{tt}_\ell + g^{tf}_\ell)(1+u_{\min})\right\} \\ &\qquad + \max\left\{\max_\ell(g^{tf}_\ell)\frac{\Delta\theta^2_{\max}}{2},\, 0\right\} + \max_\ell(\left|b^{tf}_\ell\right|)\Delta\theta_{\max} \end{aligned}$$

$$\mathcal{M}_{P^t} = \max(\mathcal{M}^1_{P^t}, \mathcal{M}^2_{P^t}) \tag{B.1.7c}$$

Calculating $\mathcal{M}_{Q^t}$

$$\mathcal{M}^1_{Q^t} \geq -Q^t_\ell - (b^{tt}_\ell + b^{tf}_\ell)(1+u) + b^{tf}_\ell \phi - g^{tf}_\ell \theta_{ft(\ell)} \tag{B.1.8a}$$

$$\begin{aligned} &\geq r_{\max} - \min\left\{\min_\ell(b^{tt}_\ell + b^{tf}_\ell)(1+u_{\max}),\, \min_\ell(b^{tt}_\ell + b^{tf}_\ell)(1+u_{\min})\right\} \\ &\qquad + \max\left\{\max_\ell(b^{tf}_\ell)\frac{\Delta\theta^2_{\max}}{2},\, 0\right\} + \max_\ell(\left|g^{tf}\right|)\Delta\theta_{\max} \end{aligned}$$

$$\mathcal{M}^2_{Q^t} \geq +Q^t_\ell + (b^{tt}_\ell + b^{tf}_\ell)(1+u) - b^{tf}_\ell \phi + g^{tf}_\ell \theta_{ft(\ell)} \tag{B.1.8b}$$

$$\begin{aligned} &\geq r_{\max} + \max\left\{\max_\ell(b^{tt}_\ell + g^{tf}_\ell)(1+u_{\max}), \max_\ell(b^{tt}_\ell + b^{tf}_\ell)(1+u_{\min})\right\} \\ &\qquad - \min\left\{\min_\ell(b^{tf}_\ell)\frac{\Delta\theta^2_{\max}}{2},\, 0\right\} + \max_\ell(\left|g^{tf}\right|)\Delta\theta_{\max} \end{aligned}$$

$$\mathcal{M}_{Q^t} = \max(\mathcal{M}^1_{Q^t}, \mathcal{M}^2_{Q^t}) \tag{B.1.8c}$$

B.2 Selecting h for Polyhedral Relaxation

Consider two tangent lines, $f(x)$ and $g(x)$, to the function $q(x) = (x - \bar{x})^2$ at x_0 and $x_1 > x_0$ respectively.

$$\begin{aligned} f(x) &= 2(x_0 - \bar{x})x + \bar{x}^2 - x_0^2 \\ g(x) &= 2(x_1 - \bar{x})x + \bar{x}^2 - x_1^2 \end{aligned} \tag{B.2.1}$$

Since both $f(x)$ and $g(x)$ lie below $q(x)$, the maximum deviation from either on the interval $[x_0, x_1]$ will be at the intersection of the two, which occurs at the interval midpoint, $x_0 + d/2$, where $d = x_1 - x_0$. The error ϵ at this point is,

$$\epsilon = q(x_0 + \frac{d}{2}) - f(x_0 + \frac{d}{2}) \tag{B.2.2a}$$

$$= (x_0 + \frac{d}{2} - \bar{x})^2 - 2(x_0 - \bar{x})(x_0 + \frac{d}{2}) - \bar{x}^2 + x_0^2 \tag{B.2.2b}$$

$$= \frac{d^2}{4}. \tag{B.2.2c}$$

Therefore, to achieve a particular ϵ, spacing d should be chosen as,

$$d = 2\sqrt{\epsilon}. \tag{B.2.3}$$

Assuming that all tangent points are place equally on the interval $[-\Delta\theta_{\max}, \Delta\theta_{\max}]$, spacing d expressed in terms of number of points minus one h is,

$$d = \frac{2\Delta\theta_{\max}}{h}. \tag{B.2.4}$$

Equating (B.2.3) and (B.2.4) and solving for h, gives the desired h given an error ϵ:

$$h = \frac{\Delta\theta_{\max}}{\sqrt{\epsilon}}. \tag{B.2.5}$$

B.3 AC-PTDF

Several algorithms in Chapter 3 make use of AC-PTDFs, or linearized sensitivities of the AC power flow problem around a particular operating point. These are briefly derived here, in a similar manner to [Wood *et al.*(2014), Appendix 8D].

The desired sensitivities link changes in bus injection to line power flow via matrix H^f[1]:

$$\begin{pmatrix} \Delta P^f \\ \Delta Q^f \end{pmatrix} = H^f \begin{pmatrix} \Delta P^{\text{bus}} \\ \Delta Q^{\text{bus}} \end{pmatrix}, \tag{B.3.1}$$

[1]The superscript f indicates power flows at the *from* end of the branch. An identical derivation can be carried out for the *to* end as well.

where,

$$H^f = \begin{pmatrix} \frac{\partial P^f}{\partial P^{\text{bus}}} & \frac{\partial P^f}{\partial Q^{\text{bus}}} \\ \frac{\partial Q^f}{\partial P^{\text{bus}}} & \frac{\partial Q^f}{\partial Q^{\text{bus}}} \end{pmatrix}. \tag{B.3.2}$$

The two Δ vectors can be expressed in terms of the changes in complex voltage state variable as:

$$\begin{aligned} \begin{pmatrix} \Delta P^{\text{bus}} \\ \Delta Q^{\text{bus}} \end{pmatrix} &= \overbrace{\begin{pmatrix} \frac{\partial P^{\text{bus}}}{\partial \theta} & \frac{\partial P^{\text{bus}}}{\partial |v|} \\ \frac{\partial Q^{\text{bus}}}{\partial \theta} & \frac{\partial Q^{\text{bus}}}{\partial |v|} \end{pmatrix}}^{J} \begin{pmatrix} \Delta\theta \\ \Delta|v| \end{pmatrix} \\ \begin{pmatrix} \Delta P^f \\ \Delta Q^f \end{pmatrix} &= \overbrace{\begin{pmatrix} \frac{\partial P^f}{\partial \theta} & \frac{\partial P^f}{\partial |v|} \\ \frac{\partial Q^f}{\partial \theta} & \frac{\partial Q^f}{\partial |v|} \end{pmatrix}}^{K} \begin{pmatrix} \Delta\theta \\ \Delta|v| \end{pmatrix}. \end{aligned} \tag{B.3.3}$$

Matrix J is the standard $2(N-1) \times 2(N-1)$ Newton method Jacobian matrix, and matrix K is an $2L \times 2(N-1)$ similar branch flow Jacobian (see [Zimmerman(2010)]). Substituting (B.3.3) in (B.3.1),

$$\begin{aligned} K \begin{pmatrix} \Delta\theta \\ \Delta|v| \end{pmatrix} &= H^f J \begin{pmatrix} \Delta\theta \\ \Delta|v| \end{pmatrix} \\ \Rightarrow H^f &= K J^{-1}. \end{aligned} \tag{B.3.4}$$

Matrix H_f is therefore, $2L \times 2(N-1)$, however, a column of zeros can be added for the slack bus to make it $2L \times 2N$. It is important to note that different slack bus choices will result in different H^f matrices.

B.4 Reactive Planning

B.4.1 Adding Shunts for Voltage Regulation

The basic reactive planning approach adopted is similar conceptually to [Birchfield *et al.*(2018)] but leverages the OPF framework with soft limit capabilities. Generator

with limits equal to zero are added to each bus, with soft limits enabled. Since the soft limits are expensive, they will be non-zero only when necessary to satisfy the voltage constraints. Once a solution is found, the desired shunt to add to node i is:

$$B_i^{sh} = \frac{s_i^{\text{qmax}} - s_i^{\text{qmin}}}{|v_i|^2}, \tag{B.4.1}$$

where s_i^{qmax} and s_i^{qmin} are violations in the positive and negative directions, respectively, of the soft limit. Note that if the units on s_i^{qmax} and s_i^{qmin} are MVAr, and v_i is in per-unit, then B_i^{sh} will be in MVAr, which is the required format for MATPOWER.

It is additionally possible to place an upper bound on the soft limits, so that the magnitude of the shunts will be limited. Furthermore, to ensure that no shunt is unreasonably small, all shunts with magnitudes greater than zero but smaller than a given threshold, t, are set to that threshold:

$$B_i^{sh} = \begin{cases} B_i^{sh} & (|B_i^{sh}| \geq t) \cup (B_i^{sh} = 0) \\ \text{sgn}(B_i^{sh})t & 0 < |B_i^{sh}| < t. \end{cases} \tag{B.4.2}$$

B.4.2 Adding Shunts to Limit Reactive Flows

Another reason to add shunts may be to limit the reactive flows. Given an operating point, sensitivities H_q:

$$H_q \Delta Q_{\text{inj}} = \Delta Q_{\text{branch}}, \tag{B.4.3}$$

can be calculated as in Appendix B.3.

Define the magnitude of the flows given a change in bus injections as,

$$Q_{\text{branch}}^{\text{new}} = |Q_{\text{branch}}^{\text{old}} + \Delta Q_{\text{branch}}|. \tag{B.4.4}$$

A reasonable objective is to minimize $Q_{\text{branch}}^{\text{new}}$ alongside the magnitude of ΔQ_{inj}. The ℓ_1-norm is used since sparse solutions, i.e. relatively few shunt elements, are desired.

Minimizing ΔQ_{inj} is of interest because a) linear sensitivities, H_q, are more accurate with smaller injection changes, and b) the number of shunts added should be limited. The full problem is formulated as,

$$
\begin{aligned}
\underset{Q^{\text{new}}_{\text{branch}},\Delta Q_{\text{inj}},s_q}{\textbf{Minimize}} \quad & \sum Q^{\text{new}}_{\text{branch}} + \sum s_q \\
\textbf{Subject to} \quad & Q^{\text{new}}_{\text{branch}} - H_q \Delta Q_{\text{inj}} \geq Q^{\text{old}}_{\text{branch}} \\
& Q^{\text{new}}_{\text{branch}} + H_q \Delta Q_{\text{inj}} \geq -Q^{\text{old}}_{\text{branch}} \\
& s_q - \Delta Q_{\text{inj}} \geq 0 \\
& s_q + \Delta Q_{\text{inj}} \geq 0 \\
& -\Delta Q_{\text{max}} \geq \Delta Q_{\text{inj}} \geq \Delta Q_{\text{max}} \\
& s_q \geq 0,\ Q^{\text{new}}_{\text{branch}} \geq 0
\end{aligned}
\tag{B.4.5}
$$

Despite the use of the ℓ_1-norm, results in ΔQ_{inj} are likely not sufficiently sparse. This is addressed rather crudely with a desired fraction specifying how many buses should have shunts. The default used is 10%, in which case a threshold value, t is found satisfying,

$$90\% = \mathbb{P}(|\Delta Q_{\text{inj}}| \leq t). \tag{B.4.6}$$

That is, t is the 90th percentile. The final shunt values are then,

$$B^{sh}_i = \begin{cases} [\Delta Q_{\text{inj}}]_i & |[\Delta Q_{\text{inj}}]_i| > t \\ 0 & \text{otherwise.} \end{cases} \tag{B.4.7}$$

Unlike the previous section, the voltage magnitude is not used when converting between reactive power and susceptance. Given the errors associated with the linearized sensitivities, it is not at all certain that such a division will increase accuracy and is therefore neglected.

B.4.3 Combining Procedures

In the specific application of Section 3.4.5 the following procedure is used:

1. Shunts are added according to Section B.4.1.

2. After resolving the OPF, shunts are added again according to Section B.4.2.

3. The original values from step 1 are subtracted from the current shunt elements to avoid cumulative effects, and the procedure in Section B.4.1 is performed again.

APPENDIX C

TRANSMISSION & DISTRIBUTION CO-SIMULATION DETAILS

C.1 Translation Code From MATPOWER to GridLAB-D

```
function str = mpc2gld(mpc,omega,varargin)
%%% convert a matpower case structure to a gridlabd string.
%%% Since gridlabd does not support PV buses, all PV buses are converted to
%%% PQ. Phase shifts are not supported currently but off-nominal tap ratios
%%% are.
%%%
%%% KNOWN ISSUES:
%%%     Base KV MUST be specified in the mpc.bus matrics, otherwise all
%%%     voltages will be set to 0 in the glm model, which wll result in
%%%     errors.
%%%
%%% INPUTS:
%%%         mpc: matpower case
%%%         omega: power radian frequency (2*pi*f)
%%% OPTIONAL NAME VALUE PAIRS:
%%%         exclude_buses: default empty.
%%%                        vector of bus numbers to exclude from the model.
%%%                        example: mpc2gld(mpc,omega,'exclude_buses',[5,7])
%%%                        nodes 5 and 7 will not be created. However, edges
%%%                        connecting to nodes 5 and 7 will still be
%%%                        written!!! The assumption is that these nodes
%%%                        will be added elsewhere as part of a feeder
%%%                        model.
%%%          no_shunt: default true.
%%%                    If false, no susceptances will be added to the glm.
%%% OUTPUTS:
%%%         str: formated string in glm format (note: preamble such as
%%%         module loading/clock etc. is provided.)
%%%
%%% written July, 2017 by Eran Schweitzer (eranschweitzer@gmail.com) at PNNL

idx = find(strcmp(varargin,'exclude_buses'));
if ~isempty(idx)
    exclude_buses = varargin{idx + 1};
else
    exclude_buses = [];
end

idx = find(strcmp(varargin,'with_shunt'));
if ~isempty(idx)
    shunt = varargin{idx+1};
else
    shunt = true;
end


define_constants;
str = '';
nmap = sparse(mpc.bus(:,BUS_I),1,1:size(mpc.bus,1));

for n = 1:size(mpc.bus,1)
    if ~any(mpc.bus(n,BUS_I) == exclude_buses)
        if (abs(mpc.bus(n,PD)) > 0) || (abs(mpc.bus(n,QD)) > 0) || ...
           (abs(mpc.bus(n,GS)) > 0) || (abs(mpc.bus(n,BS)) > 0)
            str = strcat(str,load_str(mpc.bus(n,:)));
        else
            str = strcat(str,node_str(mpc.bus(n,:)));
        end
    end
end

branch_mask = false(size(mpc.branch,1),1);
sorted_branches = [min(mpc.branch(:,1:2),[],2), max(mpc.branch(:,1:2),[],2) ];
for b = 1:size(mpc.branch,1)
    if branch_mask(b)
        continue
    end
    if mpc.branch(b,BR_STATUS)
        par_mask = parallel_mask(sorted_branches,b);
```

```
70
            par_mask(b:end) = false;
            branch_mask(b) = true;
            dummy_num = sum(par_mask);
            if dummy_num > 0
75              %parallel branch, add dummy node
                str = strcat(str,dummy_node(mpc.bus(nmap(mpc.branch(b,F_BUS)),:), ...
                                            mpc.branch(b,T_BUS),dummy_num));
            end

80          % a transformer has any of the following properties:
            % 1) different voltages at the ends of the branch
            % 2) a tap setting not equal to 0 (even tap of 1 will be used as a
            % transfomer)
            xfmr_check = mpc.bus(nmap(mpc.branch(b,F_BUS)),BASE_KV) ~= ...
85                       mpc.bus(nmap(mpc.branch(b,T_BUS)),BASE_KV);
            xfmr_check = xfmr_check || (mpc.branch(b,TAP) ~= 0);
            if ~xfmr_check
                Zbase = mpc.bus(nmap(mpc.branch(b,F_BUS)),BASE_KV)^2/mpc.baseMVA;
                z = Zbase*(mpc.branch(b,BR_R) + 1i*mpc.branch(b,BR_X));
90              if shunt
                    c = 1e9*mpc.branch(b,BR_B)/(omega*Zbase);
                else
                    c = 0;
                end
95              str = strcat(str,line_str(mpc.branch(b,:),z,c,dummy_num));
            else
                % treat as a transformer
                z = mpc.branch(b,BR_R) + 1i*mpc.branch(b,BR_X);
                if shunt
100                 bshunt = mpc.branch(b,BR_B);
                else
                    bshunt = 0;
                end
                if bshunt ~= 0
105                 zshunt = 1/(1i*bshunt);
                    str = strcat(str,xfmr_shunt(mpc.branch(b,F_BUS),...
                    mpc.branch(b,T_BUS),...
                    mpc.bus(nmap(mpc.branch(b,F_BUS)),BASE_KV), ...
                    mpc.bus(nmap(mpc.branch(b,T_BUS)),BASE_KV),...
110                 mpc.baseMVA,zshunt,dummy_num));
                else
                    zshunt = 0;
                end
                str = strcat(str,xfmr_str(mpc.branch(b,:), z, zshunt, mpc.baseMVA,...
115                 mpc.bus(nmap(mpc.branch(b,F_BUS)),BASE_KV), ...
                    mpc.bus(nmap(mpc.branch(b,T_BUS)),BASE_KV),dummy_num));
            end
        end
    end
120
    for g = unique(mpc.gen(:,GEN_BUS))'
        rows = find(mpc.gen(:,GEN_BUS) == g);
        for gnum = 1:length(rows)
            if mpc.gen(rows(gnum),GEN_STATUS) > 0
125             str = strcat(str,gen_str(mpc.gen(rows(gnum),:),...
                                 gnum,mpc.bus(nmap(g),BASE_KV)));
            end
        end
    end
130
    end

    function str = dummy_node(bus_row,tobus,dummy_num)
        str = node_str(bus_row,sprintf('_to%d_dummy%d',tobus,dummy_num));
135     str = strcat(str,sprintf(['\nobject switch {\n',...
            'name dummy_switch%d_bus%d_to%d;\n',...
            'phases ABC;\n',...
            'from bus%d;\n',...
            'to bus%d_to%d_dummy%d;\n',...
140         'status CLOSED;\n',...
            '}\n'],...
```

```
        dummy_num,bus_row(1),tobus,bus_row(1),bus_row(1),tobus,dummy_num));
end
function mask = parallel_mask(branches,bid)
    mask = (branches(:,1) == branches(bid,1)) & ...
           (branches(:,2) == branches(bid,2));
end

function str = gen_str(gen_row,gnum,baseKV)
    %generators will simply be treated like negative loads

    define_constants;
    %negative since treated as load in gld.
    S = -( gen_row(PG) + 1i*gen_row(QG) );
    str = sprintf(['\nobject load {\n',...
        '\tname gen%d_bus%d;\n',...
        '\tparent bus%d;\n',...
        '\tphases ABC;\n',...
        '\tnominal_voltage %0.3f kV;\n',...
        '\tconstant_power_A %s MVA;\n',...
        '\tconstant_power_B %s MVA;\n',...
        '\tconstant_power_C %s MVA;\n',...
        '}\n'],gnum,gen_row(GEN_BUS),gen_row(GEN_BUS),baseKV/sqrt(3),...
        complex_string(S/3),complex_string(S/3),complex_string(S/3));
end

function str = xfmr_shunt(from,to,baseKV1,baseKV2,baseMVA,zpu,dummy_num)

    if dummy_num > 0
        from = sprintf('%d_to%d_dummy%d',from,to,dummy_num);
    else
        from = sprintf('%d',from);
    end

    Zbase1 = baseKV1^2/baseMVA;
    Zbase2 = baseKV2^2/baseMVA;
    str = sprintf(['\nobject load {\n',...
        '\tname xfmr_%s_%d_shunt_from;\n',...
        '\tparent bus%s;\n',...
        '\tphases ABC;\n',...
        '\tnominal_voltage %0.3f kV;\n',...
        '\tconstant_impedance_A %s Ohm;\n',...
        '\tconstant_impedance_B %s Ohm;\n',...
        '\tconstant_impedance_C %s Ohm;\n',...
        '}\n'],from,to,from,baseKV1/sqrt(3),...
        complex_string(2*zpu*Zbase1),complex_string(2*zpu*Zbase1),...
        complex_string(2*zpu*Zbase1));

    str = strcat(str,sprintf(['\nobject load {\n',...
        '\tname xfmr_%s_%d_shunt_to;\n',...
        '\tparent bus%d;\n',...
        '\tphases ABC;\n',...
        '\tnominal_voltage %0.3f kV;\n',...
        '\tconstant_impedance_A %s Ohm;\n',...
        '\tconstant_impedance_B %s Ohm;\n',...
        '\tconstant_impedance_C %s Ohm;\n',...
        '}\n'],from,to,to,baseKV2/sqrt(3),...
        complex_string(2*zpu*Zbase2),complex_string(2*zpu*Zbase2),...
        complex_string(2*zpu*Zbase2)));
end

function str = xfmr_str(branch_row,z, zshunt, baseMVA,baseKV1,baseKV2,dummy_num)


    [F_BUS, T_BUS, BR_R, BR_X, BR_B, RATE_A, RATE_B, RATE_C, ...
    TAP, SHIFT, BR_STATUS, PF, QF, PT, QT, MU_SF, MU_ST, ...
    ANGMIN, ANGMAX, MU_ANGMIN, MU_ANGMAX] = idx_brch; %#ok<ASGLU>

    if dummy_num > 0
        dummy_name = sprintf('_dummy%d',dummy_num);
        dummy_from = sprintf('_to%d_dummy%d',branch_row(T_BUS),dummy_num);
    else
        dummy_name = '';
```

```
        dummy_from = '';
    end


    tap = branch_row(TAP);
    if tap == 0
        tap = 1;
    end

    from = branch_row(F_BUS);
    to   = branch_row(T_BUS);

    str = sprintf(['\n',...
    'object transformer_configuration {\n',...
    '\tname trans_branch_config_%d_%d%s;\n',...
    '\tconnect_type WYE_WYE;\n',...
    '\tpower_rating %0.1f_MVA;\n',...
    '\tprimary_voltage %0.2f_kV;\n',...
    '\tsecondary_voltage %0.2f_kV;\n',...
    '\tresistance %0.6f;\n',...
    '\treactance %0.6f;\n'],...
        branch_row(F_BUS),branch_row(T_BUS),dummy_name,baseMVA,...
        baseKV1*tap,baseKV2,max(real(z),1e-6),imag(z));

    str = strcat(str,sprintf('\n}\n'));

    str = strcat(str,sprintf(['\nobject transformer {\n',...
    '\tname trans_branch_%d_%d%s;\n',...
    '\tphases ABC;\n',...
    '\tfrom bus%d%s;\n',...
    '\tto bus%d;\n',...
    '\tconfiguration trans_branch_config_%d_%d%s;\n',...
    '}\n'],...
    branch_row(F_BUS),branch_row(T_BUS),dummy_name,...
    from,dummy_from,to,...
    branch_row(F_BUS),branch_row(T_BUS),dummy_name));

end

function str = line_str(branch_row,z,c,dummy_num)

    [F_BUS, T_BUS, BR_R, BR_X, BR_B, RATE_A, RATE_B, RATE_C, ...
    TAP, SHIFT, BR_STATUS, PF, QF, PT, QT, MU_SF, MU_ST, ...
    ANGMIN, ANGMAX, MU_ANGMIN, MU_ANGMAX] = idx_brch; %#ok<ASGLU>

    if dummy_num > 0
        dummy_name = sprintf('_dummy%d',dummy_num);
        dummy_from = sprintf('_to%d_dummy%d',branch_row(T_BUS),dummy_num);
    else
        dummy_name = '';
        dummy_from = '';
    end

    str = sprintf(['\nobject line_configuration {\n',...
            '\tname line_config_%d_%d%s;\n',...
            '\tz11 %s Ohm/mile;\n',...
            '\tz22 %s Ohm/mile;\n',...
            '\tz33 %s Ohm/mile;\n',...
            '\tc11 %0.4f nF/mile;\n',...
            '\tc22 %0.4f nF/mile;\n',...
            '\tc33 %0.4f nF/mile;\n',...
            '}\n'],branch_row(F_BUS),branch_row(T_BUS),dummy_name,...
            complex_string(z),complex_string(z),complex_string(z),...
            c,c,c);

     str = strcat(str,sprintf(['\nobject overhead_line {\n',...
            '\tname line_%d_%d%s;\n',...
            '\tphases ABC;\n',...
            '\tfrom bus%d%s;\n',...
            '\tto bus%d;\n',...
            '\tlength 1 mile;\n',...
            '\tconfiguration line_config_%d_%d%s;\n}\n'],...
```

```
                branch_row(F_BUS), branch_row(T_BUS), dummy_name, ...
                branch_row(F_BUS), dummy_from, branch_row(T_BUS), ...
                branch_row(F_BUS), branch_row(T_BUS), dummy_name));
end

function str = load_str(bus_row)
    [PQ, PV, REF, NONE, BUS_I, BUS_TYPE, PD, ...
    QD, GS, BS, BUS_AREA, VM, ...
    VA, BASE_KV, ZONE, VMAX, VMIN, ...
    LAM_P, LAM_Q, MU_VMAX, MU_VMIN] = idx_bus; %#ok<ASGLU>
    str = sprintf(['\nobject load {\n', ...
        '\tname bus%d;\n', ...
        '\tphases ABC;\n', ...
        '\tnominal_voltage %0.3f kV;\n', ...
        '\tbustype %s;\n'], bus_row(BUS_I), bus_row(BASE_KV)/sqrt(3), ...
        bustype(bus_row(BUS_TYPE)));

    v = bus_row(VM)*exp(1i*bus_row(VA)*pi/180)*bus_row(BASE_KV)/sqrt(3);
    a = exp(1i*120*pi/180);
    str = strcat(str, sprintf(['\n\tvoltage_A %s kV;\n', ...
        '\tvoltage_B %s kV;\n', ...
        '\tvoltage_C %s kV;\n'], ...
        complex_string(v,'format','polar'), ...
        complex_string(v*a^2,'format','polar'), ...
        complex_string(v*a,'format','polar')));

    if (abs(bus_row(PD)) > 0) || (abs(bus_row(QD)) > 0)
        S = bus_row(PD) + 1i*bus_row(QD);
        str = strcat(str, sprintf(['\n\tconstant_power_A %s MVA;\n', ...
                '\tconstant_power_B %s MVA;\n', ...
                '\tconstant_power_C %s MVA;\n'], ...
                complex_string(S/3), complex_string(S/3), ...
                complex_string(S/3)));
    end

    if (abs(bus_row(GS)) > 0) || (abs(bus_row(BS)) > 0)
        S = bus_row(GS) - 1i*bus_row(BS); %power in MVA
        Z = bus_row(BASE_KV)^2/(conj(S)); %impedance in Ohm.
        str = strcat(str, sprintf(['\n\tconstant_impedance_A %s Ohm;\n', ...
                '\tconstant_impedance_B %s Ohm;\n', ...
                '\tconstant_impedance_C %s Ohm;\n'], ...
                complex_string(Z), complex_string(Z), complex_string(Z)));
    end

    str = strcat(str, sprintf('\n}\n'));
end

function str = cap_str(bus_row)

    [PQ, PV, REF, NONE, BUS_I, BUS_TYPE, PD, ...
    QD, GS, BS, BUS_AREA, VM, ...
    VA, BASE_KV, ZONE, VMAX, VMIN, ...
    LAM_P, LAM_Q, MU_VMAX, MU_VMIN] = idx_bus; %#ok<ASGLU>

    str = sprintf(['\nobject capacitor {\n', ...
        '\tname cap%d;\n', ...
        '\tparent bus%d;\n', ...
        '\tphases ABC;\n', ...
        '\tphases_connected ABC;\n', ...
        '\tnominal_voltage %0.3f kV;\n', ...
        '\tcapacitor_A %0.3f MVAr;\n', ...
        '\tcapacitor_B %0.3f MVAr;\n', ...
        '\tcapacitor_C %0.3f MVAr;\n', ...
        '}\n'], ...
        bus_row(BUS_I), bus_row(BUS_I), bus_row(BASE_KV)/sqrt(3), ...
        bus_row(BS)/3, bus_row(BS)/3, bus_row(BS)/3);

end

function str = node_str(bus_row,dummy_name)
    if nargin == 1
        dummy_name = '';
```

```
    end
    [PQ, PV, REF, NONE, BUS_I, BUS_TYPE, PD, ...
    QD, GS, BS, BUS_AREA, VM, ...
    VA, BASE_KV, ZONE, VMAX, VMIN, ...
    LAM_P, LAM_Q, MU_VMAX, MU_VMIN] = idx_bus; %#ok<ASGLU>
    str = sprintf(['\nobject node {\n',...
        '\tname bus%d%s;\n',...
        '\tphases ABC;\n',...
        '\tnominal_voltage %0.3f kV;\n',...
        '\tbustype %s;\n'],bus_row(BUS_I),dummy_name,...
        bus_row(BASE_KV)/sqrt(3), bustype(bus_row(BUS_TYPE)));

    v = bus_row(VM)*exp(1i*bus_row(VA)*pi/180)*bus_row(BASE_KV)/sqrt(3);
    a = exp(1i*120*pi/180);
    str = strcat(str,sprintf(['\n\tvoltage_A %s kV;\n',...
        '\tvoltage_B %s kV;\n',...
        '\tvoltage_C %s kV;\n'],...
        complex_string(v,'format','polar'),...
        complex_string(v*a^2,'format','polar'),...
        complex_string(v*a,'format','polar')));

    str = strcat(str,sprintf('\n}\n'));
end

function str = bustype(n)
    switch n
        case 1
            str = 'PQ';
        case 2
            str = 'PQ'; % PV buses are not implemented in gridlabd!
        case 3
            str = 'SWING';
    end
end

function str = complex_string(v,varargin)
    idx = find(strcmp(varargin,'format'),1);
    if ~isempty(idx)
        fmt = varargin{idx + 1};
    else
        fmt = 'rect';
    end
    if strcmp(fmt,'rect')
        if imag(v) < 0
            str = sprintf('%0.4f%0.4fj',real(v),imag(v));
        else
            str = sprintf('%0.4f+%0.4fj',real(v),imag(v));
        end
    elseif strcmp(fmt,'polar')
        if angle(v) < 0
            str = sprintf('%0.4f%0.4fd',abs(v),angle(v)*180/pi);
        else
            str = sprintf('%0.4f+%0.4fd',abs(v),angle(v)*180/pi);
        end
    end
end
```

APPENDIX D

DISTFLOW DETAILS

D.1 Three-Phase Connection Matrix Example

Figure D.1.1 is used to illustrate how the connection matrices for a multiphase feeder are formed.

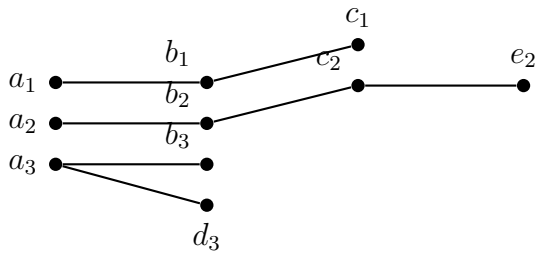

Figure D.1.1: Example multiphase feeder.

The connection matrices are:

$$\boldsymbol{F} = \begin{array}{c} \\ \ell^{ab}_{11} \\ \ell^{ab}_{21} \\ \ell^{ab}_{31} \\ \ell^{ab}_{12} \\ \ell^{ab}_{22} \\ \ell^{ab}_{32} \\ \ell^{ab}_{13} \\ \ell^{ab}_{23} \\ \ell^{ab}_{33} \\ \ell^{bc}_{11} \\ \ell^{bc}_{21} \\ \ell^{bc}_{12} \\ \ell^{bc}_{22} \\ \ell^{ad}_{33} \\ \ell^{ce}_{22} \end{array} \begin{array}{c} \begin{array}{ccccccccccccccccccccccccc} a_{11} & a_{21} & a_{31} & a_{12} & a_{22} & a_{32} & a_{13} & a_{23} & a_{33} & b_{11} & b_{21} & b_{31} & b_{12} & b_{22} & b_{32} & b_{13} & b_{23} & b_{33} & c_{11} & c_{21} & c_{12} & c_{22} & d_{33} & e_{22} \end{array} \\ \left(\begin{array}{ccccccccccccccccccccccccc} 1 & & & & & & & & & & & & & & & & & & & & & & & & \\ & 1 & & & & & & & & & & & & & & & & & & & & & & & \\ & & 1 & & & & & & & & & & & & & & & & & & & & & & \\ & & & 1 & & & & & & & & & & & & & & & & & & & & & \\ & & & & 1 & & & & & & & & & & & & & & & & & & & & \\ & & & & & 1 & & & & & & & & & & & & & & & & & & & \\ & & & & & & 1 & & & & & & & & & & & & & & & & & & \\ & & & & & & & 1 & & & & & & & & & & & & & & & & & \\ & & & & & & & & 1 & & & & & & & & & & & & & & & & \\ \hline & & & & & & & & & 1 & & & & & & & & & & & & & & & \\ & & & & & & & & & & 1 & & & & & & & & & & & & & & \\ & & & & & & & & & & & & 1 & & & & & & & & & & & & \\ & & & & & & & & & & & & & 1 & & & & & & & & & & & \\ \hline & & & & & & & & 1 & & & & & & & & & & & & & & & & \\ & & & & & & & & & & & & & & & & & & & & & & & 1 & \end{array}\right) \end{array} \tag{D.1.1a}$$

$$\boldsymbol{T} = \begin{array}{c} \\ \ell^{ab}_{11} \\ \ell^{ab}_{21} \\ \ell^{ab}_{31} \\ \ell^{ab}_{12} \\ \ell^{ab}_{22} \\ \ell^{ab}_{32} \\ \ell^{ab}_{13} \\ \ell^{ab}_{23} \\ \ell^{ab}_{33} \\ \ell^{bc}_{11} \\ \ell^{bc}_{21} \\ \ell^{bc}_{12} \\ \ell^{bc}_{22} \\ \ell^{ad}_{33} \\ \ell^{ce}_{22} \end{array} \begin{array}{c} \begin{array}{ccccccccc} a_{11} & a_{21} & a_{31} & a_{12} & a_{22} & a_{32} & a_{13} & a_{23} & a_{33} \end{array} \\ \left(\begin{array}{ccccccccc} & & & & & & & & \\ & & & & & & & & \\ & & & & & & & & \\ & & & & & & & & \\ & & & & & & & & \\ & & & & & & & & \\ & & & & & & & & \\ & & & & & & & & \\ & & & & & & & & \\ \hline & & & & & & & & \\ & & & & & & & & \\ & & & & & & & & \\ & & & & & & & & \\ \hline & & & & & & & & \\ & & & & & & & & \end{array}\right) \end{array} \begin{array}{c} \overbrace{\begin{array}{ccccccccccccccc} b_{11} & b_{21} & b_{31} & b_{12} & b_{22} & b_{32} & b_{13} & b_{23} & b_{33} & c_{11} & c_{21} & c_{12} & c_{22} & d_{33} & e_{22} \end{array}}^{\boldsymbol{T}_E} \\ \left(\begin{array}{ccccccccccccccc} 1 & & & & & & & & & & & & & & \\ & 1 & & & & & & & & & & & & & \\ & & 1 & & & & & & & & & & & & \\ & & & 1 & & & & & & & & & & & \\ & & & & 1 & & & & & & & & & & \\ & & & & & 1 & & & & & & & & & \\ & & & & & & 1 & & & & & & & & \\ & & & & & & & 1 & & & & & & & \\ & & & & & & & & 1 & & & & & & \\ \hline & & & & & & & & & 1 & & & & & \\ & & & & & & & & & & 1 & & & & \\ & & & & & & & & & & & 1 & & & \\ & & & & & & & & & & & & 1 & & \\ \hline & & & & & & & & & & & & & 1 & \\ & & & & & & & & & & & & & & 1 \end{array}\right) \end{array} \tag{D.1.1b}$$

$$\boldsymbol{M}_0 = \begin{array}{c} \\ \ell^{ab}_{11} \\ \ell^{ab}_{21} \\ \ell^{ab}_{31} \\ \ell^{ab}_{12} \\ \ell^{ab}_{22} \\ \ell^{ab}_{32} \\ \ell^{ab}_{13} \\ \ell^{ab}_{23} \\ \ell^{ab}_{33} \\ \hline \ell^{bc}_{11} \\ \ell^{bc}_{21} \\ \ell^{bc}_{12} \\ \ell^{bc}_{22} \\ \hline \ell^{ad}_{33} \\ \ell^{ce}_{22} \end{array} \overbrace{\begin{array}{ccccccccc} a_{11} & a_{21} & a_{31} & a_{12} & a_{22} & a_{32} & a_{13} & a_{23} & a_{33} \end{array}}^{m_0} \overbrace{\begin{array}{ccccccccccccccc} b_{11} & b_{21} & b_{31} & b_{12} & b_{22} & b_{32} & b_{13} & b_{23} & b_{33} & c_{11} & c_{21} & c_{12} & c_{22} & d_{33} & e_{22} \end{array}}^{\boldsymbol{M}} \left(\begin{array}{ccccccccc|ccccccc} 1 & & & & & & & & & -1 & & & & & & & \\ & 1 & & & & & & & & & -1 & & & & & & \\ & & 1 & & & & & & & & & -1 & & & & & \\ & & & 1 & & & & & & & & & -1 & & & & \\ & & & & 1 & & & & & & & & & -1 & & & \\ & & & & & 1 & & & & & & & & & -1 & & \\ & & & & & & 1 & & & & & & & & & -1 & \\ & & & & & & & 1 & & & & & & & & & -1 \\ \hline & & & & & & & & 1 & & & & & & & & \\ \hline & & & & & & & & & 1 & & & & & & & \\ & & & & & & & & & & 1 & & & & & & \\ & & & & & & & & & & & 1 & & & & & \\ & & & & & & & & & & & & 1 & & & & \\ \hline & & & & & & & & 1 & & & & & & & & \\ \hline & & & & & & & & & & & & & 1 & & -1 & \\ & & & & & & & & & & & & & & 1 & & -1 \end{array}\right)$$

(D.1.1c)

$$\overbrace{\begin{array}{ccccccccc} a_{11} & a_{21} & a_{31} & a_{12} & a_{22} & a_{32} & a_{13} & a_{23} & a_{33} \end{array}}^{\mathrm{ph}(\mathbf{1}_{|\mathscr{N}|}\otimes\mathbb{I}_{|\Phi_0|})} \begin{array}{c} a_{11} \\ a_{21} \\ a_{31} \\ a_{12} \\ a_{22} \\ a_{32} \\ a_{13} \\ a_{23} \\ a_{33} \\ \hline b_{11} \\ b_{21} \\ b_{31} \\ b_{12} \\ b_{22} \\ b_{32} \\ b_{13} \\ b_{23} \\ b_{33} \\ \hline c_{11} \\ c_{21} \\ c_{12} \\ c_{22} \\ \hline d_{33} \\ \hline e_{22} \end{array} \left(\begin{array}{ccccccccc} 1 & & & & & & & & \\ & 1 & & & & & & & \\ & & 1 & & & & & & \\ & & & 1 & & & & & \\ & & & & 1 & & & & \\ & & & & & 1 & & & \\ & & & & & & 1 & & \\ & & & & & & & 1 & \\ & & & & & & & & 1 \\ \hline 1 & & & & & & & & \\ & 1 & & & & & & & \\ & & 1 & & & & & & \\ & & & 1 & & & & & \\ & & & & 1 & & & & \\ & & & & & 1 & & & \\ & & & & & & 1 & & \\ & & & & & & & 1 & \\ & & & & & & & & 1 \\ \hline 1 & & & & & & & & \\ & 1 & & & & & & & \\ & & 1 & & & & & & \\ & & & 1 & & & & & \\ & & & & 1 & & & & \\ \hline & & & & & & & & 1 \\ \hline & & & & 1 & & & & \end{array}\right) \left(\begin{array}{c} [v_0^2]_{11} \\ [v_0^2]_{21} \\ [v_0^2]_{31} \\ [v_0^2]_{12} \\ [v_0^2]_{22} \\ [v_0^2]_{32} \\ [v_0^2]_{13} \\ [v_0^2]_{23} \\ [v_0^2]_{33} \end{array}\right) = \begin{array}{c} a_{11} \\ a_{21} \\ a_{31} \\ a_{12} \\ a_{22} \\ a_{32} \\ a_{13} \\ a_{23} \\ a_{33} \\ \hline b_{11} \\ b_{21} \\ b_{31} \\ b_{12} \\ b_{22} \\ b_{32} \\ b_{13} \\ b_{23} \\ b_{33} \\ \hline c_{11} \\ c_{21} \\ c_{12} \\ c_{22} \\ \hline d_{33} \\ \hline e_{22} \end{array} \left(\begin{array}{c} [v_0^2]_{11} \\ [v_0^2]_{21} \\ [v_0^2]_{31} \\ [v_0^2]_{12} \\ [v_0^2]_{22} \\ [v_0^2]_{32} \\ [v_0^2]_{13} \\ [v_0^2]_{23} \\ [v_0^2]_{33} \\ \hline [v_0^2]_{11} \\ [v_0^2]_{21} \\ [v_0^2]_{31} \\ [v_0^2]_{12} \\ [v_0^2]_{22} \\ [v_0^2]_{32} \\ [v_0^2]_{13} \\ [v_0^2]_{23} \\ [v_0^2]_{33} \\ \hline [v_0^2]_{11} \\ [v_0^2]_{21} \\ [v_0^2]_{12} \\ [v_0^2]_{22} \\ \hline [v_0^2]_{33} \\ \hline [v_0^2]_{22} \end{array}\right)$$

(D.1.2)

$$\Rightarrow \boldsymbol{M}_0 \,\mathrm{ph}(\mathbf{1}_{|\mathscr{N}|} \otimes \mathbb{I}_{|\Phi_0|}) v_0^2 = \mathbf{0}_E \tag{D.1.3}$$